UNIVERSITY of NAPLES
FEDERICO II

DEPARTEMENT OF CHEMICAL, MATERIALS
AND PRODUCTION ENGINEERING

RESEARCH DOCTORATE IN

INDUSTRIAL PRODUCT AND PROCESS ENGINEERING
XXIX CYCLE

INVESTIGATING THE MECHANICS OF TUMOUR: FROM SINGLE CELL MECHANICS TO THE BIOPHYSICAL INTERPLAY BETWEEN CELLS AND ECM

COORDINATOR
CH.MO PROF. G. MENSITIERI

SUPERVISOR
CH.MO PROF. P.A. NETTI

ADVISOR
PH.D. S.FUSCO

PH.D. STUDENT
ING. IDA MUSELLA

ABSTRACT

This PhD project has focused the attention on the mechanical characterization of cancer cells and their surroundings. It is well known that the mechanical properties of cells and extracellular matrix (ECM), especially stiffness, play an important role in many biological processes such as cell growth, migration, division and differentiation. The pathological state of a cell implicates the alteration of the cytoskeletal structure and, consequently, of its functions, determining a variation of cell and ECM mechanical properties. In particular, the aim of this work is to investigate how cancer progression changes cell and ECM mechanical properties *in vitro* and *ex vivo* conditions. In the first experimental studies, particle tracking microrheology and Atomic Force Microscopy (AFM) techniques were performed to compare the mechanical properties of murine normal and virus-transformed cell lines cultured on glass. The first goal of the work was the identification of several biophysical parameters to discriminate between tumour and healthy cells. They have been useful to understand how virus transformation influence cell physiological processes and mechanical properties and, as a consequence, to identify the existence of a relationship between biological functions and cell mechanics. We observed that the effects of virus induced-transformation are the intensification of cell proliferation, the enhanced capability of transformed cells to migrate, the reduced adhesion capability, the reduction of cell cytoskeletal organization and the increased cell deformability. Successively, taking into account the results collected on the single murine cells, we moved to the characterization of human lung cells with different metastatic potential. Also in this case, combining the analyses of phenotypic characteristics and the biophysical properties of the cells, in particular elasticity, we were able to discriminate benign from cancer cells and, among them, to distinguish the grade of aggressiveness. Thus, we achieved the first milestone of this work with the definition of a new and accurate biomarker of cell metastatic potential.

The second goal of the work concerned the investigation of the crosstalk between cancer cells and the surrounding ECM, through the study of *ex vivo* human biopsy tissues, removed from patients affected by lung adenocarcinoma. To this aim a new

technique, based on multiple particle tracking (MPT) has been developed. To perform, at the same time, the mechanical classification of cells and ECM of each sample and a comparison with the healthy equivalent for the entire pool of patients, the ECM structure and morphology of cancer and healthy tissues were investigated and compared. Moreover, results and mechanical phenotypes were correlated to the stage and the grade of cancer, previously classified by the classic immunodiagnostic method. The cancerous transformation of tissues had a remarkable effect on the dynamics of the tracer beads and contributes a sort of symmetric modification of the mechanical properties of the cells and ECM. Indeed, compared to the healthy tissues, particles introduced into the cells of adenocarcinoma tissues increase their motion. Otherwise, unlike healthy tissues, the reduced motion of the beads probing the surrounding ECM suggests that cell in tumour tissues reside in a stiffer matrix. These increased mechanical properties of ECM are associated to an enhancement of collagen cross-linking, also confirmed through the structural and morphological analyses of tissue biopsies. The obtained mechanical properties of cells and their surrounding ECM from MPT represents a reliable indicator of the malignant transformation process and we believe that it can be used in combination with the classical immunohistochemistry-based diagnostic tools to obtain a more effective and precise diagnosis of the cancer.

Abbreviations

AFM	Atomic force microscopy
BSA	Bovine serum albumin
CSK	Cytoskeleton
E	Young's modulus
ECM	Extracellular matrix
EMT	Epithelial to mesenchymal transition
FA(s)	Focal adhesion(s)
MPM	Malignant pleural mesothelioma
MPT	Multiple particles tracking
MSD(s)	Mean squared displacement(s)
NA	Numerical aperture
OCT	Optimal cutting temperature
PAAm	Polyacrylamide
PBS	Phosphate-buffered saline
PTM	Particle tracking microrheology
R_g	Radius of gyration
SE	Standard error
SHG	Second harmonic generation

1

Introduction

1.1 Cell Biology: the role of cytoskeleton

Cells, often called the *building blocks of life*, are the basic structural, functional and biological unit of all known living organisms. Cells are the smallest unit of life, not visible to naked eyes; in fact, most of the biological cells are 1-100 μm in size. The cell comprises many constituents: it consists of *cytoplasm* enclosed within a phospholipid bilayer membrane, *cell membrane*, and a *nucleus*, that is the control centre of the cell. The cell membrane separates the material outside the cell, the extracellular matrix (ECM), from the material inside the cell. It maintains the integrity of a cell and controls the passage of materials into and out of the cell. Cells are highly dynamic systems that continuously change their chemical and physical characteristics. Many aspects of cellular physiology rely on the ability to control mechanical stimuli across the cell: i) cells subjected to external stress must be able to maintain their shape; ii) during cell migration and division, forces generated within cell are required to drive morphogenic changes with extremely high spatial and temporal precision; iii) adherent cells also generate force on their surrounding environment; cellular force generation is required in remodelling of ECM and tissue morphogenesis. This varied mechanical behaviour of cells is determined, to a large degree, by a complex machinery formed by a network of filamentous proteins, called the cytoskeleton (CSK) (1). The cytoskeleton spans the cytoplasm and interconnects the cell nucleus with the ECM, thereby forming a structural bridge between gene expression and molecules involved in cell communication and adhesion on a subcellular scale. Despite the connotations of the word “skeleton”, the cytoskeleton is not a fixed structure, but it is a dynamic and adaptive structure, composed of three main types of polymer: actin filaments, microtubules and intermediate filaments. All three are organized into networks that resist deformation but can reorganize in response to externally applied forces, and they have important roles in arranging and maintaining the integrity of intracellular compartments. The cytoskeleton carries out three broad functions: i) it spatially organizes the content of the cell; ii) it connects the cell physically and biochemically to the external environment and iii) generates coordinated forces that enable the cell to move and change shape. Thus, the correct functioning of cellular processes depends on the maintenance of the CSK structure. As a consequence,

changes in such a crucial cellular structure lead to pathological condition and many diseases have now been associated with abnormalities in cytoskeleton, including cancer (2–4).

1.2 Hallmarks of cancer cells

Cancer is a disease characterized by an altered behaviour of normal cells, due to genetic defects. Nowadays, cancer is one of the leading causes of death worldwide. The study of this disease is really complex because of the existence of hundreds distinct types of cancer, and subtypes of tumours can be found within specific organs. Despite this complexity, Hanahan and Weinberg (5) suggested that the vast catalogue of cancer cell genotypes is a manifestation of six essential alterations in cell physiology (Fig.1) that collectively dictate malignant growth:

- *Self-sufficiency in growth signals*: normal cells require mitogenic growth signals (GS) before they can move from a quiescent state into an active proliferative state. These signals are transmitted into the cell by transmembrane receptors that bind distinctive classes or signalling molecules. In the absence of these signals, the cell is not able to proliferate. However, tumour cells lack of this exogenous growth signalling dependence and acquire GS independently, disrupting the normal homeostasis mechanism.
- *Insensitivity to antigrowth signals*: within normal tissues, multiple antiproliferative signals operate to maintain cellular quiescence and tissue homeostasis. Indeed, in the case of cancer, cells result insensitivity to these antigrowth signals.
- *Evading apoptosis*: apoptotic program is present in latent form in all cell types. Cancer cells acquire also resistance to apoptosis, that is a form of programmed cell death, initiated when a cell is damaged or infected.
- *Limitless in replicative potential*: independently of the cell-cell signalling pathways, cells carry an intrinsic program that limits their multiplication. Once cells have progressed through a certain number of doublings, they stop growing through a process known as senescence. Cancer cells escape this limit and are apparently capable of indefinite growth and division.

- *Sustained angiogenesis*: cells should be close to the blood vessels to get the oxygen and nutrients necessary for cell function and survival. Angiogenesis is the process of growth of new blood vessels, that is transitory and carefully regulated once a tissue is formed. However, during tumour progression, an "angiogenic switch" is almost always activated and remains on, causing normal quiescent vasculature to continually sprout out new vessels that help sustain expanding neoplastic growths.
- *Tissue invasion and metastasis*: the most well-known property of cancer cells is their ability to invade surrounding tissues and travel to distant sites (metastasis). Successful invasion and metastasis depend upon all of other five acquired hallmark capabilities. The multistep process of invasion and metastasis begins with local invasion, then intravasation by cancer cells into nearby blood and lymphatic vessels, transit of cancer cells through the lymphatic and haematogenous systems, followed by escape of cancer cells from the lumina of such vessels into the parenchyma of distant tissues (extravasation), the formation of small nodules of cancer cells (micro-metastases), and finally the growth of micro-metastatic lesions into macroscopic tumours, this last step being termed *colonization*.

The hallmarks of cancer, described above, are acquired functional capabilities that allow cancer cells to survive, proliferate and disseminate. These functions are acquired in different tumour types via distinct mechanism and at various times during the course of multistep tumorigenesis. Their acquisition is made possible by the development of genomic instability in cancer cells, which generates random mutations, and the inflammatory state of premalignant and frankly malignant lesions that is driven by cells of the immune system, some of which serve to promote tumour progression through various means.

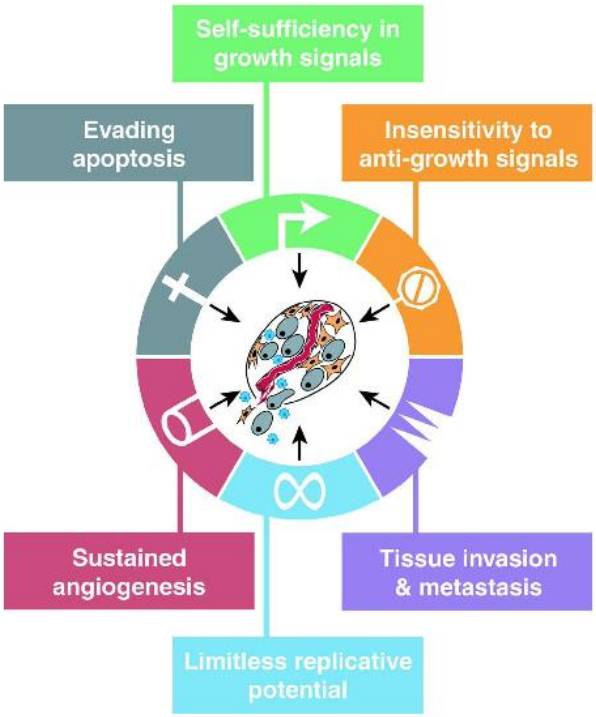

Figure 1 Acquired capabilities of cancer cells.

Yet other distinct attributes of cancer cells have been proposed to be functionally important for the development of cancer and might therefore be added to the list of core hallmarks (6):

- *Reprogramming of cellular energy metabolism*: cancer cells have to change their energy metabolism to sustain continuous cell growth and proliferation. Under aerobic conditions, normal cells process glucose, first to pyruvate via glycolysis in the cytosol and thereafter to carbon dioxide in the mitochondria; under anaerobic conditions, glycolysis is favoured and relatively little pyruvate is dispatched to the oxygen-consuming mitochondria. Cancer cells, even in the presence of oxygen, can reprogram their glucose metabolism and thus their energy production, by limiting their energy metabolism largely to glycolysis, leading to a state that has been termed "anaerobic glycolysis".
- *Evading the immune system*: cells and tissues are constantly monitored by an ever-alert immune system. The complex crosstalk between immunity and cancer cells occurs through events that usually eventually climax either in successful tumour eradication or immune evasion by the tumour (7).

In order to define the malignant transformation of neoplasms and finally reveal the functional pathway that enables cancer cells to promote cancer progression, the eight classical hallmarks of cancer, described above, require the inclusion of specific mechanical properties of cancer cells and their microenvironment, such as the ECM and embedded cells (8,9). Physical measurements can improve classical approaches that investigate cancer and inflammatory disease and, thus, physical insights can be integrated into classical biological approaches. This ninth hallmark of cancer considers that the primary tumour and the tumour microenvironment alter the survival conditions and cellular properties of a certain set of cancer cells, which subsequently favours the selection of an aggressive (highly invasive) subtype of cancer cells. Cancer progression is characterized by nine hallmarks, that can be organized in three groups: neoplasm formation, transformation of cancer cells into aggressive and invasive cells and tumour growth (Fig.2).

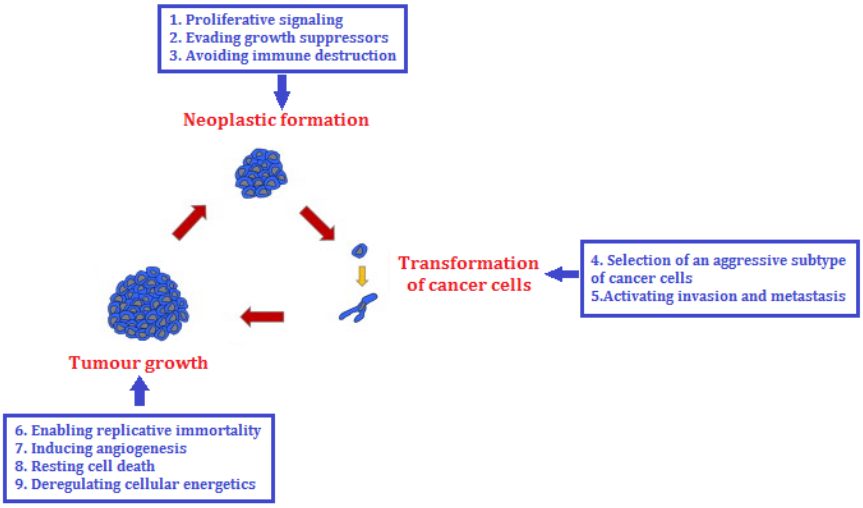

Figure 2 Schematic representation of the eight hallmarks of cancer, defined by Hanahan and Weinberg, including the mechanical properties of cells and their microenvironment as a new possible hallmark of cancer.

1.3 The role of cell mechanics in cancer disease

The classical tumour biology research, using biochemical or molecular genetic methods, has proposed eight hallmarks of cancer, such as sustaining proliferative signalling, evading growth suppressors, avoiding immune destruction, activating invasion and metastasis, enabling replicative immortality, inducing angiogenesis,

resisting cell death and deregulating cellular energetics. As classical biological and biochemical approaches have not captured the full complexity of the cancer disease, physical-based cancer research has gained knowledge about the malignant progression of cancer. A ninth hallmark, which combines the aspect of physics into classical cancer research, has added to the classical hallmarks of cancer. It is represented by the biomechanical properties of cancer cells and their microenvironment.

In the last decade, the interest on the correlation between biomechanical and biophysical properties of cells and subcellular structures and the onset and progression of human diseases, in particularly cancer, has significantly increased (10). Disease not only causes biological and functional alterations but also results in abnormalities in the physical and structural characteristics of cells. It is now well accepted that mechanical properties of cancer cells and their microenvironment have a fundamental role to define the malignant transformation of neoplasms and finally reveal the functional pathways which enable cancer cells to promote cancer progression (6). To facilitate tumour progression and finally to metastasize in target organs, cancer cells are able to remodel and adapt their microenvironment, including its mechanical properties. The tumour microenvironment is, hence, an active compartment, which has a key role to provide adjuvant conditions for malignant cancer progression (11,12).

The mechanical properties of cells are largely determined by the cytoskeleton, an internal polymer network, which determines the cell's mechanical strength and morphology (13). Cell cytoskeleton plays an important role in several cellular structural and functional roles, such as cell morphology, signalling, intracellular transport, migration, adhesion and proliferation. As a consequence, any changes to normal cellular function are mirrored in the cytoskeleton. During the cell's progression from a fully mature, post mitotic state to a replicating, motile, and immortal cancerous cell, the cytoskeleton devolves from a rather ordered and rigid structure to a more irregular and compliant state. These changes in cytoskeletal content and structure should be reflected in the overall mechanical properties of the cell (14). Thus, the measure of the cell's rigidity should provide information about its biological state and may be considered as a new biological marker for cellular

phenotypic events, associated with alterations in cytostructure and adhesion during malignant transformation. Previous studies on the mechanical properties of cells, measured by using different characterization techniques (shown below), have demonstrated that, independently of the cancer type (bladder, melanoma, prostate, breast, colon), the cancer cells are more compliant than their healthy counterparts (14–17). Furthermore, the decrease in cell stiffness seems to be greater in cells with higher malignancy and metastatic potential (18,19) The determination of cell stiffness enables an effective detection and identification of cancerous cells and the difference in cell deformability can be exploited to discriminate between cancer and healthy cells and also to distinguish cancer cells with different aggressiveness.

To fully understand the mechanobiology of a tumour, it is necessary to study the individual specialized cell types within the tumour microenvironment. Cells indeed can communicate with the surrounding environment, which is formed by other cells and the ECM, through cell adhesion proteins that act as a receptor and tie matrix through the cytoskeleton (20). A normal cell not only applies the forces but also responds to them, through cytoskeleton organization and other cellular processes, regardless of whether they derive from normal tissue matrix, synthetic substrate, or even an adjacent cell. Furthermore, physical properties of tissues can change in disease and cellular responsiveness to matrix solidity can likewise change (21). Tumour microenvironment seems to be highly critical for all steps of the cancer metastatic process. The physical interaction between a cancer cell and the ECM has a key role in allowing cancer cells to migrate from a tumour to nearby tissues. The most abundant fibrous protein within ECM is collagen, that plays structural roles and contributes to mechanical properties, molecular architecture, and shape of tissues. The changes in cellular mechanical properties are accompanied by some very specific variations in the mechanical properties of ECM. Tumours with high invasive potential have a stiff extracellular environment (22,23). In fact, during malignant transformation, an increase in the crosslinking of the collagen fibres has been observed. In a growing tumour, the fibres in the ECM undergo extensive remodelling in terms of degradation, re-polymerization and alignment, due to cell metastasis and invasion of the extracellular environment (24–26). The realignment of ECM fibres and strain-induced stretching can alter the ECM mechanical properties (27). In order to

understand how single cells sense mechanical signals of the surrounding environment, early studies have been performed on synthetic gels, including polyacrylamide, that mimic the physiological stiffness of healthy and pathologic tissues (28–31). However, the relevance of single cell measurements has been questioned given the lack of a proper three-dimensional tissue environment (32). Recently, to understand how the malignancy alters the mechanical properties of cells within the tumour microenvironment, *ex vivo* studies on human biopsies have also been performed (33).

Besides cell-ECM interaction, also cell-cell adhesion has to be considered in determining tissue architecture. The most important proteins that ensure tight adhesion junction between neighbouring cells are the cadherins. During tumour progression, in the case of epithelial cells, the cell-cell junctions are down-regulate, cell morphology changes and cellular motility enhances. During this process, known as epithelial to mesenchymal transition (EMT), cell-cell contacts are inhibited, because of the switching of the expression from E-cadherin to N-cadherin and active signals, that support tumour cell migration, invasion, and metastatic dissemination, are produced (34).

To summarize, in the past recent years it was established that the mechanical properties of cells and surrounding environment have a key role in cancer progression. They regulate the transformation of cancer cells into aggressive subtypes of cancer cells, they have the capability to down-regulate cell-cell adhesions, alter cell-matrix adhesions, in order to facilitate the transmigration of cancer cells through the basement membrane and their migration into neighbouring tissues.

1.4 Tools to study cell mechanics

A variety of methods has been developed to study the mechanics of cell cytoskeleton. The experimental approaches to cell mechanics can be divided in two broad classes: active and passive techniques. The first engages the application of a stress (or strain) to measure the corresponding strain (or stress). The second analyses the thermal fluctuations of particles injected directly into the cytoplasm or detects the forces that cells exert on flexible substrates. In particular, the dominant techniques belonging to

the first class are micropipette aspiration, optical tweezers, magnetic tweezers and atomic force microscopy (AFM). On the other side, passive techniques include, among others, particle tracking microrheology (PTM), microfabricated posts and traction force microscopy (TFM). In this section, the working principles of the principle techniques, in view of their application to cell mechanics, are illustrated.

1.4.1 Micropipette aspiration

Micropipette aspiration applies an hydrostatic suction pressure to cell surface via micropipette (Fig. 3) and measures the mechanical properties of single cells by the observation of cell deformation upon pressure suction. Cells are aspired into a micropipette and examining the resulting cell deformation, elastic and viscoelastic properties of cells are extrapolated (35). Micropipette aspiration is one of the most widely used techniques for probing suspended cells.

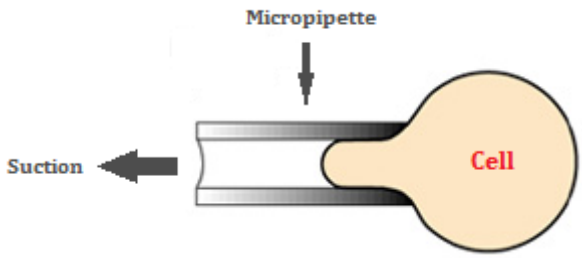

Figure 3 Schematic representation of the working principle of micropipette aspiration to measure cell deformability.

The study of suspended cells is important in the diagnosis of cancer, because a canonical feature of many cancer cells is the loss of anchorage dependence, thus these cells grow in suspension (36). This technique can be used on isolated cells, both in suspension and substrate-attached, but it only tests the extracellular surface and probes the mechanical properties of sub-membrane cytoskeleton (37).

1.4.2 Optical and magnetic tweezers

Optical tweezers use a highly focused laser beam to trap and manipulate microscopic, neutral objects such as small dielectric spherical particles. The beam is typically focused sending it through the interior of a microscope, filling the back aperture of a microscope object. Typically, the system is implemented using a high numerical

aperture (NA) objective to ensure true three dimensional trapping. Dielectric particles experience two kinds of forces: the scattering force, due to light scattering, that is proportional to light intensity and acts in the direction of propagation of light and the gradient force, produced by a gradient of field light intensity. Scattering and gradient forces exerted on the particles depend on the wavelength of the laser beam and on the particle size (38). Optical tweezers technique has been extensively used for the study of biological systems (39), and later to investigate the mechanical properties of the cell cytoskeleton (40–43). A spherical bead is used as a probe to study the mechanical response of living cells and generate a small or moderate stress to the cell in the approximate range 1-100 $pN/\mu m^2$. Optical tweezer appears a valuable tool for high precision measurements of small forces. Nevertheless, the amount of force that can be applied using this method is inherently limited. In particular, in order to enhance optical forces, an increase in the laser power is required, with the risk of inducing local heating of the cell that might damage cell structure and alter its mechanical properties. To increase the amount of optical forces, leaving minimal photo-damage, another type of optical manipulation technique can be performed. It involves coupling a laser light to another optical fibre that enables trapping and stretching of the whole cell (44) By combining this optical stretcher technique with a microfluidic platform, high throughput mechanical characterization of diseased and healthy cells in suspension has been reported (14).

Magnetic tweezers are similar in concept to optical tweezers. Optical and magnetic tweezers have notably succeeded in combining great flexibility in terms of molecular manipulation with high spatial and temporal resolution. In particular, magnetic tweezers can apply both stretching forces and torques to biological samples tethered between a surface and beads.

The apparatus of magnetic tweezers consists of magnetic micro-particles, which can be manipulated with the help of an external magnetic field. Magnetic particle in an external magnetic field experiences a force proportional to the gradient of the square of the magnetic field. A microscopic objective with a camera allows to determine the position of magnetic particles. High forces can be achieved with relatively small magnetic field strengths provided a very steep field gradient. Recent advances in

techniques which combine magnetic tweezers with microfluidic systems and fluorescence microscopy, opened new possibilities of experimental design. These advances also helped to solve one of the original weaknesses of the method, its difficulties in generating strong magnetic fields. The use of micro-manufactured magnetic poles allows a significant reduction in the separation between the bead and the pole, which helps produce stronger field gradients and stiffer magnetic traps. Thanks to such developments, sub-nanometer resolution has become possible. The method has few limitations. One of them includes difficulties in working with particles that are susceptible to magnetic fields. Among biomolecules, however, the list of such molecules is rather short and consists mostly of proteins associated with metal clusters. Perhaps the biggest limitation is the rather bulky geometry of the magnetic poles, which must be positioned close to the sample. Likewise, carrying beads around using magnetic tweezers remains a challenge and requires a specialized instrument. These limitations, however, are not especially restrictive and only underscore how versatile and powerful the technique truly is. Magnetic tweezers permit measurement of force and displacement generated by single molecules ranging from cells to protein. In particular, for the first time, magnetic tweezers were used to measure mechanical properties of cytoskeleton by Wang, by attaching a specific bead to the cytoskeleton via transmembrane receptors (45).

The irreducible differences between optical and magnetic tweezers concern the type of effort applied to the bead and the number of implicated beads. Magnetic twisting offers the ability to apply much larger force (up to 500 pN) and thus, to probe deeply into the cell, even after focal adhesion have formed. In the magnetic twisting technique, a torque is applied to each bead resulting in a mean bead deviation measured over a large number of beads, bound to a significant cell population. Thus, magnetic tweezers require that tens of thousands of cells be measured simultaneously in order to sense the average bead rotation in response to the application of a magnetic torque. Magnetic twisting technique measures a population average, so it may therefore obscure important behaviours of individual cells. The basic device was modified to measure mechanical properties of individual living cells (46). On the other side, in the optical tweezers technique, a unidirectional force is applied to a unique

attached bead and results in bead translation or rather in a combination of rotation and translation.

1.4.3 Atomic Force Microscopy

The AFM technique is based on detection of forces acting between a sharp probe, known as AFM tip, and the sample surface. The tip is attached to the end of a flexible cantilever. The tip is brought to contact or near-contact with the surface of interest. Forces between the tip and the sample surface cause the cantilever to bend. The deflection of the cantilever is detected optically, while the sample is scanned under the tip. AFM system records the deflection of the cantilever, due to very small forces between the atoms of the probe and the surface, with sub-nanometer precision. To detect the position of the cantilever, most AFM set up uses a laser beam which bounces off the back of the cantilever and onto a Quadrant Photo Detector (QPD). As the cantilever bends, the position of the laser beam on the detector changes (Fig.4). The ratio of the path length between the cantilever and the detector to the length of the cantilever itself produces amplification. As a result, the system can detect sub-Ångstrom vertical movement at the free end of the cantilever, where the tip is located. A map of the substrate surface topography is generated by monitoring these cantilever deflections and visualized on a computer in real-time.

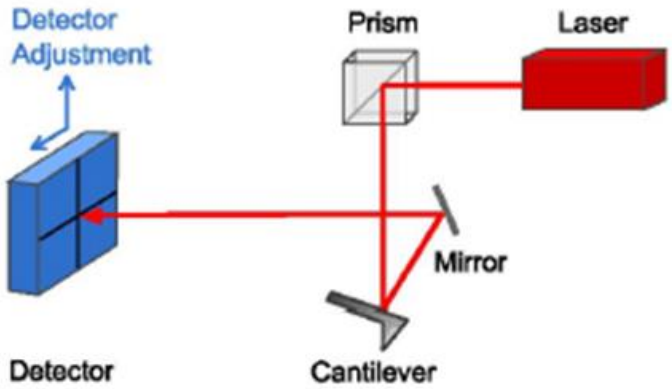

Figure 4 Schematic representation of the detection path of the laser.

AFM is a method widely applied to characterize the micro-scale stiffness for a variety of materials. Over the past few years, AFM has been used to measure the mechanical

properties of soft biological tissues and cells. Nanomechanical analysis of cells is becoming increasingly important in cancer research. Cancer progression has accompanied by alterations in mechanical properties of cells. The technique has revealed differences in stiffness of normal and cancerous cells and can also differentiate cancerous cell from non-malignant and less-differentiated cancer cells (15,47–49). In order to test soft biological samples, like cells, the choice of the indenter shape is crucial and it is recommended to use spherical probes. In this way, a lower pressure is applied to cells and a general impression of such inhomogeneous sample can be achieved.

1.4.4 Particle Tracking Microrheology

Particle tracking microrheology allows to monitor the local viscoelastic properties of living cells with high spatio-temporal resolution. It consists in the injection of microscopic fluorescent beads directly in the cytoplasm of living cells. These beads rapidly disperse through the cytoplasm, undergo to Brownian motions and are subsequently tracked by fluorescent microscopy. Thus, this technique does not apply any external forces, but rather monitors the thermal fluctuations of microscopic probes embedded in the cytoplasm. Videos of beads embedded into the cells are acquired to track their displacements and to describe their trajectories. Once the nanoparticle trajectory has been obtained, to gather information about intracellular structure and mechanics (50), the mean squared displacements (MSDs) are calculated. However, in active systems such as living cells, the MSD of particle motion cannot be directly correlated with rheological parameters, such as creep compliance and dynamic moduli (50). Deduction of rheological parameters from the MSD requires the generalized Stokes-Einstein relation, developed under the assumption of exclusively thermal driving forces; in fact, the generalization also requires the material to be a (hydrodynamic) continuum, homogeneous, isotropic, and incompressible. Driving forces in cells are, however, a combination of thermal fluctuations and active contributions from motor transport and cytoskeleton remodelling, leading to system far from equilibrium. Although the MSD is not enough to fully characterize the complex intracellular microenvironment, it is a good estimator of the mechanics of the

environment investigated by particles: MSDs are higher if probes explored a more deformable regions. Comparison between MSDs of particles introduced in healthy and diseased cells could suggest the difference of deformability of the cytoplasmic environment.

1.5 The PhD Project

The role of the mechanical properties of cells and surrounding ECM is crucial in many biological processes, such as cell growth, migration, division and differentiation. Indeed, the maintenance of the cell mechanical architecture, depending mainly on the cytoskeleton, is fundamental to guarantee the correct functioning of several cellular functions. The malignant transformation induces the alteration of the cytoskeletal structure and determines a variation of cell and ECM mechanical properties. This implicates the modification of their crosstalk and of the biological functions. The strong correlation existing between cell stiffness and cell malignancy allows to use cell mechanical properties as a new powerful biomarker, not only to distinguish malignant from benign cells, but also to discriminate between cancer cells with different aggressive potential. Nevertheless, it is necessary to consider that cells are not isolated systems, but they continuously interact with their surrounding environment. Indeed, cells rearrange their cytoskeleton in response to the biophysical properties of surrounding ECM. These structural modifications induce alterations in the cytoskeletal-generated forces that, in turn, are able to remodel the ECM. The disease advancement causes the loss of this mechanical interplay between cells and extracellular environment. Thus, it is essential to consider in which way the changes of biophysical cues and, in particular, of the mechanical properties of matrix could influence cancer development from genesis to invasion.

In this review chapter an overview of the current knowledge about genetic and mechanical changes of cells and their surroundings due to the malignant transformation is presented. Moreover, the most common tools used to test cell mechanical properties are introduced. In chapter 2, the materials employed and the procedures followed in the experiments are described in detail. The thesis, then, is organized in three more chapters written in form of research articles.

In chapter 3, several parameters, able to characterize the biophysical state of cells, have been considered and compared to discriminate between tumour and healthy cells. The comparison of murine normal and virus-transformed cell lines was developed. In particular, the analysis of these parameters has been useful to understand how virus transformation influences cell physiological processes and cell mechanical properties and, finally, to identify the existent relationship between biological functions and cell mechanics.

In chapter 4, we adopt the tumorous biophysical characterization, developed on single cells in the previous chapter, to human lung cells with different metastatic potential. The distinction of cancer and benign cells and the discrimination of cancer cells with different aggressiveness have been reached combining the analyses of phenotypic characteristics and the characterization of the cell biophysical properties. In particular, the cell elasticity has been identified as a new accurate biomarker of metastatic potential.

Finally, chapter 5 focuses the attention on the crosstalk between cells and their surrounding ECM. Human biopsy tissues, removed from patients affected by lung adenocarcinoma, were analysed. A new technique is presented for the mechanical characterization of cells embedded in 3D matrices. This technique gave us the possibility to perform a mechanical classification of cells and ECM of each sample and a comparison with the healthy equivalent for the entire pool of patients and, thus, to investigate the influence of ECM biophysical properties on cell tumour modifications and evolutions.

In summary, in this study, we have investigated the mechanics of tumour starting from single cell mechanical characterization to the biophysical interplay between cells and their surroundings. Single cell mechanical properties result to be a new label free marker of cancer progression. In fact, we observed that, during malignant transformation, cytoskeleton devolves from a rather ordered and rigid structure to a more irregular and compliant state. These changes in cytoskeletal content and structure reflect in the overall mechanical properties of the cells, that increase their deformability, but also determine enhanced proliferative and migratory capacity and reduced adhesiveness to the substrate. These aspects are considered hallmarks of

cancer and, thus, the study of the single cell mechanical properties should provide information about its biological state.

Nevertheless, the investigation of single cell mechanical properties neglects the ancillary role of the tumour microenvironment in tumorigenesis and cancer progression. In order to study the complex interplay cell-ECM, we analysed *ex vivo* biopsy tissues, with the aim of mechanically phenotyping the tissues at cellular and ECM levels. This double-check mechanical characterization offers new diagnostic markers of the biophysical properties of the cells and ECM and gives new interpretative analytical points relating to the cancer mechanobiology.

1.6 References of Chapter 1

1. Gardel ML, Kasza KE, Brangwynne CP, Liu J, Weitz DA. Chapter 19 Mechanical Response of Cytoskeletal Networks. In: Methods in Cell Biology [Internet]. Elsevier; 2008 [cited 2017 Jan 15]. p. 487–519. Available from: http://linkinghub.elsevier.com/retrieve/pii/S0091679X08006195

2. Ramaekers FC, Bosman FT. The cytoskeleton and disease: The cytoskeleton and disease. J Pathol. 2004 Nov;204(4):351–4.

3. Hall A. The cytoskeleton and cancer. Cancer Metastasis Rev. 2009 Jun;28(1–2):5–14.

4. Fife CM, McCarroll JA, Kavallaris M. Movers and shakers: cell cytoskeleton in cancer metastasis: Cytoskeleton and cancer metastasis. Br J Pharmacol. 2014 Dec;171(24):5507–23.

5. Hanahan D, Weinberg RA. The Hallmarks of Cancer. Cell. 2000 Jan;100(1):57–70.

6. Hanahan D, Weinberg RA. Hallmarks of Cancer: The Next Generation. Cell. 2011 Mar;144(5):646–74.

7. Becker JC, Andersen MH, Schrama D, Thor Straten P. Immune-suppressive properties of the tumor microenvironment. Cancer Immunol Immunother CII. 2013 Jul;62(7):1137–48.

8. Mierke CT. Physical break-down of the classical view on cancer cell invasion and metastasis. Eur J Cell Biol. 2013 Mar;92(3):89–104.

9. Mierke CT. The fundamental role of mechanical properties in the progression of cancer disease and inflammation. Rep Prog Phys. 2014 Jul 1;77(7):76602.

10. Suresh S. Biomechanics and biophysics of cancer cells☆. Acta Mater. 2007 Jul;55(12):3989–4014.

11. Engler AJ, Sen S, Sweeney HL, Discher DE. Matrix Elasticity Directs Stem Cell Lineage Specification. Cell. 2006 Aug;126(4):677–89.

12. Mierke CT. The Biomechanical Properties of 3d Extracellular Matrices and Embedded Cells Regulate the Invasiveness of Cancer Cells. Cell Biochem Biophys. 2011 Nov;61(2):217–36.

13. Elson EL. Cellular Mechanics as an Indicator of Cytoskeletal Structure and Function. Annu Rev Biophys Biophys Chem. 1988 Jun;17(1):397–430.

14. Guck J, Schinkinger S, Lincoln B, Wottawah F, Ebert S, Romeyke M, et al. Optical Deformability as an Inherent Cell Marker for Testing Malignant Transformation and Metastatic Competence. Biophys J. 2005 May;88(5):3689–98.

15. Li QS, Lee GYH, Ong CN, Lim CT. AFM indentation study of breast cancer cells. Biochem Biophys Res Commun. 2008 Oct;374(4):609–13.

16. Kirmizis D. Atomic force microscopy probing in the measurement of cell mechanics. Int J Nanomedicine. 2010 Mar;137.

17. Remmerbach TW, Wottawah F, Dietrich J, Lincoln B, Wittekind C, Guck J. Oral Cancer Diagnosis by Mechanical Phenotyping. Cancer Res. 2009 Feb 10;69(5):1728–32.

18. Cross SE, Jin Y-S, Rao J, Gimzewski JK. Nanomechanical analysis of cells from cancer patients. Nat Nanotechnol. 2007 Dec;2(12):780–3.

19. Swanton C, Burrell RA, Futreal PA. Breast cancer genome heterogeneity: a challenge to personalised medicine? Breast Cancer Res [Internet]. 2011 Feb [cited 2017 Feb 7];13(1). Available from: http://breast-cancer-research.biomedcentral.com/articles/10.1186/bcr2807

20. Schwartz MA. Integrins and Extracellular Matrix in Mechanotransduction. Cold Spring Harb Perspect Biol. 2010 Dec 1;2(12):a005066–a005066.

21. Discher DE. Tissue Cells Feel and Respond to the Stiffness of Their Substrate. Science. 2005 Nov 18;310(5751):1139–43.

22. Erler JT, Weaver VM. Three-dimensional context regulation of metastasis. Clin Exp Metastasis. 2009 Jan;26(1):35–49.

23. Levental KR, Yu H, Kass L, Lakins JN, Egeblad M, Erler JT, et al. Matrix Crosslinking Forces Tumor Progression by Enhancing Integrin Signaling. Cell. 2009 Nov;139(5):891–906.

24. Vader D, Kabla A, Weitz D, Mahadevan L. Strain-Induced Alignment in Collagen Gels. Langowski J, editor. PLoS ONE. 2009 Jun 16;4(6):e5902.

25. Paszek MJ, Zahir N, Johnson KR, Lakins JN, Rozenberg GI, Gefen A, et al. Tensional homeostasis and the malignant phenotype. Cancer Cell. 2005 Sep;8(3):241–54.

26. Yang C-M, Chien C-S, Yao C-C, Hsiao L-D, Huang Y-C, Wu CB. Mechanical Strain Induces Collagenase-3 (MMP-13) Expression in MC3T3-E1 Osteoblastic Cells. J Biol Chem. 2004 May 21;279(21):22158–65.

27. Stein AM, Vader DA, Weitz DA, Sander LM. The micromechanics of three-dimensional collagen-I gels. Complexity. 2011 Mar;16(4):22–8.

28. Schrader J, Gordon-Walker TT, Aucott RL, van Deemter M, Quaas A, Walsh S, et al. Matrix stiffness modulates proliferation, chemotherapeutic response, and dormancy in hepatocellular carcinoma cells. Hepatology. 2011 Apr;53(4):1192–205.

29. Ulrich TA, de Juan Pardo EM, Kumar S. The mechanical rigidity of the extracellular matrix regulates the structure, motility, and proliferation of glioma cells. Cancer Res. 2009 May 15;69(10):4167–74.

30. Pelham RJ, Wang Y l. Cell locomotion and focal adhesions are regulated by substrate flexibility. Proc Natl Acad Sci U S A. 1997 Dec 9;94(25):13661–5.

31. Wells RG. The role of matrix stiffness in regulating cell behavior. Hepatology. 2008 Jan 7;47(4):1394–400.

32. Lin EY, Jones JG, Li P, Zhu L, Whitney KD, Muller WJ, et al. Progression to Malignancy in the Polyoma Middle T Oncoprotein Mouse Breast Cancer Model Provides a Reliable Model for Human Diseases. Am J Pathol. 2003 Nov;163(5):2113–26.

33. Plodinec M, Loparic M, Monnier CA, Obermann EC, Zanetti-Dallenbach R, Oertle P, et al. The nanomechanical signature of breast cancer. Nat Nanotechnol. 2012 Oct 21;7(11):757–65.

34. Thiery JP, Acloque H, Huang RYJ, Nieto MA. Epithelial-Mesenchymal Transitions in Development and Disease. Cell. 2009 Nov;139(5):871–90.

35. Hochmuth RM. Micropipette aspiration of living cells. J Biomech. 2000 Jan;33(1):15–22.

36. Zhou EH, Quek ST, Lim CT. Power-law rheology analysis of cells undergoing micropipette aspiration. Biomech Model Mechanobiol. 2010 Oct;9(5):563–72.

37. Oh M-J, Kuhr F, Byfield F, Levitan I. Micropipette Aspiration of Substrate-attached Cells to Estimate Cell Stiffness. J Vis Exp [Internet]. 2012 Sep 27 [cited 2017 Jan 23];(67). Available from: http://www.jove.com/video/3886/micropipette-aspiration-substrate-attached-cells-to-estimate-cell

38. Zhang H, Liu K-K. Optical tweezers for single cells. J R Soc Interface. 2008 Jul 6;5(24):671–90.

39. Svoboda K, Block SM. Biological Applications of Optical Forces. Annu Rev Biophys Biomol Struct. 1994 Jun;23(1):247–85.

40. Potard US, Butler JP, Wang N. Cytoskeletal mechanics in confluent epithelial cells probed through integrins and E-cadherins. Am J Physiol. 1997 May;272(5 Pt 1):C1654-1663.

41. Choquet D, Felsenfeld DP, Sheetz MP. Extracellular Matrix Rigidity Causes Strengthening of Integrin–Cytoskeleton Linkages. Cell. 1997 Jan;88(1):39–48.

42. Hénon S, Lenormand G, Richert A, Gallet F. A new determination of the shear modulus of the human erythrocyte membrane using optical tweezers. Biophys J. 1999 Feb;76(2):1145–51.

43. Dao M, Lim CT, Suresh S. Mechanics of the human red blood cell deformed by optical tweezers. J Mech Phys Solids. 2003 Nov;51(11–12):2259–80.

44. Guck J, Ananthakrishnan R, Mahmood H, Moon TJ, Cunningham CC, Käs J. The Optical Stretcher: A Novel Laser Tool to Micromanipulate Cells. Biophys J. 2001 Aug;81(2):767–84.

45. Wang, Ning and Butler, James P and Ingber, Donald E and other. Mechanotransduction Across the Cell Surface and Through the Cytoskeleton.pdf. Science; 1993.

46. Alenghat FJ, Fabry B, Tsai KY, Goldmann WH, Ingber DE. Analysis of Cell Mechanics in Single Vinculin-Deficient Cells Using a Magnetic Tweezer. Biochem Biophys Res Commun. 2000 Oct;277(1):93–9.

47. Lekka M, Gil D, Pogoda K, Dulińska-Litewka J, Jach R, Gostek J, et al. Cancer cell detection in tissue sections using AFM. Arch Biochem Biophys. 2012 Feb 15;518(2):151–6.

48. Cross SE, Jin Y-S, Tondre J, Wong R, Rao J, Gimzewski JK. AFM-based analysis of human metastatic cancer cells. Nanotechnology. 2008 Sep 24;19(38):384003.

49. Faria EC, Ma N, Gazi E, Gardner P, Brown M, Clarke NW, et al. Measurement of elastic properties of prostate cancer cells using AFM. The Analyst. 2008;133(11):1498.

50. Gal N, Lechtman-Goldstein D, Weihs D. Particle tracking in living cells: a review of the mean square displacement method and beyond. Rheol Acta. 2013 May;52(5):425–43.

2

MATERIALS AND METHODS

2.1 Polyacrilamide substrate preparation

Polyacrylamide (PAAm) substrates were prepared by mixing acrylamide, methylene-bis-acrylamide, 1/100 total volume of 10% ammonium persulfate and 1/1000 total volume N,N,N',N'-tetramethylethylenediamide (TEMED). Different combinations of acrylamide and bis-acrylamide were used to obtain 0.3 kPa (3 wt/vol% acrylamide and 0.04 wt/vol% bis-acrylamide), 4 kPa (6 wt/vol% acrylamide and 0.06 wt/vol% bis-acrylamide), 13 kPa (10 wt/vol% acrylamide and 0.06 wt/vol% bis-acrylamide), 30 kPa (10 wt/vol% acrylamide and 0.3 wt/vol% bis-acrylamide) hydrogels. To allow for cell adhesion, substrates were functionalized with collagen, by using a bifunctional photolinker, N-sulphosuccinimidyl-6-(4'-azido-2'-nitrophenylamino) hexanoate (sulpho-SANPAH) as a cross-linking agent to immobilize collagen. The freshly prepared sulpho-SANPAH solution at a concentration of 0.2 mg/ml was placed onto PAAm substrates and exposed to UV light for 10 min. After washing with Phosphate Buffer Saline (PBS, Microtech), the hydrogels were coated with 50 µg/ml of bovine type I collagen overnight at room temperature (RT).

The local elasticity of PAAm gels was probed with a commercial AFM (JPK Instruments, Germany) mounted on an epifluorescence microscope (Olympus IX70). Gel stiffness was quantified by indenting each sample at sixty distinct points; the substrate stiffness was defined as the average of six measurements. We used glass sphere cantilevers with a force constant of 0.05 N/m (Novascan, USA). Cantilevers were calibrated by measuring the free fluctuations when unloaded (see 2.3.2.1). To quantify the stiffness, the Hertz model gave the following relation between the indentation δ and the loading force F in the case of an infinitely hard sphere of radius R (AFM tip) touching a soft planar surface:

$$F_{sphere} = \frac{4}{3}\frac{E}{(1-\nu)}\sqrt{R}\,\delta^{\frac{3}{2}}$$

where E is Young's modulus and ν is the Poisson ratio (ν_{PA} = 0.457 (1)) of the soft material.

2.2 Biological parameters

2.2.1 Proliferation

Two proliferation assays were selected to evaluate cell viability and growth. Cells were cultured at a starting concentration and then collected at different time intervals. Cell proliferation was measured by counting cells in Neubauer hemocytometer. We used Gompertz model (2) to fit experimental data and derive for the two cell populations the growth rate parameter *c*:

$$N_{cell}(t) = N_0 e^{b(1-e^{-ct})}$$

Cell proliferation was also evaluated using CellTiter 96® AQueous One Solution Cell Proliferation Assay (Promega), according to the manufacturer's protocol. 24h after seeding, cells were incubated with Cell Titer 96® One Reagent for 90min, absorbance was then read at 490 nm using a plate reading spectrophotometer. Average absorbance from six replicates for each time and treatment was calculated and expressed as fold change of control at 24 h.

2.2.2 Adhesion

To study the cell adhesion to polystyrene, cells were plated on Petri dishes at a starting concentration. After 4 h incubation at 37°C, nonadherent cells were gently washed with phosphate-buffered saline (PBS, EuroClone) and adherent cells were fixed in 4% paraformaldehyde (Sigma-Aldrich) for 20 min and nuclei were counterstained with Hoechst 33342 (Life Technologies). The adherent cells were determined by counting the stained nuclei in a representative unit area (3.6×10^5 mm^2).

2.2.3 Immunofluorescence Labelling

Cells were plated at a starting density on glass dishes (Fluorodish, World Precision Instrument) or PAAm substrates. Cells were fixed and immunostained at 24h from seeding to quantify the focal adhesions (FAs) area and the organization of the actin cytoskeleton and in particular of bundles of actin microfilaments (stress filaments). After washing two times with PBS, cells were fixed in 4% paraformaldehyde (Sigma-

Aldrich) in PBS for 20 min, rinsed twice with PBS and permeabilized in 0.1% Triton X 100 (Sigma-Aldrich) in PBS for 10 min. Cells were washed three times in PBS and blocked for 15 min in 5% bovine serum albumin (BSA, Sigma-Aldrich) in PBS to prevent unspecific binding. Cell were washed two times and then were incubated for 1 h with primary anti-paxillin antibody (Abcam) at 1:300 dilution in PBS-BSA. Then, cells were washed for three more times with PBS and incubated for 1h with secondary antibody, Alexa 488 anti-rabbit (Invitrogen), at 1:500 dilution and Alexa 568 phalloidin (Invitrogen) at 1:200 dilution in PBS-BSA. Finally, cells have been washed three times with PBS-BSA and incubated with DNA-specific fluorescent Hoechts 33342 (Life Technologies) diluted in PBS at 1:10000 for 5 min. Specimens were imaged using an Olympus IX81 inverted microscope and a 10× objective to quantify cell spreading area and cell spindle factor, while a 100× objective to quantify FA area. Fluorescent images were imported into ImageJ software (NIH, Bethesda, MD, USA) for post-processing analysis and quantification of the cell spreading area, cell spindle factor and FA area. To evaluate cell area, images of all single cells were thresholded manually on the basis of the actin stain and then the area of the thresholded cell body was calculated (Fig.1).

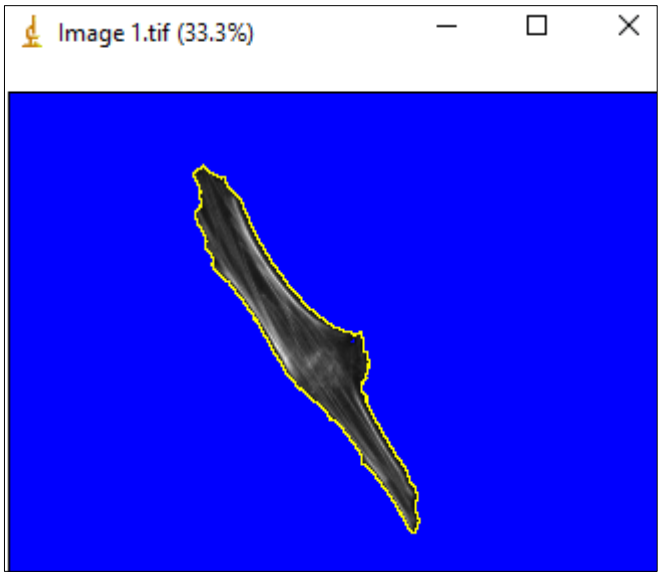

Figure 1 Image of single cell is thresholded manually on the basis of actin stain.

Changes in cell shape were quantified by a spindle factor, defined as $4\pi(\text{area})/(\text{perimeter})^2$, approaching 1 for a rounding and 0 for an elongated cell.

To quantify the focal adhesion average area, the paxillin images were assembled into a stack. First the stack was Gaussian-filtered using a radius of 30 pixels. This stack was then subtracted from the original stack to reduce diffuse background signal. Adhesions were measured by thresholding the stacks and using an ellipse-fitting function in ImageJ. Objects with area ≤0.1 μm^2 were discarded, in order to avoid possible errors due to background noise. Areas of individual focal adhesions were determined for both cell lines.

2.2.4 Migration

Cells were cultured at a starting concentration, then incubated at 37°C and 5% CO_2 for 24h. After incubation, single cell migration experiments were recorded using Olympus IX81 inverted microscope with 10× magnification, equipped with a digital camera (Hamamatsu, ORCA-Flash2.8). Phase contrast images were collected at 5 min intervals for 12 h, to allow the tracking of an average number between 100 and 200 cells. Manual cell tracking was carried out using ImageJ (Fig.2) and the Manual Tracking plugin (http://rsweb.nih.gov/ij/). Speed was calculated by analysing the acquired data with Chemotaxis and Migration Tool plugin (http://www.ibidi.de/applications/ap_chemo.html). To study collective cell migration on glass dishes, the cell wound closure assay was used. Cells were seeded in 35 mm Petri dishes and incubated until confluence. Then, a scratch was made across the monolayer and the wound closure was recorded for 12h, using the equipment previously described. The migration efficiency, expressed in term of percentage of wound closure, was calculated by measuring 3 randomly chosen distances across the wound at 4 different time intervals (0, 4, 8 and 12 h).

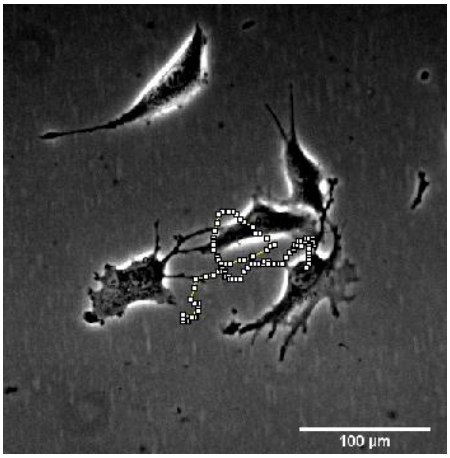

Figure 2 Manual cell tracking carried out using Image J.

2.2.5 Tissue Morphology

A Confocal Leica TCS SP5 II combined with a multi-photon laser source was used to investigate tissue morphology. To prepare the tissues for observation under microscope they have been sliced. Because of the softness of the tissues, they had to be embedded in Optimal Cutting Temperature (OCT, Killik, Bio-Optica). The tissues have been fixed in 4% paraformaldehyde (Sigma-Aldrich) in PBS for 20 min, then rinsed twice with PBS and incubated overnight in 2M sucrose (Sigma-Aldrich) in distilled water. Afterwards the samples have been embedded in OCT, snap frozen in liquid nitrogen, and stored at -80 °C. Next, the samples have been sectioned at a thickness of 10 µm using a Cryostat (Leica CM 1850 UV), then mounted on coverslips and stored in the fridge (-20 °C) until staining. For actin microfilaments and nucleus detections, the samples have been stained with Alexa 568-phalloidin (Life Technologies) and SYTOX Green (Life Technologies), respectively. The samples were permeabilized in 0.3% Triton X 100 (Sigma-Aldrich) in PBS for 5 min and then blocked in 10% BSA for 30 min to block unspecific binding. After blocking, samples have been incubated for 1 h with phalloidin at a 1:200 dilution in PBS-BSA and, finally, with SYTOX Green diluted in PBS at 1:50000 for 10 min. Two-photon excited fluorescence were used to induce second harmonic generation (SHG) and obtain high-resolution images of the unstained collagen structures. Appropriate fluorescence filters were used: 504 nm excitation/523 emission for SYTOX Green, 578/600 for phalloidin. All the samples were imaged by two-photon excited fluorescence at λex =

840 nm to induce SHG of unstained collagen structures by collecting the emission wavelength in the range λem = 420 ± 5 nm.

2.2.6 Tissue immunohistochemical analysis

Basal membrane material was highlighted by immunohistochemical detection of laminin (Novocastra; clone 4C7, diluted 1:50). A standard automated (Dako Autostainer, Glostrup, Denmark) immunoperoxidase procedure was employed, and immunoreactions were shown by a biotin-free dextran-chain detection system (Envision, Dako), and developed using diaminobenzidine as the chromogen.

2.3 Mechanical parameters

2.3.1 Particle tracking microrheology

Particle tracking microrheology, introduced by Tseng et al. (3), allows to monitor the local viscoelastic properties of living cells or extracellular microenvironment with high spatio-temporal resolution, collecting and analysing the Brownian motions of particles embedded in the cytoplasm of cells or ECM, respectively. Measurements are typically conducted using carboxylated polystyrene beads or polyethylene glycol (PEG)-coated beads because they do not interact with subcellular structures. Videos of beads have been acquired to track their displacements. To generate the point tracking trajectories, an *ad hoc* Matlab (Matlab 7) code performed two distinct steps: first, it detected the beads in each frame and, then, it linked the points into trajectories. Each position has been determined by intensity measurements through its centroid, and it has been compared frame by frame to identify the trajectory for each particle, based on the principle that the closest positions in successive frames belonged to the same particle (proximity principle). Once the nanoparticle trajectory was obtained, two parameters could be calculated to gather information about intracellular structure and mechanics (4): MSDs and the radius of gyration (R_g). MSDs were calculated as:

$$< \Delta r^2(\tau) >=< [x(t-\tau) - x(t)]^2 + [y(t-\tau) - y(t)]^2 >$$

where angular brackets mean time average, τ is the time scale and t the elapsed time. The R_g was calculated as the average of the distances between all measured positions in a trajectory :

$$R_g^2 = \frac{1}{2N^2}\sum_{i=1}^{N}\sum_{j=1}^{N}\left(\overrightarrow{R_i} - \overrightarrow{R_j}\right)^2$$

The particles embedded in regions with a thickness similar to or smaller than the particle diameter were excluded from the analysis (cell lamellar regions). In general, local viscoelastic properties of explored regions were extrapolated from MSDs by using the generalized Stokes–Einstein equation where angular brackets meant time average, τ was the time scale and t the elapsed time:

$$G^*(\omega) = \frac{k_B T}{\pi i \omega \Im_u\{< \Delta r^2(\tau) >\}}$$

Being G*(ω) the complex shear modulus, k_B the Boltzmann constant, ω the frequency and $\Im_u$ the unilateral Fourier transform of MSDs (5,6). However, in active systems such as living cells, the MSD of particle motion cannot be directly correlated with rheological parameters, such as creep compliance and dynamic moduli (4). Deduction of rheological parameters from the MSD requires the generalized Stokes-Einstein relation, developed under the assumption of exclusively thermal driving forces; in fact, the generalization also requires the material to be a (hydrodynamic) continuum, homogeneous, isotropic, and incompressible. Driving forces in cells are, however, a combination of thermal fluctuations and active contributions from motor transport and cytoskeleton remodelling, leading to system far from equilibrium. Although the MSD is not enough to fully characterize the complex intracellular and extracellular microenvironment, it is a good estimator of the mechanics of the environment investigated by particles: MSDs are higher if probes explored a more deformable regions. Comparison between MSDs of particles introduced in healthy and diseased cells or tissues could suggest the difference of deformability of the cytoplasmic environment.

2.3.2 Atomic force microscopy

Atomic force microscopy is a relatively novel technique arising out of and a form of Scanning Probe Microscopy (SPM), invented in 1986 (7). This method has been widely applied to investigate morphology or characterize the micro-scale stiffness of a variety of materials ranging from metal surfaces to soft biological tissues and cells. The system is based on detection of forces acting between a sharp probe, known as AFM tip, and the sample's surface. The tip is attached to a very flexible cantilever. The local attractive and repulsive forces between the tip and the sample are converted into a bending, or deflection, of the cantilever. The instrument measures the deflection of the cantilever as it scans. Any motion of the cantilever is detected and converted into an electrical signal, proportional to the cantilever deflection. The detection system uses a laser beam that is reflected from the back of the cantilever onto a detector. A small change in the bending angle of the cantilever is converted to a measurably large deflection in the position of the reflected spot. The position of the laser spot is measured by comparing the signals from different sections of the detector. Most AFMs use a photodiode that is made of four quadrants, so that the laser spot position can be calculated in two directions, by comparing the signals. The vertical deflection (measuring the interaction force) can be calculated by comparing the amount of signals from the "top" and "bottom" halves of the detector. The lateral twisting of the cantilever can also be calculated by comparing the "left" and "right" halves of the detector. The deflection signal is recorded digitally and is visualized on computer in real-time (Fig. 3a). The AFM is best known for its high-resolution imaging capabilities, but it is also a powerful tool for sensitive force measurements. When used in imaging mode, the AFM cantilever is scanned laterally over the surface of the specimen and the force is held constant. In force spectroscopy measurements, the lateral position is set at a fixed point, and the z position of the cantilever is scanned. The force spectroscopy curves plot the cantilever deflection versus the piezoelectric position on the z axis (Fig. 3b). After calibrating the cantilever, the corresponding force can be calculated multiplying the cantilever deflection by the spring constant. AFM is particularly suited for biological applications, because the samples can be analysed in

physiological conditions. High resolution imaging and force spectroscopy measurements are possible in physiological buffer or medium, and over a range of temperatures. Differently from particle tracking microrheology technique, AFM typically probes the cellular surface and not intracellular environment. It is also possible to infer bulk properties with large indentations depth, but interpretation is more difficult. An important advantage is that AFM measurements can be made in liquid and actually *in-situ* during an experiment.

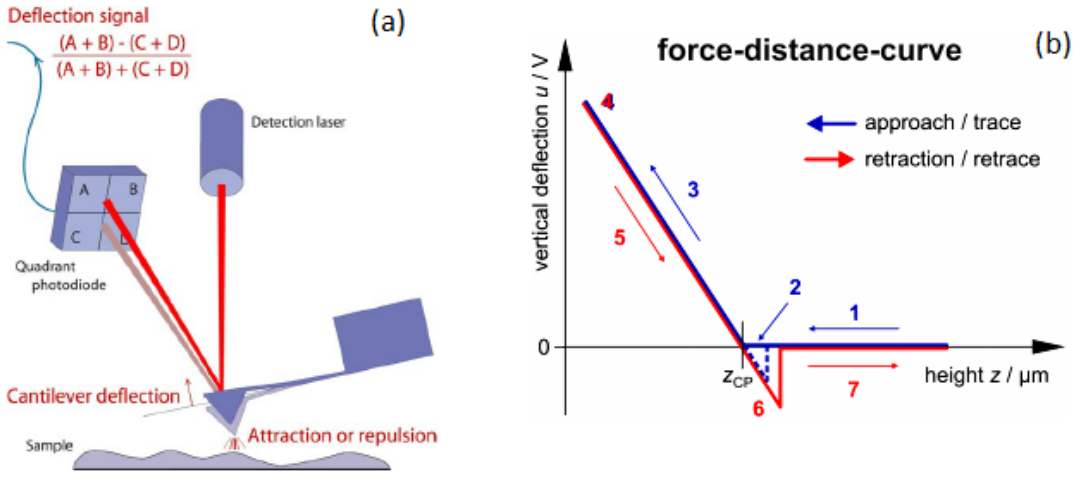

Figure 3 Working principles of AFM. (a) A laser beam was reflected from the back of the cantilever onto a detector. The cantilever deflection, caused by the attractive and repulsive force between the tip and the sample, was detected: the angle of the reflected laser beam changed, and the spot fell on a different part of the photodetector.(b) Working in force spectroscopy the result was the so-called force-distance-curve. Each scan produced two curves: trace and retrace curve. Trace curve: the cantilever was moved down without touching the sample. (1) Very close to the surface the cantilever can be suddenly attracted by the sample due to adhesion forces (e.g. electrostatic interaction), (2). When the cantilever is moved further down, the cantilever is bent upwards in direct proportion to the z-piezo height (3). This characteristic linear slope can be used for calibration of the cantilever. Retrace: As soon as a defined setpoint of deflection is reached (4), the cantilever is withdrawn. The cantilever gets more and more unbent, while moving upwards again (5). Then, the tip usually keeps attracted to the surface by adhesion, which causes the cantilever to bend in the opposite direction, until it suddenly loses contact and flicks up into its initial position (6). Further retraction results no longer in a vertical deflection (7).

2.3.2.1 Calibration of the cantilever deflection

To convert the photodetector signal into a quantitative value of force, the calibration of cantilever deflection is required. The first stage is to calibrate the distance that the cantilever actually deflects for a certain measured change in photodetector voltage. This value depends on the type of cantilever, but also on the optical path of the AFM detection laser, and could be slightly different each time

the cantilever is mounted in the instrument. For this purpose, the sensitivity of the experimental setup was determined first. This is a measurement of the deflection of the tip in nanometres for a given moment of the deflection laser on the photodetector, obtained using a force curve between a plain cantilever tip and a bare hard substrate. The repulsive contact region, where the deflection rises steeply upwards, is linear for a hard surface and tip. Therefore the software could easily determine the factor for converting Volts into nanometres. Once the deflection of cantilever is known as a distance, the spring constant is needed to convert this value into a force, using the Hooke's law. Thanks to the calibration of the spring constant, the vertical deflection signal from the detector could be converted from Volts into Newtons. The approach used to calibrate the spring constant of the AFM cantilever is the thermal noise analysis. This method is based on measuring the thermal fluctuations of the cantilever, and using the equipartition theorem to relate this to the spring constant. Essentially, the thermal energy calculated from the absolute temperature should be equal to the energy measured from the oscillation of the cantilever spring.

2.3.2.2 Determining the elastic modulus of biological samples

AFM is a useful tool to determine the elastic properties of biological samples, like cells. To calculate the parameters of interest various models can be used to fit the force-indentation curve. In the case of spherical indenter the Hertz model is adopted. The Hertz model makes several assumptions to calculate the Young's modulus (E): the sample is approximated as an isotropic and linear elastic solid occupying an infinitely extending half space. Furthermore it is assumed that the indenter is not deformable and that there are no additional interactions between indenter and sample. But most biological materials are neither homogeneous nor absolutely elastic. The energy delivered by the indenter is not completely given back by a cell (as it would be done by an absolute elastic material) but dissipated owing to plastic behaviour that also appeared as hysteresis between the extend and the retract part of the force curve. One time scale describing this behaviour is the viscous relaxation time, which brought variations in force indentation measurements if different indentation velocities are tested (8,9). An appropriate

speed should be applied to reduce the influence of this time-dependent behaviour and to prevent a too high viscous response or reorganization of the cell, respectively caused by too high or too low indentation velocities. Moreover, the Hertz model is valid only for small indentations (up to 5-10% of the height of the cell) where the substrate does not influence the calculations, so the indentation depth has to be optimized. Thus, in spite of some limitation of Hertz model, keeping in mind and considering all these issues is possible to obtain reasonable and reproducible results.

2.3.2.3 AFM setup and experimental approach

Analyses were performed on Nano Wizard AFM system, combined with an optical inverted microscope (Zeiss) that allows the precise lateral positioning of the AFM tip over cells. The choice of the appropriate cantilever depended on the stiffness of the sample. For cells, that are soft and delicate materials, the use of soft cantilever is recommended. Another point to consider is the choice of the indenter shape. For soft biological samples, the use of spherical probes is preferred to sharp pyramidal or conical tip. In fact, using spherical probes the force is applied to a wider sample area than the case if a pyramidal or conic tip was used, which results in a lower pressure. Moreover, spherical probes yielded a general impression for inhomogeneous materials, such as cells or tissues. For these reasons, in the experiments a silicon nitride cantilever, V-shaped, 170 μm long, with a nominal spring constant of 0.07 N/m from BRUKER (MLCT-O10), modified gluing a spherical polystyrene bead of 6 μm diameter, has been used. Bead size was selected to offer a general idea of the inhomogeneous tested area, but at the same time to allow high resolution, to test single cells. The polystyrene bead (Sigma-Aldrich) was glued onto the front of the tipless cantilever using an optical adhesive (NOA63, Norland). This could be easily done by preparing a microscope slide where spheres where deposited on one part and optical adhesive on an adjacent part. Beads were suspended in water, so a drop was put on the slide and dried. The cantilever was first dipped into the glue. To remove excess glue, one or more additional approaches to the surface were performed on a clean glass area. Finally, to attach a sphere, another approach was run with the tip positioned over a sphere

bead. Once the bead was attached, the spherical probe was ready to test cell mechanical properties. To quantify mechanical (Young's modulus) parameters, at least 10 square arrays of 8×8 indentations, covering (1×1) μm^2 areas of cells were performed. Measurements were conducted in cell culture medium supplemented with 12.5 mM Hepes buffer (EuroClone) at 37°C. Cells were indented approximately on cytoplasmic region. The indentation depth was chosen to be 50 nm. The force indentation curves were analysed using Hertz model to obtain the local Young's moduli of each cell. In fact, the Hertz model gives the following relation between the indentation δ and the loading force F in the case of an infinitely hard sphere of radius R (AFM tip) touching a soft planar surface:

$$F_{sphere} = \frac{4}{3} \frac{E}{(1-\nu)} \sqrt{R}\, \delta^{\frac{3}{2}}$$

where the Poisson ratio, ν, is generally set to 0.5 for biological material (incompressible materials like rubber).

2.4 Statistical Analysis

Data are reported as mean ± standard error (SE), unless otherwise indicated. Statistical comparisons were performed with a Student's unpaired test. P values < 0.05 denote statistical significance.

2.5 References of Chapter 2

1. Takigawa T, Morino Y, Urayama K, Masuda T. Poisson's ratio of polyacrylamide (PAAm) gels. Polym Gels Netw. 1996 Jan;4(1):1–5.

2. Gompertz B. On the Nature of the Function Expressive of the Law of Human Mortality, and on a New Mode of Determining the Value of Life Contingencies. Philos Trans R Soc Lond. 1825;115:513–83.

3. Tseng Y, Kole TP, Lee S-HJ, Wirtz D. Local dynamics and viscoelastic properties of cell biological systems. Curr Opin Colloid Interface Sci. 2002 Aug;7(3–4):210–7.

4. Gal N, Lechtman-Goldstein D, Weihs D. Particle tracking in living cells: a review of the mean square displacement method and beyond. Rheol Acta. 2013 May;52(5):425–43.

5. Brangwynne CP, Koenderink GH, MacKintosh FC, Weitz DA. Intracellular transport by active diffusion. Trends Cell Biol. 2009 Sep;19(9):423–7.

6. Hoffman BD, Massiera G, Van Citters KM, Crocker JC. The consensus mechanics of cultured mammalian cells. Proc Natl Acad Sci. 2006 Jul 5;103(27):10259–64.

7. Binnig G, Quate CF, Gerber C. Atomic Force Microscope. Phys Rev Lett. 1986 Mar 3;56(9):930–3.

8. Rosenbluth MJ, Lam WA, Fletcher DA. Force Microscopy of Nonadherent Cells: A Comparison of Leukemia Cell Deformability. Biophys J. 2006 Apr;90(8):2994–3003.

9. Li QS, Lee GYH, Ong CN, Lim CT. AFM indentation study of breast cancer cells. Biochem Biophys Res Commun. 2008 Oct;374(4):609–13.

3

BIOPHYSICAL CHARACTERIZATION OF HEALTHY AND TUMOUR FIBROBLAST

3.1 Introduction

Cancer has long been one of the leading causes of death worldwide and is presently responsible for about 25% of all deaths. Oncogenic transformation is driven by both intrinsic genomic changes in the constituent tumour cells and the integrated response of the tissue or organ to extrinsic cues, such as growth factors, cytokines, and chemotactic stimuli. Cancer transformation leads to a distinct phenotype of cancerous cells in several aspects, such as variations in cellular growth, differentiation and interactions with neighbouring cells and/or the ECM (1,2). In cell monolayer culture, transformed cells do not exhibit the contact inhibition that normally arrests the proliferation of healthy cells when they come in contact. Transformed cells are not anchorage-dependent, while normal cells require attachment to a solid substrate. Unlike normal cells, cancer cells lose the ability to "self-destruct", a process known as apoptosis, a form of programmed cell death. Genetic transformation caused also aberrant migration of cancer cells and over the past few years, dysregulated cell motility has been recognized as a key step in tumour invasion and metastasis (3,4). During these cell functions the cytoskeletal network is dynamically remodelled and the maintenance of the cytoskeletal architecture is essential for the correct functioning of cellular processes. Therefore, alterations to the cell functions, due to biochemical processes, are connected to the variation in the cytoskeleton dynamics, that significantly alter the mechanical properties of cancer cells (5). For this reason, biomechanics of cancer cells, in particular cell stiffness, has been identified as an important factor relating to cancer cell function, adherence, motility, transformation and invasion. During cancer progression, the cytoskeleton devolves from a rather ordered and rigid structure to a more irregular and compliant state. These changes are commonly related to either a partial loss of actin filaments (3) or disorganization of microtubules (6) being in fact the consequence of lower density of the cellular scaffold.

Part of this chapter is included in the paper "*X-rays effects on cytoskeleton mechanics of healthy and tumor cells.*", Panzetta V., De Menna M., Musella I., Pugliese M., Quarto M., Netti P. A., & Fusco S., published on Cytoskeleton (2016); and in "*Effects of High Energy X-rays on Cell Morphology and Functions*", Panzetta V, Musella I., Pugliese M., Piccolo C, Pasqua G., Netti P.A. and. Fusco S., published on Bioengineering (ENBENG)(2017).

The reduced cytoskeletal strength and decreased organization allow cancer cells to infiltrate and invade tissues, and migrate to distant sites. Malignant cells, in fact, are marked by replication and motility, both of which are inconsistent with a rigid cytoskeleton. Alterations in cytoskeletal content and structure are reflected in the overall mechanical properties of the cell. Consequently, measurements of cytoskeleton rigidity provide information about cell state and composition and may be viewed as a new biomarker of cancer progression (5,7,8) Since the malignant transformation determines an altered behaviour of cancer cells, several cell biophysical parameters can be identified to discriminate between healthy and tumour cells. Among these, the cellular mechanical properties has been studied for a long time using various techniques, such as micropipette aspiration, microfluidic systems, optical tweezers, atomic force microscopy, in order to discriminate healthy from cancer cells (9–12). *In vitro* studies, performed by using different techniques, showed the larger deformability of tumour cells for various cancers, such as bladder, prostate, thyroid and ovarian ones (10,13–19).

This work has focused the attention on the biophysical characterization of Simian virus 40 transformed BALB/c 3T3 (SVT2) cells and their normal counterpart BALB/c 3T3 fibroblasts. The aim of this study was to identify several cell biophysical parameters to discriminate between tumour and healthy behaviour. These parameters help to understand how virus transformation could influence cell physiological processes and cell mechanical properties and, finally, to identify the existence of a relationship between biological functions and cell mechanics. Thus, first, we investigated the influence of virus transformation on peculiar cell functions, then its effect on cell mechanics. We identified some biophysical parameters, such as cell proliferation, adhesion at cell and focal adhesion level, cell migration, and we used them to predict cell malignancy and distinguish normal from transformed cells. PTM and AFM techniques were used to compare the mechanical properties of murine normal and virus-transformed cell lines cultured on glass. Results show that the consequences of Sv40 induced-transformation are the intensification of cell proliferation, the enhanced capability of transformed cells to migrate, the reduced adhesion capability, the reduction of cell cytoskeletal

organization and the increased cell deformability. Finally, considering the key role of extracellular matrix in cancer, we investigated in which way normal and transformed fibroblasts modulate their biophysical properties and in particular their cytoskeletal organization in response to substrate rigidity, by using PAAm gels of various stiffness.

3.2 Materials and Methods

3.2.1 Polyacrylamide substrate preparation and mechanical characterization

PAAm substrates were prepared by mixing different combination of acrylamide and methylene-bis-acrylamide, as described in Section 2.1, to obtain 0.3 kPa, 4 kPa, 30 kPa hydrogels. To allow for cell adhesion, substrates were functionalized with collagen, by using a bifunctional photolinker, sulpho-SANPAH.

3.2.2 Cell culture

Experiments were performed on murine fibroblast BALB/c 3T3 and SVT2 cells, as a model of normal and tumour cell lines, respectively. Cell lines were cultured at 37°C in 5% CO_2 in Dulbecco's modified Eagle's medium (Euroclone Ltd., UK) supplemented with 10% fetal bovine serum (FBS, BioWhatter, MD), 2 mM L-glutamine (Sigma, St. Louis, MO), 1000 U/L penicillin (Sigma, St. Louis, MO), and 100 mg/L streptomycin (Sigma, St. Louis, MO).

3.2.3 Cell proliferation and adhesion

To evaluate cell viability and growth, BALB/c 3T3 and SVT2 were cultured at a starting concentration of 200 cells/cm^2 and then collected at different time intervals (0, 1, 3, 6 days). Fibroblast cell proliferation was evaluated using two assays, described in detail in Section 2.2.1.

To study the cell adhesion to polystyrene, 2×10^4 cells were washed, trypsinised and plated on 35-mm Petri dishes. The adherent cells were determined following the procedure in 2.2.2.

3.2.4 Immunofluorescence labelling

Cells were fixed and immunostained at 24h from seeding to quantify the FAs area and the organization of the actin cytoskeleton and in particular of bundles of actin microfilaments (stress filaments). To quantify changes in cell shape, we calculated the spindle factor, previously defined in 2.2.3.

3.2.5 Cell migration

BALB/c 3T3 and SVT2 were respectively cultured at a concentration of 1000 cells/cm^2 and 2000 cells/cm^2, then incubated at 37°C and 5% CO_2 for 24h. After incubation, cell migration experiments were recorded using the equipment described in Section 2.2.4. Cells were manually tracked using Image J.

3.2.6 Particle tracking microrheology

BALB/c3T3 and SVT2 cells were cultured in 35 mm dishes (Corning Incorporated) until confluence. Carboxyl-modified fluorescent polystyrene particles (0.500 μm diameter, Invitrogen, Molecular Probes) were introduced into the cytoplasm of cells through ballistic injection. Once bombarded, cells were washed extensively in order to prevent the nanoparticles that do not penetrate the cytoplasm from entering the cells via endocytosis. The cells were allowed to recover for 24 h, before re-plating. After incubation, videos of beads embedded into the cells were recorded for a total of 5 sec at 100 fps to track their displacements. Once the nanoparticle trajectory was obtained, the MSDs and the R_g were calculated to gather information about intracellular structure and mechanics (see Section 2.3.1).

3.2.7 Atomic force microscopy

To quantify mechanical (Young's modulus) parameters, cells (2000/cm^2) were cultured on 23 mm Fluorodish (WPI), incubated at 37°C and tested 24h after seeding. For each cell line, we selected 20 cells and (1×1) μm^2 area of each cell was indented. At least 10 square arrays of 8×8 indentations were performed. Measurements were conducted in cell culture medium supplemented with 12.5 mM Hepes buffer (EuroClone) at 37°C. Cells were indented approximately on

cytoplasmic region. The indentation depth was chosen to be 50 nm. The force indentation curves were analysed using Hertz model to obtain the local Young's moduli of each cell (see Section 2.3.2).

3.2.8 Statistical Analysis

Data are reported as mean ± standard error (SE), unless otherwise indicated. Statistical comparisons were performed with a Student's unpaired test. P values < 0.05 denote statistical significance.

3.3 Results

3.3.1 Cell proliferation and adhesion

Proliferation of BALB/c 3T3 and SVT2 was determined by directly counting cells at 1, 3 and 6 days from seeding and by using CellTiter 96® AQueous One Solution. Both testes indicated that the proliferative capacity of transformed cells was significantly higher than those of BALB/c 3T3 (Fig.1), as already observed (20). By fitting experimental data with Gompertz model, previously described in the *Materials and Methods* section, we found that the growth rate value for SVT2 cells was about 50% higher than those of BALB/c 3T3 (Table 1).

Adhesion experiments were performed to evaluate the adhesive capacity of normal and transformed cells. Adhesiveness of SVT2 cells was significantly lower than BALB/c 3T3 (Fig.2), as has already been observed for many malignant cells both in tissues (21) and on tissue culture substrates (22,23).

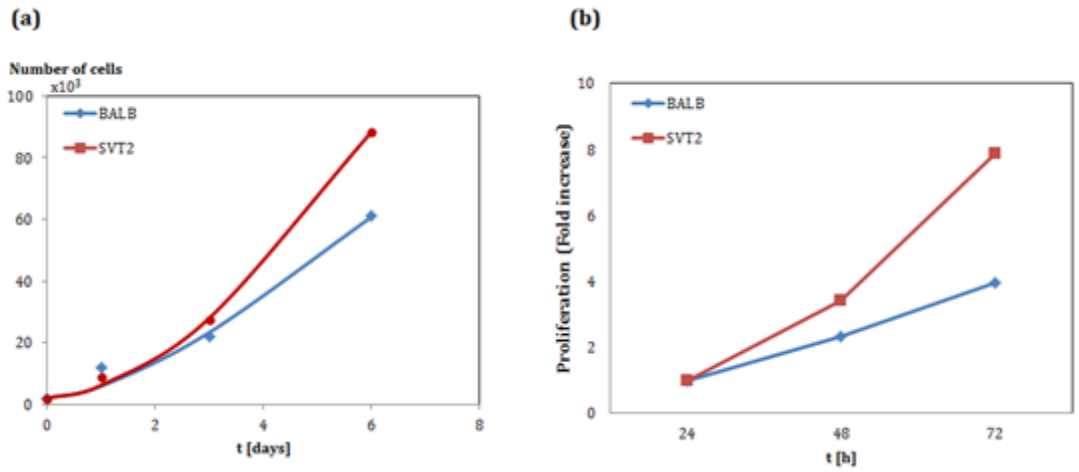

Figure 1(a) Growth curve of BALB c/3T3 (blue) and SVT2 (red) cell lines, derived by fitting experimental data (dot points at three different investigated times) with Gompertz model; (b)Proliferation curves obtained by CellTiter 96® AQueous One Solution assay. Values represent the mean of six replicates ±SD.

	Growth Rate [Ncellh^{-1}]
BALB/c 3T3	4.9
SVT2	7.2

Table 1 Values of growth rate [$N_{cell}h^{-1}$] derived by fitting experimental data with Gompertz model for both cell lines in all investigated conditions.

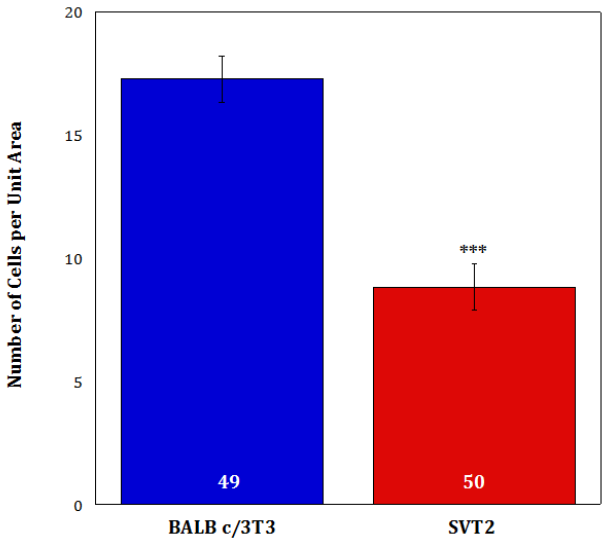

Figure 2 BALB/c 3T3 and SVT2 cell adhesion to polystryrene dishes. Bars represent the mean of number of adhering cells per unit area ± SEM and the number of cells analysed is indicated in the bars. Data presented are pooled means of, at least, 46 images. ***P < 0.001 as compared with normal cells.

3.3.2 Cell morphological changes and FA size

Using fluorescent microscopy, we examined the morphology and cytoskeletal organization of cells. In particular, we analysed cell spreading as the initial kinetic process that follows adhesion events once the cell touches the substrate. It represents a good prototype of simplifying the cell-substrate interactions. Starting from cell spreading area, we evaluated the spindle-shape factor, a parameter which gives indirect information about the typical organization of the CSK of fibroblasts into elongated filament bundles (stress fibres) parallel to the polarization direction. Figure 3 shows morphology and cytoskeleton of BALB/c 3T3 and SVT2 cells. BALB/c 3T3 cells exhibits elongated cell bodies, high spreading and well organized actin cytoskeleton compared to SVT2 cells, which presents a round morphology, low spreading areas and less structured cytoskeleton. In terms of spindle factor, from the normal to the transformed cells, a significant increase of the spindle-factor ($p<0.001$) was observed (Fig.3c), due to the enhanced spreading area.

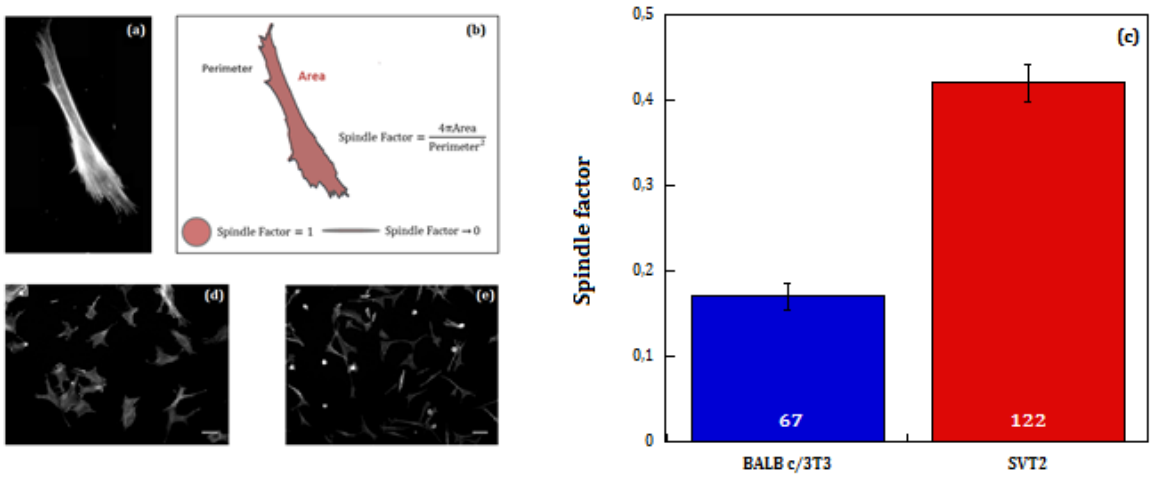

Figure 3(a)Representative image of cell morphology. (b) Schematic representation of the morphological descriptor, spindle shape factor, which was used in this study. (c) The spindle factor data were presented as mean ± SEM and the number of cells analysed is indicated in the bars. $P < 0.001$ as compared with normal cells. (d-e)The morphology and cytoskeleton in BALB/c 3T3 and SVT2 cells were compared. Scale bar, 50 μm.

We also examined the area of single FA, that typically increases in the direction of their associated stress fibres through a process driven by actomyosin-mediated

tension. SVT2 cells showed significantly smaller focal adhesion areas compared to BALB/c 3T3 (Fig.4).

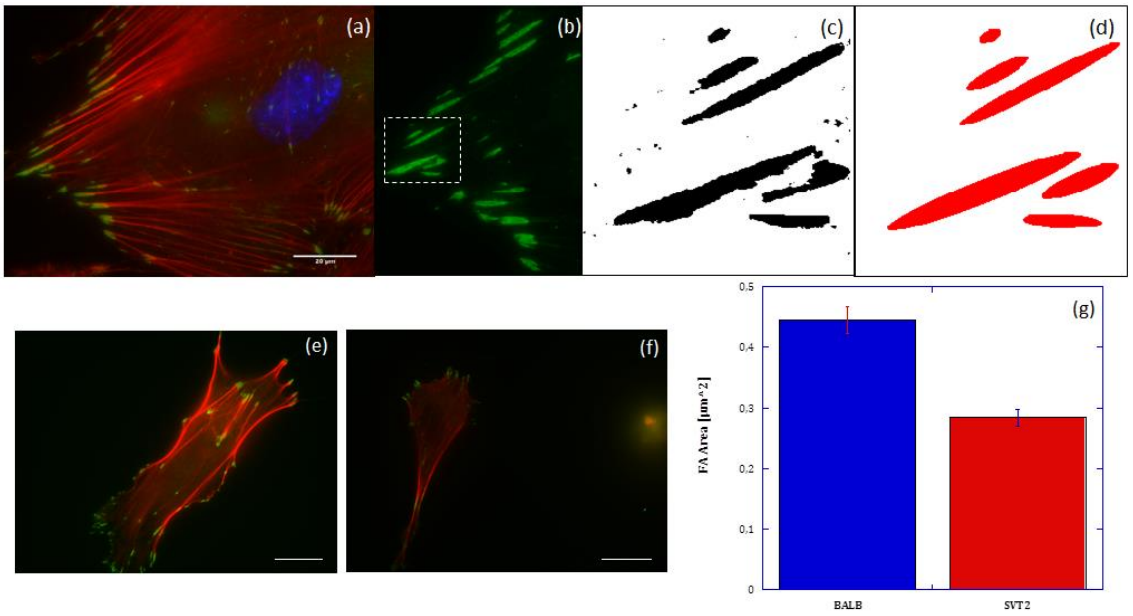

Figure 4 BALB/c 3T3 and SVT2 cells were fixed and stained with phalloidin (red, actin) and immunostained to detect paxillin (green, FAs). Representative images of the organization of actin filaments (a) and FAs (b) of BALB/c 3T3 cell, binary image of FAs obtained by thresholding methods (c), best-fit ellipses of FAs (d). Representative images of actin filaments and FAs (e-f). Data related to FA areas are presented as mean ± SEM and the number of FAs analysed is indicated in the bars. P<0.001 as compared with normal cells. Scale bar, 10 μm.

To investigate the influence of substrate stiffness on cell behaviours, we chose artificial substrates of polyacrylamide functionalized at the surface with collagen I (see Section 2.1). In Figure 5, the dependence of cell spreading on substrate stiffness is presented. Both normal and transformed cells exhibit a significant increase in cell spreading on 30 kPa gels, compared to 0.3 kPa gels. Independently from gel stiffness, BALB/c 3T3 continues to present wider area than SVT2 cells (Fig 5a).

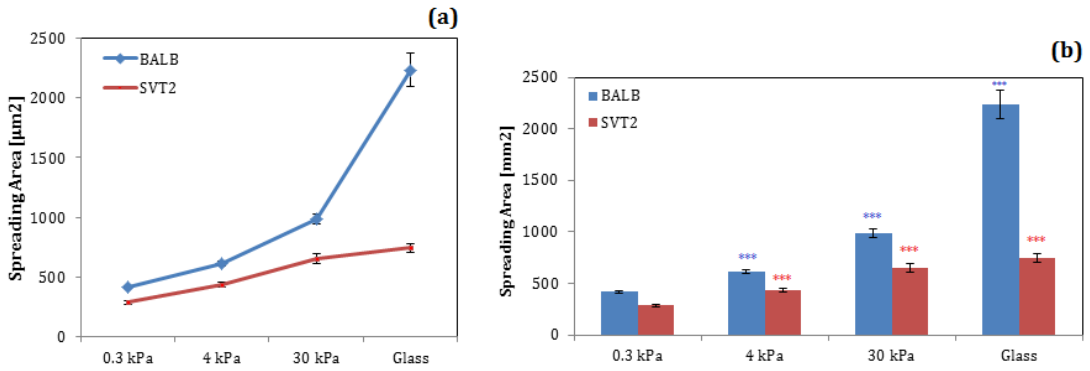

Figure 5 The dependence of spreading of BALB c/3T3 and SVT2 cells on substrates stiffness.(a) SVT2 cells show wider spreading, independently from gel stiffness. (b)The spreading data on glass and polyacrylamide substrates were presented as mean ±S.E.M. Statistical difference are shown as ***P<0.001 by Student's t test, as compared to 0.3 kPa.

3.3.3 Cell migration

Cell migration could be considered a fundamental parameter to describe the pathological condition of cells. Aberrant regulation of cell migration drives progression of cancer, invasion and metastasis (4,24). As expected, quantitative time-lapse videomicroscopy analysis revealed random motility speeds of transformed cells were significantly increased (0.76±0.41 µm/min), compared to speeds of BALB/c 3T3 (0.35±0.18 µm/min). The migration rate of single cells is shown in Fig.6.

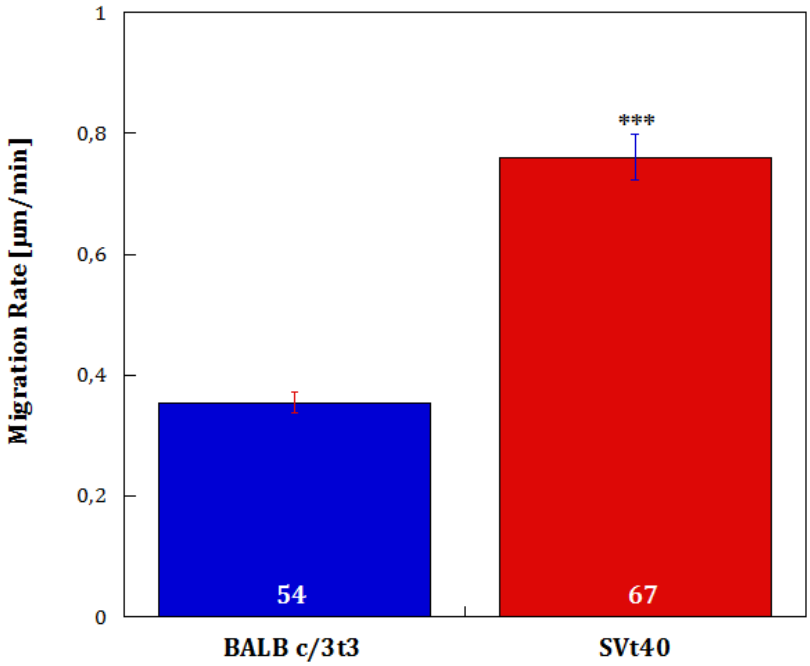

Figure 6 BALB c/3T3 and SVT2 cell migration. Sv40 transformation induced a significantly (***P<0.001 by Student's t test)increase in migration rate. Results were presented as mean ±S.E.M and the number of cells analysed was indicated in the bars.

3.3.4 Cell mechanics

Particle tracking microrheology and atomic force microscopy were performed to probe the mechanical properties of individual living cells.

With PTM we calculated the MSD of nanoprobes embedded in cell. They provides information about the motion of particles in cytoplasm and, indirectly, about the mechanics of the cell microenvironment. Then, we compared the MSDs of normal and tumour fibroblasts. Figure 7 shows the cumulative distribution functions in the two cell lines, for two different parameters: we measured the R_g (Fig. 7a), that is an averaged measure of the particle trajectory size and the distance travelled by the MSD at τ = 1 s (Fig. 7b). The two analyses showed similar results: a lognormal distribution of particle displacements in both cells, with higher values in transformed cells. In particular, the radii of gyration in transformed SVT2 cells were significantly higher than in BALB/c 3T3, indicating that the particles move further, according with the higher MSD amplitude.

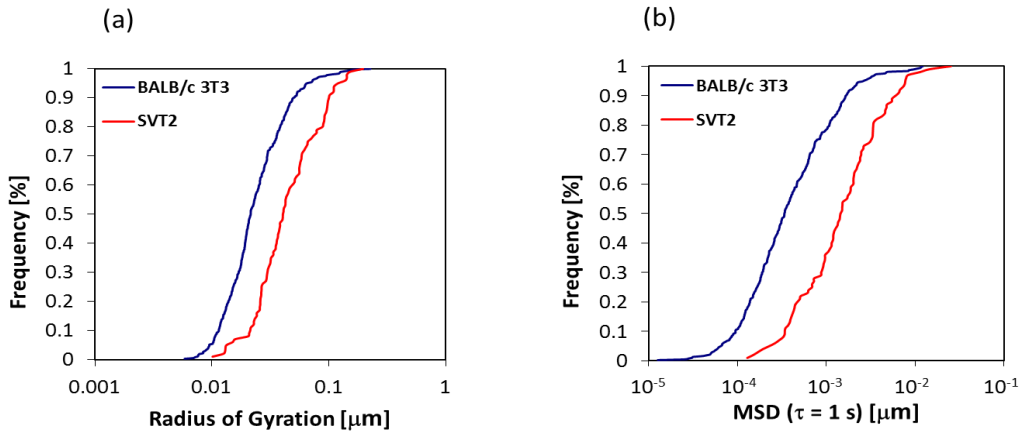

Figure 7 Cumulative distribution functions of BALB/c3T3 (blue curve) and SVT2 (red curve) cells by calculation of the radius of gyration (a) and MSD (τ=1 s) (b).

The reduced stiffness of the transformed cell line was also confirmed by AFM. Cells (2000/cm^2) were cultured on 23 mm Fluorodish (WPI), incubated at 37°C and tested 24h after seeding. For each cell line, we selected 20 cells and (1×1) μm^2 area of each cell was indented. Figure 8 shows the average values of the Young's modulus of normal BALB/c 3T3 and transformed cells, obtained using Hertz's contact model. The average stiffness (mean±s.d.) of normal cell was found to be 2.3±3.2 kPa, significantly higher than transformed cells (1.1±1.1 kPa). Thus, SVT2 exhibited a Young's modulus approximatively 0.5 times lower than normal BALB/c 3T3.

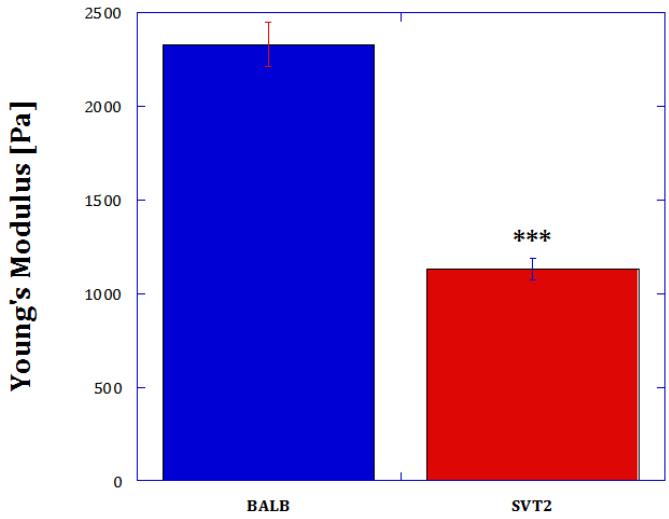

Figure 8 Apparent Young's modulus for BALB c/3T3 (E=2.3±0.084 kPa) and SVT2 (E=1.1±0.029 kPa) cells. Results were presented as mean ±S.E.M. Student's t test was applied to measure statistical differences. ***P<0.001 as compared to normal cells.

3.4 Discussion and conclusions

A large number of pathologies are associated to cytoskeletal and nucleoskeletal proteins alterations: cancer (25,26), cardiovascular disease syndromes (27,28), neurodegenerative diseases (29), lung injury (30) and others. In particular, cancer metastasis is a process connected to the capability of malignant cells to change their shape and increase their deformability, to lose their interaction with other cells and ECM and thus, to enhance their ability to move and invade adjacent tissues and migrate towards distant sites. Indeed during this process, changes in cytoskeletal networks and cell–cell/cell-ECM interactions have a key role and the mechanical properties and deformability of cancer cells are of paramount importance (25). Several works demonstrated that the aggressive phenotype of cancer cells is correlated with alterations of adhesion receptors and CSK architecture, deregulation of CSK dynamics mediators and changes in migratory properties (31,32). All these alterations result in variations of cell mechanical characteristics: as cancer cells become more aggressive and invasive, they present decreased cell stiffness. In this context, stiffness is not only a predictor of invasive potential, but it can be used also as a gauge of effectiveness of anti-cancer treatments.

For these reasons, we have characterized some of the peculiar cell functions (i.e., proliferation, adhesion, migration) in terms of cytoskeleton organization of highly aggressive murine tumour cells (SVT2) and their normal counterpart (BALB/c 3T3). We studied the direct effects of Sv40-induced transformation on the cytoskeleton structure of BALB/c 3T3 cells, by evaluating CSK mechanics and its direct crosstalk with adhesion substrate via FAs. We showed that the malignancy of transformed cell line, SVT2, was associated with significantly increase of proliferative capacity, profound reduction in cell-substrate adhesions and with impaired organization of the actin bundles, high motility and reduced cell mechanical properties. It is, nevertheless, that the reduced adhesiveness of tumour cells activates metastatic process, by allowing the malignant cells to detach for the primary tumour, and to reach distal tissues via the lymphatics and bloodstream (33).

As already stated, the malignant phenotype of SVT2 cells was associated with weak and altered expression of FA proteins. Some studies provided evidence that a reduction in cytoskeletal proteins such as actin, tropomyosin and vinculin, was often a key feature of cell transformation(34). The smaller size of FAs we observed in transformed cells was probably responsible for the modest adhesiveness to the culture dish (Fig.2), but also for the SVT2 abilities to grow in suspension in a semisolid medium (35) and the loss of adhesion-dependent growth control (36). Indeed, the decrease in paxillin level stimulated the disassembly of stable FAs, as demonstrated by the reduced dimensions of FAs in SVT2 cells, shifting the dynamic equilibrium between soluble and assembled FA proteins.

The reduction of FAs size in transformed cells was strictly correlated to the cell morphological variations: it was demonstrated that in fibroblasts FAs grown in the direction of major cell-axis, were co-aligned with stress fibres and governed cell polarization, giving the cell its typical elongated shape (37). The reduction of FA dimensions in SVT2 cells was associated with an alteration of the CSK protein expression and organization (38). The direct consequence of this dysregulation was a profound reduction in cell-substrate adhesion and a round cellular morphology (39). BALB/c 3T3 were characterized by high spreading, elongated cell bodies with extended processes which gave cells the spindle-like shape, well organized cell cytoskeleton that were completely lost due to Sv40-induced transformation (Fig.3). As previously reported, we found a strong correlation between cell adhesion, FAs assembly, actin-CSK architecture and cell mechanical properties (38).

We used PTM to evaluate the intracellular mechanics of BALB/c3T3 and SVT2 cells, measuring MSDs and radii of gyration of tracked beads. The presence of CSK non-thermal driving forces did not allow us to derive viscoelastic moduli, nevertheless MSD amplitude was shown to be inversely related to intracellular stiffness (40). Working on that principle, we performed PTM experiments, that revealed changes in the internal mechanism and activity of transformed cells. Our results show how MSDs and radii of gyration in SVT2 cells were sensitively higher than in BALB/c 3T3 cells, due to a less dense and more active cytoskeletal network. These results suggested that the tumorigenicity of cells was probably correlated

with a decrease in stiffness and structural density and an increase in intracellular activity.

The architectural changes concerning transformed cells were confirmed by AFM. Using AFM, we measured the local stiffness of BALB/c 3T3 and SVT2 cells and we found that mechanical properties of transformed cells were decreased of 100%, compared with normal cells. These results suggest that when adhesion and CSK structure are compromised (decreased cell spreading area, reduced actin polymerization and focal adhesions), SVT2 cells result softer and more able to deform, increase motility and invade other tissues (41). Thus, the primary consequence of Sv40-induced transformation was the increase of aggressiveness of normal cells.

PTM and AFM explored two regions of the same system. Particle tracking localized mechanical measurements inside the cytoplasm of living cells. Tracer particles embedded in cells were subjected to the combined action of thermal fluctuations and active contributions from cytoskeleton remodelling and myosin-actin generated forces. AFM examined the combined local elastic response due to cell membrane and subcortical actin network. Combining AFM with fluorescent microscopy, the regional cell mechanics can be correlate with underlying cytoskeletal components (42–44).

Results from PTM and AFM could not be compared, because they tested different regions of cells. Nevertheless, both techniques came to the conclusion that, in case of malignancy, cell mechanical properties were drastically reduced.

Finally, we considered that biological properties of tumour cells including growth, morphology and migratory properties can be modulated by the rigidity of ECM. Previously studies (45) concluded that cancer cells can be classified in two categories: “rigidity independent” lines, whose behaviour does not change across a tested spectrum of matrix stiffness and “rigidity dependent” lines, which exhibit increasing cell growth as extracellular rigidity increased. We investigated the ability of transformed and normal cells to spread on gel substrates of different stiffness. Our results show that SVT2 cells appear “rigidity dependent”, because

they exhibited significant increases in cell spreading and substrate adhesiveness on stiffer gels.

To conclude, we presented a single-cell biophysical characterization to discriminate benign from malignant cells. To this aim, we have identified several cell biophysical parameters for the screening of cancer. We found that the main features of malignant phenotype are increased cell proliferation, reduced cell adhesion to substrate, altered cellular morphology, enhanced migration capacity and lower cell mechanical properties. In particular, we found that single cell mechanics characterization is a quick and efficient marker of cell malignancy and may become a powerful support for cancer diagnosis.

3.5 References of Chapter 3

1. Hanahan D, Weinberg RA. Hallmarks of Cancer: The Next Generation. Cell. 2011 Mar;144(5):646–74.

2. Jinka R, Kapoor R, Sistla PG, Raj TA, Pande G. Alterations in Cell-Extracellular Matrix Interactions during Progression of Cancers. Int J Cell Biol. 2012;2012:1–8.

3. Yamaguchi H, Condeelis J. Regulation of the actin cytoskeleton in cancer cell migration and invasion. Biochim Biophys Acta BBA - Mol Cell Res. 2007 May;1773(5):642–52.

4. Yamaguchi H, Wyckoff J, Condeelis J. Cell migration in tumors. Curr Opin Cell Biol. 2005 Oct;17(5):559–64.

5. Suresh S. Biomechanics and biophysics of cancer cells☆. Acta Mater. 2007 Jul;55(12):3989–4014.

6. Pachenari M, Seyedpour SM, Janmaleki M, Shayan SB, Taranejoo S, Hosseinkhani H. Mechanical properties of cancer cytoskeleton depend on actin filaments to microtubules content: Investigating different grades of colon cancer cell lines. J Biomech. 2014 Jan;47(2):373–9.

7. Brunner C, Niendorf A, Käs JA. Passive and active single-cell biomechanics: a new perspective in cancer diagnosis. Soft Matter. 2009;5(11):2171.

8. Lee GYH, Lim CT. Biomechanics approaches to studying human diseases. Trends Biotechnol. 2007 Mar;25(3):111–8.

9. Guo Q, Park S, Ma H. Microfluidic micropipette aspiration for measuring the deformability of single cells. Lab Chip. 2012;12(15):2687.

10. Guck J, Schinkinger S, Lincoln B, Wottawah F, Ebert S, Romeyke M, et al. Optical Deformability as an Inherent Cell Marker for Testing Malignant Transformation and Metastatic Competence. Biophys J. 2005 May;88(5):3689–98.

11. Rosenbluth MJ, Lam WA, Fletcher DA. Force Microscopy of Nonadherent Cells: A Comparison of Leukemia Cell Deformability. Biophys J. 2006 Apr;90(8):2994–3003.

12. Zhang H, Liu K-K. Optical tweezers for single cells. J R Soc Interface. 2008 Jul 6;5(24):671–90.

13. Lekka M, Laidler P, Gil D, Lekki J, Stachura Z, Hrynkiewicz AZ. Elasticity of normal and cancerous human bladder cells studied by scanning force microscopy. Eur Biophys J. 1999 May 25;28(4):312–6.

14. Faria EC, Ma N, Gazi E, Gardner P, Brown M, Clarke NW, et al. Measurement of elastic properties of prostate cancer cells using AFM. The Analyst. 2008;133(11):1498.

15. Xu W, Mezencev R, Kim B, Wang L, McDonald J, Sulchek T. Cell Stiffness Is a Biomarker of the Metastatic Potential of Ovarian Cancer Cells. Batra SK, editor. PLoS ONE. 2012 Oct 4;7(10):e46609.

16. Lekka M, Pogoda K, Gostek J, Klymenko O, Prauzner-Bechcicki S, Wiltowska-Zuber J, et al. Cancer cell recognition – Mechanical phenotype. Micron. 2012 Dec;43(12):1259–66.

17. Prabhune M, Belge G, Dotzauer A, Bullerdiek J, Radmacher M. Comparison of mechanical properties of normal and malignant thyroid cells. Micron. 2012 Dec;43(12):1267–72.

18. Li QS, Lee GYH, Ong CN, Lim CT. AFM indentation study of breast cancer cells. Biochem Biophys Res Commun. 2008 Oct;374(4):609–13.

19. Rebelo LM, de Sousa JS, Mendes Filho J, Radmacher M. Comparison of the viscoelastic properties of cells from different kidney cancer phenotypes measured with atomic force microscopy. Nanotechnology. 2013 Feb 8;24(5):55102.

20. Carrino D, Gershman H. Division of BALB/c mouse 3T3 and simian virus 40-transformed 3T3 cells in cellular aggregates. Proc Natl Acad Sci U S A. 1977 Sep;74(9):3874–8.

21. McCutcheon M, Coman DR, Moore FB. Studies on invasiveness of cancer. Adhesiveness of malignant cells in various human adenocarcinomas. Cancer. 1948 Sep;1(3):460–7.

22. Franks LM, Henzell S. The development of 'spontaneous' neoplastic transformation in vitro of cells from young and old mice. Eur J Cancer 1965. 1970 Oct;6(5):357–64.

23. Weber MJ, Hale AH, Losasso L. Decreased adherence to the substrate in Rous sarcoma virus-transformed chicken embryo fibroblasts. Cell. 1977 Jan;10(1):45–51.

24. Sahai E. Mechanisms of cancer cell invasion. Curr Opin Genet Dev. 2005 Feb;15(1):87–96.

25. Suresh S, Spatz J, Mills JP, Micoulet A, Dao M, Lim CT, et al. Connections between single-cell biomechanics and human disease states: gastrointestinal cancer and malaria. Acta Biomater. 2005 Jan;1(1):15–30.

26. Raz A, Geiger B. Altered organization of cell-substrate contacts and membrane-associated cytoskeleton in tumor cell variants exhibiting different metastatic capabilities. Cancer Res. 1982 Dec;42(12):5183–90.

27. Hein S. The role of the cytoskeleton in heart failure. Cardiovasc Res. 2000 Jan 14;45(2):273–8.

28. Heling A, Zimmermann R, Kostin S, Maeno Y, Hein S, Devaux B, et al. Increased Expression of Cytoskeletal, Linkage, and Extracellular Proteins in Failing Human Myocardium. Circ Res. 2000 Apr 28;86(8):846–53.

29. Goldman JE, Yen S-H. Cytoskeletal protein abnormalities in neurodegenerative diseases. Ann Neurol. 1986 Mar;19(3):209–23.

30. Dudek SM, Garcia JG. Cytoskeletal regulation of pulmonary vascular permeability. J Appl Physiol Bethesda Md 1985. 2001 Oct;91(4):1487–500.

31. Lark AL, Livasy CA, Dressler L, Moore DT, Millikan RC, Geradts J, et al. High focal adhesion kinase expression in invasive breast carcinomas is associated with an aggressive phenotype. Mod Pathol. 2005 Oct;18(10):1289–94.

32. Desgrosellier JS, Cheresh DA. Integrins in cancer: biological implications and therapeutic opportunities. Nat Rev Cancer. 2010 Jan;10(1):9–22.

33. Tsukita S, Itoh M, Nagafuchi A, Yonemura S, Tsukita S. Submembranous junctional plaque proteins include potential tumor suppressor molecules. J Cell Biol. 1993 Dec;123(5):1049–53.

34. Rodríguez Fernández JL, Geiger B, Salomon D, Sabanay I, Zöller M, Ben-Ze'ev A. Suppression of tumorigenicity in transformed cells after transfection with vinculin cDNA. J Cell Biol. 1992 Oct;119(2):427–38.

35. Stoker M, O'Neill C, Berryman S, Waxman V. Anchorage and growth regulation in normal and virus-transformed cells. Int J Cancer. 1968 Sep;3(5):683–93.

36. Shin SI, Freedman VH, Risser R, Pollack R. Tumorigenicity of virus-transformed cells in nude mice is correlated specifically with anchorage independent growth in vitro. Proc Natl Acad Sci U S A. 1975 Nov;72(11):4435–9.

37. Prager-Khoutorsky M, Lichtenstein A, Krishnan R, Rajendran K, Mayo A, Kam Z, et al. Fibroblast polarization is a matrix-rigidity-dependent process controlled by focal adhesion mechanosensing. Nat Cell Biol. 2011 Nov 13;13(12):1457–65.

38. Fusco S, Panzetta V, Embrione V, Netti PA. Crosstalk between focal adhesions and material mechanical properties governs cell mechanics and functions. Acta Biomater. 2015 Sep;23:63–71.

39. Panzetta V, De Menna M, Bucci D, Giovannini V, Pugliese M, Quarto M, et al. X-RAY IRRADIATION AFFECTS MORPHOLOGY, PROLIFERATION AND MIGRATION RATE OF HEALTHY AND CANCER CELLS. J Mech Med Biol. 2015 Apr;15(2):1540022.

40. Brangwynne CP, Koenderink GH, MacKintosh FC, Weitz DA. Intracellular transport by active diffusion. Trends Cell Biol. 2009 Sep;19(9):423–7.

41. Gal N, Weihs D. Intracellular Mechanics and Activity of Breast Cancer Cells Correlate with Metastatic Potential. Cell Biochem Biophys. 2012 Jul;63(3):199–209.

42. Henderson E, Haydon P, Sakaguchi D. Actin filament dynamics in living glial cells imaged by atomic force microscopy. Science. 1992 Sep 25;257(5078):1944–6.

43. Rotsch C. AFM IMAGING AND ELASTICITY MEASUREMENTS ON LIVING RAT LIVER MACROPHAGES. Cell Biol Int. 1997 Nov;21(11):685–96.

44. Wu HW, Kuhn T, Moy VT. Mechanical properties of L929 cells measured by atomic force microscopy: effects of anticytoskeletal drugs and membrane crosslinking. Scanning. 1998 Aug;20(5):389–97.

45. Tilghman RW, Cowan CR, Mih JD, Koryakina Y, Gioeli D, Slack-Davis JK, et al. Matrix Rigidity Regulates Cancer Cell Growth and Cellular Phenotype. Hotchin NA, editor. PLoS ONE. 2010 Sep 23;5(9):e12905.

4

AFM INVESTIGATION OF MESOTHELIAL CELLS MECHANICS AND THEIR MECHANOSENSING OF ECM

4.1 Introduction

Malignant pleural mesothelioma (MPM) is a rare and highly aggressive disease that develops in the pleura, a thin layer of the tissue surrounding the lungs. Asbestos exposure is considered the major cause and the long interval between exposure and the development of disease is the reason for the relatively late discovery of this correlation (1). Malignant mesothelioma, indeed, results from the neoplastic transformation of mesothelial cells and is associated with phenotypic modifications and genetic changes that alter cell-cell and cell-matrix interactions and regulation of cell proliferation and cell death (2–4). Common symptoms presented in patients are the diminished breath sound and chest movement on the affected side of the chest, the decreased vocal resonance and additionally pleural effusion, which can be used for diagnostic purposes. When the first symptoms appear, an imaging test, usually a simple chest X-ray, can determine whether pleural effusion is present. The fluid will show up on the X-ray once the accumulation has reached about 300 mL. Prior to that, it may be difficult to spot the fluid on a chest image. Currently, the initial step in the diagnostic work-up of patients with suspected malignant pleural effusions concerns the cytological analysis of pleural fluid. In order to improve the diagnostic yield of such examination, repeated pleural fluid cytological specimens are analysed, thus effusion cytology may take weeks or months to establish the diagnosis. Furthermore, standard pleural fluid cytology has limited sensitivity (30-60%) for diagnosis MPM (5). For patients with inconclusive results following cytological analysis of the pleural fluid, the next step is a thoracoscopic pleural biopsy, which is an invasive procedure that requires a skilled operator. For these reasons, alternative methods of investigation are necessary to support the diagnosis of pleural effusion. Mechanical phenotyping of individual cells appears a great opportunity having the potential to aid in diagnosis and, thus, to influence the clinical decision-making. In fact, it has been observed that the maintenance of the cell mechanical architecture, depending mainly on the cytoskeleton, is fundamental to guarantee the correct functioning of several cellular functions.

The cytoskeleton of living cells is a highly dynamic structure, constantly remodelled, for its key role in many cellular functions as cell adhesion, proliferation, migration,

differentiation. As consequence, abnormalities of the cytoskeleton led to a variety of disease, such as cardiovascular disease (6), neurodegenerative disease (7), cancer (8,9). In particular, in the case of cancer, alterations in cell cytoskeleton affect cell proliferation, adhesion, ability to remodel the surrounding matrix and migration (10,11). Changes in the cytoskeletal structure are also connected to changes in cell stiffness that entailed a softening of tumour cells in comparison with healthy ones (12–14). The strong correlation existing between cell stiffness and cell malignancy allowed to use cell mechanical properties as a new powerful biomarker, not only to distinguish malignant from benign cells, but also to discriminate between cancer cells with different aggressive potential (15–17). Many techniques of noticeable capability are developing to probe cellular properties at single cell level directly on living cells (18–21). Among these, AFM enables to quantify the elastic modulus (Young's modulus) of single cells in condition close to the natural environment. AFM has rapidly become a valuable tool also to discriminate cancer cell with different metastatic potential (22,23). Nevertheless, deeply understand the malignant transformation process from a mechanical point of view, is necessary to consider that cells are not isolated systems, but they continuously interact with their surrounding environment. Indeed, cells rearrange their cytoskeleton in function of the biophysical properties of surrounding ECM. These structural modifications induce alterations in the cytoskeletal-generated forces that, in turn, are able to remodel the ECM. When such mechanical interplay between cells and extracellular environment is loss, the disease advances. Thus, it is essential to consider in which way the changes of biophysical signalling and, in particular, of the mechanical properties of matrix could influence cancer development from genesis to invasion.

In this study we report the mechanical phenotyping of human MPM cells. The interest in this relatively rare but devastating tumour arises from the fact that its incidence is increasing worldwide. MPM remains a challenge for pathologist and clinicians to treat because of difficulties in early diagnosis and resistance to conventional therapies. We examined a normal mesothelial cell line (MeT-5A) and two epithelioid MPM cell lines (REN and MPP-89). Here, we investigated how the malignant transformation influences cell normal functions, such as cell proliferation, migration and spreading

area. In particular, migration assays revealed that different types of cancer cell migration exists, due to the loss of cell-cell adhesions that induces alterations in the peculiar collective moving of epithelial cells, in favour of a solitary migration. These changes are correlated to enhanced aggressiveness of cancer cells and promote their metastatic dissemination in the body and the formation of metastasis. The phenotypic alterations in cell behaviour, due to the malignant transformation, were associated to the reorganization of the cell cytoskeleton. Cytoskeleton remodelling caused also variations in cell mechanical properties, probed by AFM. This technique has previously been demonstrated to be a new and fast support in the pathologist diagnosis of pleural effusions (16). In particular, we verified a reduction in cancer cell stiffness compared to healthy cells. Combining the analyses of cellular phenotypical events to physical properties, in particular cell stiffness, we could discriminate cancer from benign cells and distinguish cancer cells with different aggressiveness. Finally, we studied the influence of substrate stiffness on cell mechanics. To this aim, mechanical properties of cells were examined on PAAm gels of different stiffness.

4.2 Materials and Methods

4.2.1 Polyacrylamide substrata preparation and mechanical characterization

Different combination of acrylamide and methylene-bis-acrylamide were mixed to obtain 0.3 kPa, 4 kPa, 13 kPa, 30 kPa hydrogels, as described in Section 2.1. To allow for cell adhesion, substrates were functionalized with collagen, by using a bifunctional photolinker, sulpho-SANPAH.

4.2.2 Cell culture

Experiments were performed on benign human mesothelial cells (MeT-5A) and two malignant human mesothelioma cells (REN, MPP-89), with different metastatic potential. Cell lines were cultured in RPMI 1640 (Microtech) supplemented with 10% fetal bovine serum (FBS, BioWhatter, MD), 2 mM L-glutamine (Sigma, St. Louis, MO), 1000 U/L penicillin (Sigma, St. Louis, MO), and 100 mg/L streptomycin (Sigma, St. Louis, MO).

4.2.3 Cell proliferation and migration

In proliferation experiments, cells ($5x10^4$/well) were seeded in 6-well plates. Cell aliquots were collected and counted after 24 h and 48 h from seeding in Neubauer hemocytometer.

Single cell and collective migration were investigated to study cell migratory behaviour both on glass dishes and PAAm substrates. To examine single cell migration, cells (2000/cm^2) were seeded and incubated at 37°C and 5% CO_2 for 24h in order to allow cell adhesion. To study collective cell migration on glass dishes, the cell wound closure assay was used. Cells were seeded in 35 mm Petri dishes and incubated until confluence. The procedure and the equipment are described in 2.2.4.

4.2.4 Cell spreading area

Cells were plated at a density of 2000/cm^2 on 23 mm glass dishes (Fluorodish, World Precision Instrument) and PAAm substrates. Cells were fixed and immunostained to evaluate the spreading area at 24h from seeding (see Section 2.2.3).

4.2.5 Atomic force microscopy to study cell mechanics

The mechanical properties of mesothelial cells cultured on glass and PAAm substrates were studied using AFM (see Section 2.3.2). To investigate the dependence of cell Young's modulus on cellular density, experiments were performed on both single cells and cell monolayer cultured on 23 mm glass (Fluorodish, World Precision Instrument). Cells were plated at a density of 2000/ cm^2 and until confluence to test, respectively, single cell and cell monolayer mechanical properties. Measurements were conducted in cell culture medium supplemented with 12.5 mM Hepes buffer (EuroClone) at 37°C.

4.2.6 Statistical Analysis

Data are reported as mean ± standard error (SE), unless otherwise indicated. Statistical comparisons were performed with a Student's unpaired test. P values < 0.05 denote statistical significance.

4.3 Results

4.3.1 Cell proliferation and migration

Cell proliferation and migration are considered two fundamental parameters to describe the aggressiveness of tumour cells. We found that the rate of proliferation of malignant cell lines was higher than benign one. Moreover, among malignant cell lines, MPP-89 and REN exhibited higher proliferation rate after 48h compared to MeT-5A, while there is not great difference between MPM cell lines (Fig.1).

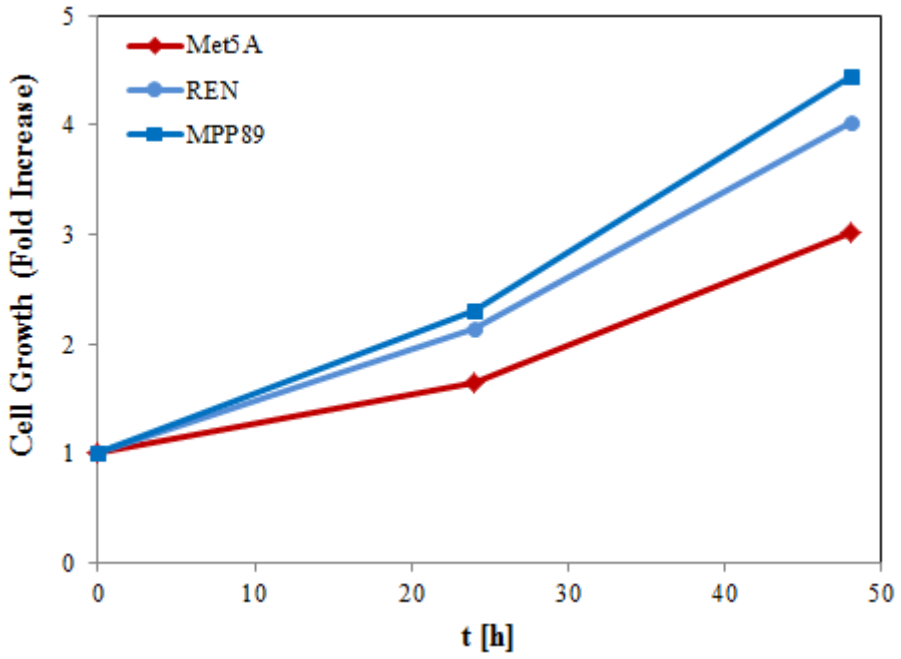

Figure 1 Cell proliferation was monitored for 48 h. Proliferative capacity of malignant cell lines was significantly higher than benign MeT-5A.

Single cell migration was initially examined on glass petri dish. Quantitative time-lapse microscopy revealed that, respect to healthy cells, the malignant cells moved quickly. Among them, MPP-89 cells migrated faster (Fig 2). To analyse the influence of substrate stiffness on single cell migration, we examined also cell migration on PAAm gels. Results showed that, independently from substrate stiffness, tumour cells displayed an increased motility compared to the healthy cell line, except for the case of 0.3 kPa, where REN migration was approximatively the same of the healthy counterpart. MPP-89 was still faster than REN cells on all PAAm substrates. Moreover, our results showed that malignant cell lines had a biphasic migration-velocity dependence on substrate stiffness, reaching the maximum velocity on 4 kPa

hydrogels (Fig.3). Differently from malignant cells, MeT-5A cell velocity seemed to increase monotonically as a function of gel stiffness (Fig.3). We wondered if a maximum in cell velocity exists also in the case of MeT-5A and, examining also cell migration on 13 kPa, we discovered that, on this substrate stiffness, MeT-5A reached a maximum in velocity (Fig.4).

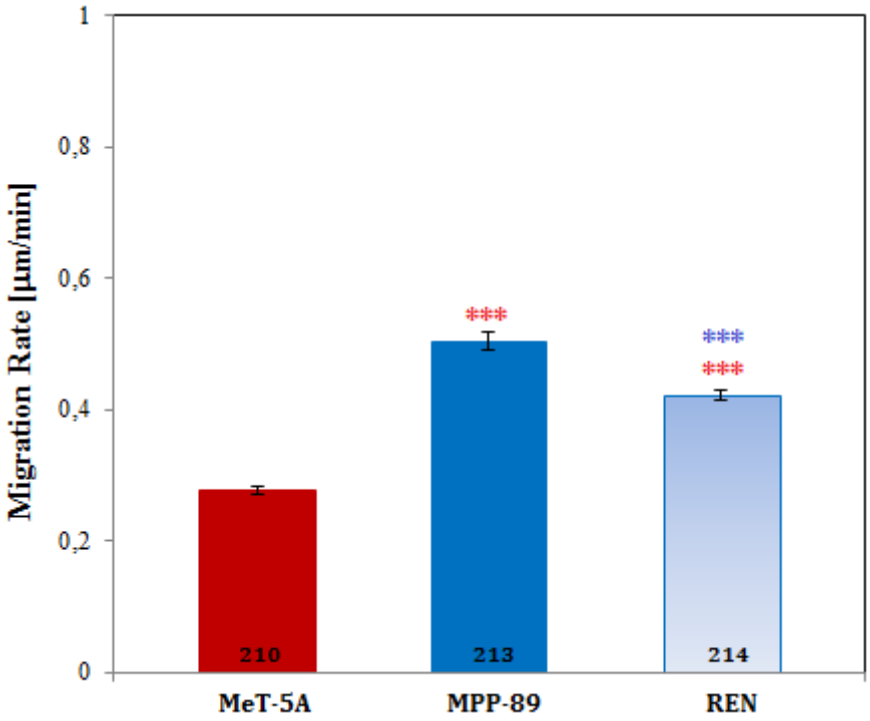

Figure 2 Single cell migration rate on glass dish. MPM cells exhibited significantly (***P<0.001 by Student's t test) higher migration rate compared to benign cells. Moreover, MPP-89 resulted significantly (***P<0.001 by Student's t test) faster than REN cells. Results were presented as mean ±S.E.M and the number of cells analysed was indicated in the bars

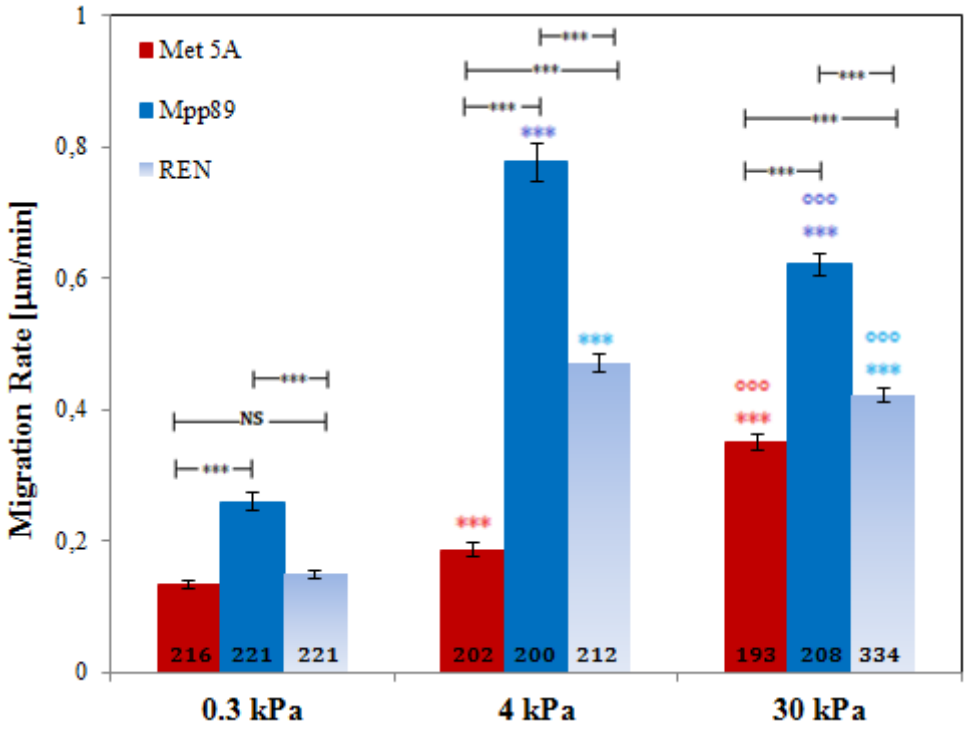

Figure 3 Single cell migration rate on PAAm. MPM cells exhibited increasing motility compared to the healthy cell line, except for the case of 0.3 kPa, where REN migration was approximatively the same of the healthy counterpart. Results were presented as mean ±S.E.M and the number of cells analysed was indicated in the bars. Statistical comparisons were performed with a Student's unpaired test. ***/°°°P<0.001, compared to 0.3 kPa/4kPa; NS P>0.05.

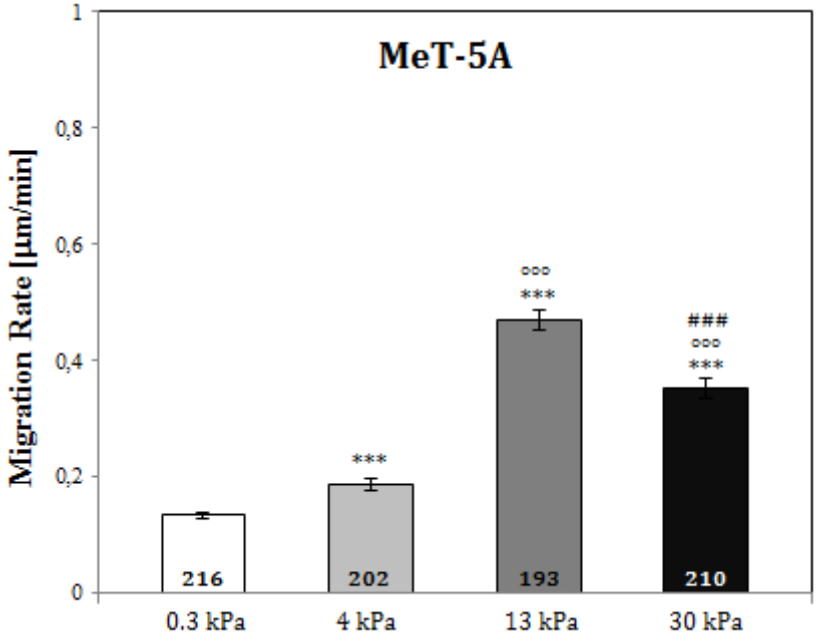

Figure 4 MeT-5A single cell migration rate on PAAm. MeT-5A cells reached a maximum in velocity on 13 kPa. Results were presented as mean ±S.E.M and the number of cells analysed was indicated in the bars. Statistical comparisons were performed with a Student's unpaired test. ***/°°°/### P<0.001 compared to 0.3 kPa, 4 kPa and 13 kPa, respectively.

Collective migration on glass was analysed through the wound healing assay, as previously described. While the benign control was not able to close the wound in 12 h, REN cells closed the wound approximately after 12 h. Similarly to the control cells, MPP-89 cells were not able to close the wound in 12h, due to their lack of ability to migrate in a directional way. Instead, they preferentially proliferated and migrated in lateral direction rather than in the direction of wound closure (Fig.5). Moreover, we examined migration velocity of cells at the far ends of the wound. Cells seeded in confluent conditions showed a decreased velocity in comparison to single cells. Also in confluent conditions, malignant cell lines continued to show higher velocity than healthy one, even if, as already said, REN cells preserved a directional migratory ability differently from MPP-89 cells (Fig. 6).

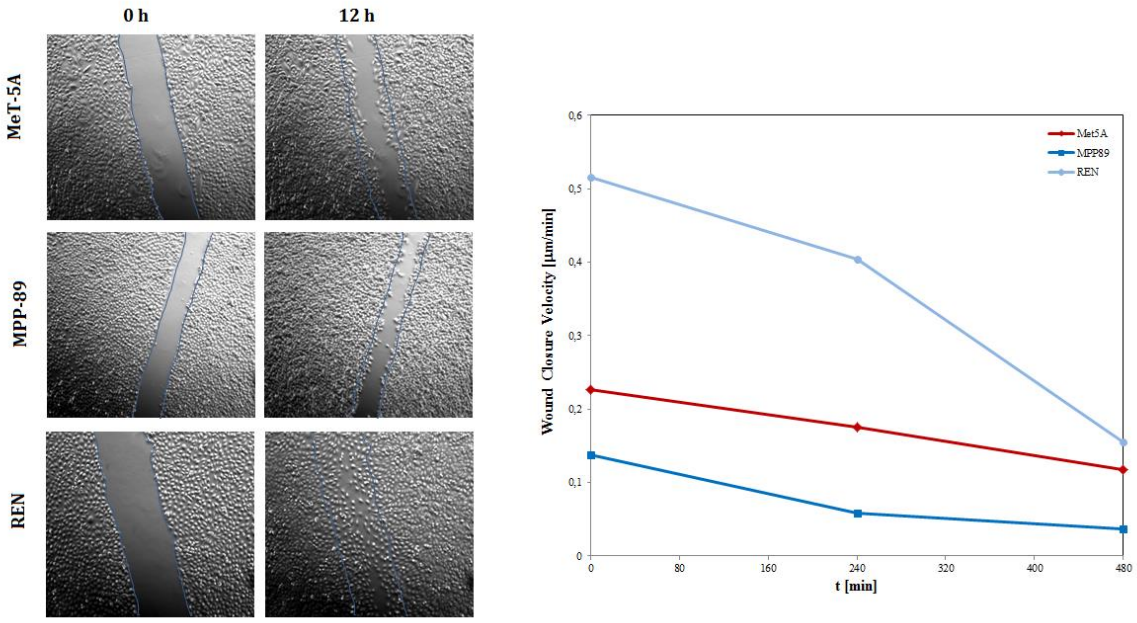

Figure 5 Confluent cell monolayers were wounded with pipette tip. REN cells closed the wound approximately after 12 h, while MPP-89 were not able to close the wound in the investigated interval of time. Collective migration velocity was expressed in terms of wound closure velocity.

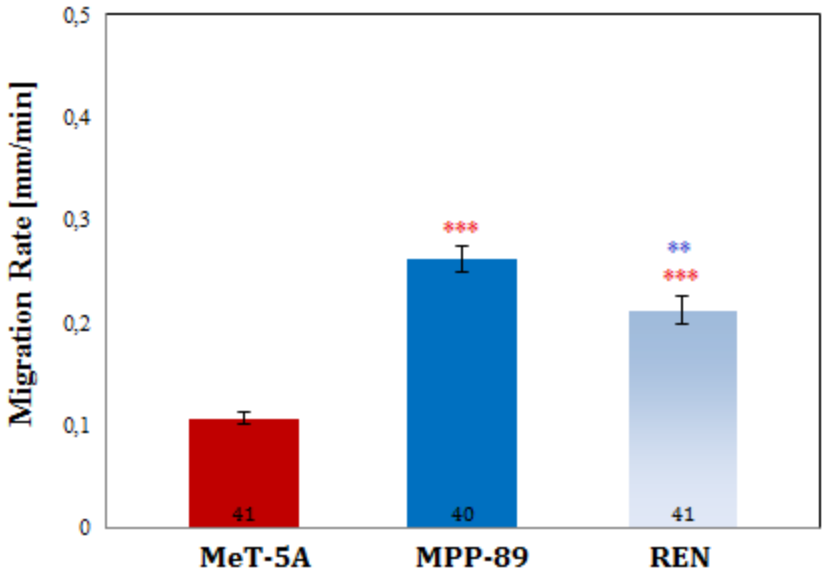

Figure 6 Migration velocity of cells at the far ends of the wound. Also in confluent conditions, malignant cell lines continued to show significantly (***P<0.001, by Student's t test)higher velocity than healthy one. MPP-89 cells migrated faster than REN cells (**P<0.05, by Student's t test). Results were presented as mean ±S.E.M and the number of cells analysed was indicated in the bars.

4.3.2 Cell morphological changes

We monitored how cell spreading area changed with substrate stiffness. Images were taken 24h after seeding, to allow cell spreading completely. Furthermore, we analysed cells that spread without contact with adjacent cells, to avoid any interference in cell spreading by the cell-cell contact. Unexpectedly, REN cells seeded on glass showed a wide spreading area, higher than MeT-5A, while MPP-89 exhibited the smallest spreading area (Fig. 7,8). On PAAm gels, cell area grew with increasing of substrate stiffness for all cell lines, except for REN cell lines, whose area did not exhibit variation up to 0.3 kPa (Fig. 9,10). These results showed the preserved ability of both normal and malignant cells to sense matrix stiffness in terms of adhesion properties to matrix.

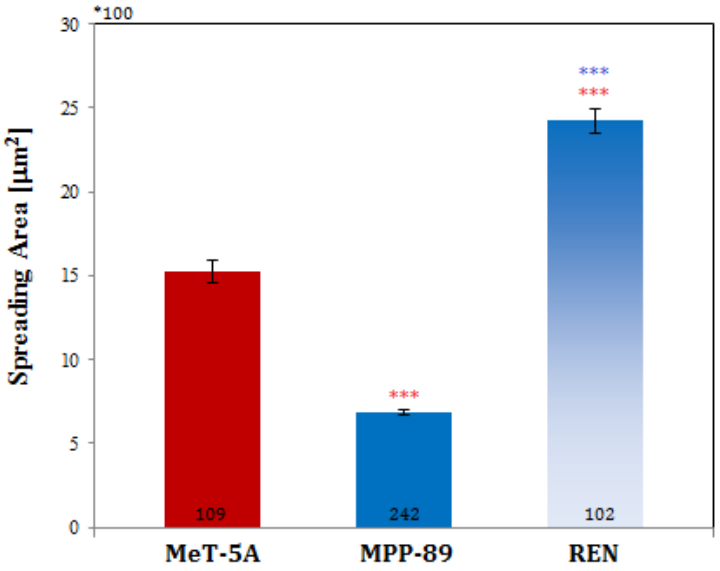

Figure 7 Cell spreading area on glass. REN cells seeded on glass showed a significantly wider spreading area compared to MeT-5A (***P<0.001) and MPP-89(***P<0.001). MPP-89 exhibited the smallest spreading area, significantly (***P<0.001) tiny compared to MEeT-5A.

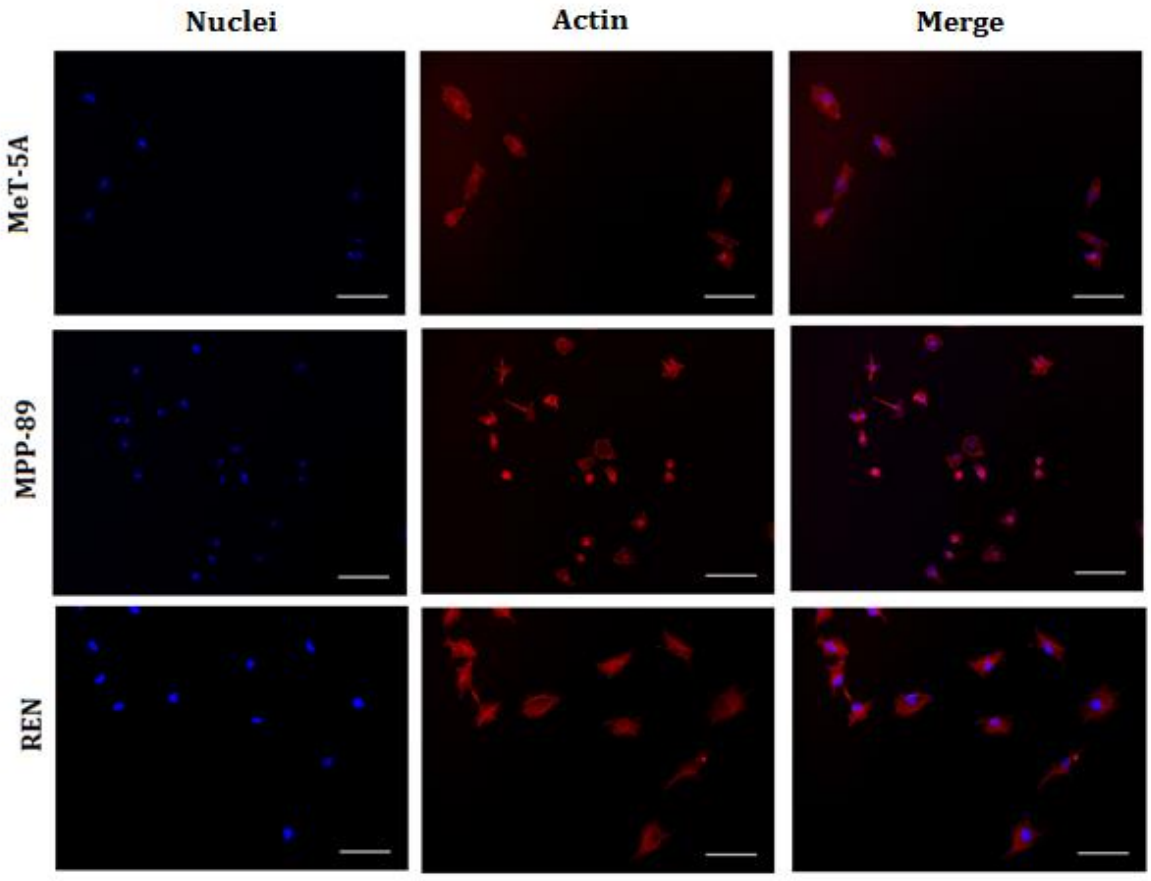

Figure 8 Cells were fixed and stained with phalloidin(red, actin) and HOECHST (blue, nuclei). Representative images of cell nuclei and actin filaments of mesothelial and MPM cells on glass . Scale bar 100 µm.

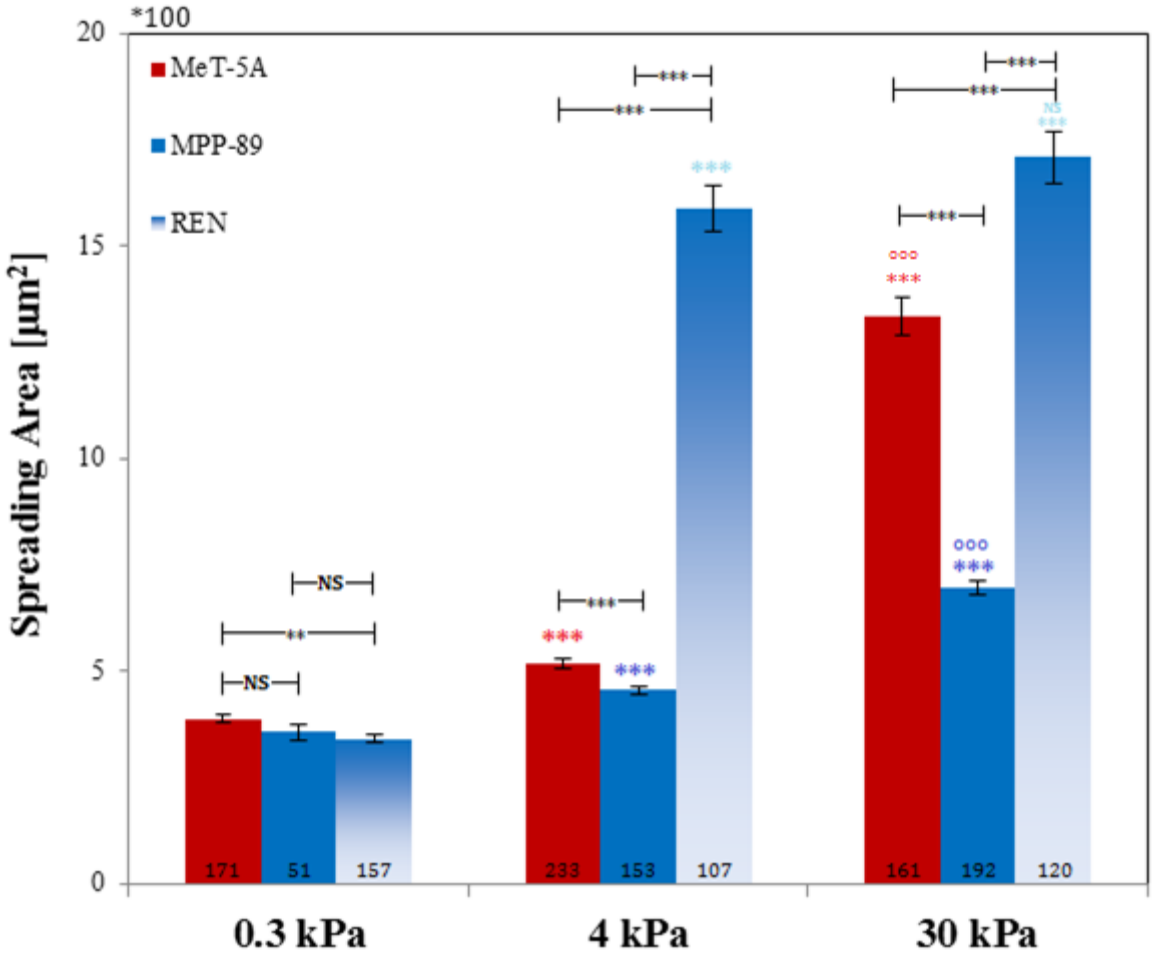

Figure 9 Cell spreading area on PAAm. Spreading area grew with increasing of substrate stiffness for all cell lines, except for REN cell lines, whose area did not exhibit variation up to 0.3 kPa Results were presented as mean ±S.E.M and the number of cells analysed was indicated in the bars. Statistical comparisons were performed with a Student's unpaired test. ***/°°°P<0.001, **P<0.05 NS P>0.05.

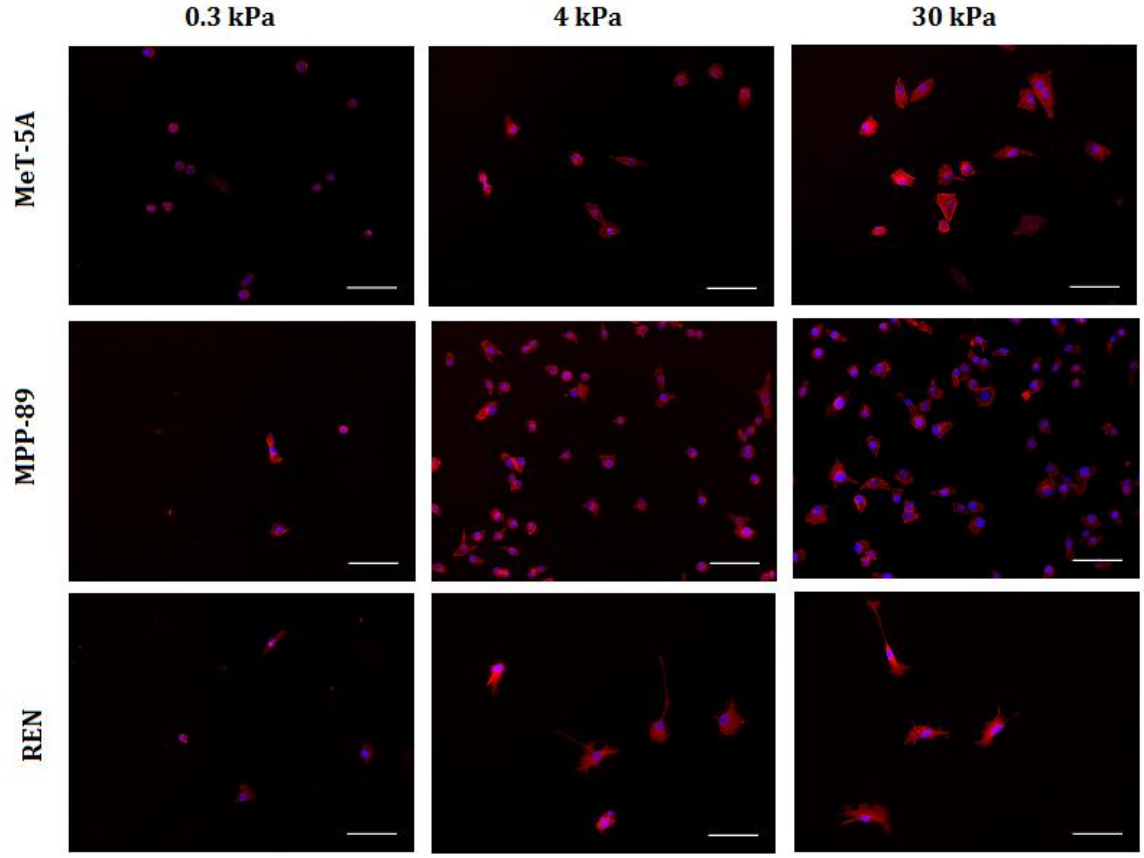

Figure 10 Cells were fixed and stained with phalloidin(red, actin) and HOECHST (blue, nuclei). Representative images of cell nuclei and actin filaments of mesothelial and MPM cells on PAAm . Scale bar 100 μm.

4.3.3 Cell mechanics

Cell mechanical properties were studied thanks to AFM. As a first step, we tested both single cells and cell monolayer on glass to analyse the influence of cell density on mechanical properties. In both culture conditions, benign cells exhibited higher Young's moduli than malignant ones (Fig. 11a). In particular, the average stiffness (mean±s.d.) of single tumour cells were found to be 0.29±0.16 kPa (MPP-89) and 0.53±0.23 kPa (REN). Thus, cancer cells showed reduction in stiffness with increasing metastatic potential. Otherwise, benign mesothelial cells expressed a significantly increased average cellular elasticity, with a value of 1.46±1.1 kPa. Results of experiments performed on cell monolayer presented the same trend of single cells (Fig. 11b), but higher elastic moduli were measured. The average stiffness of tumour cell in confluent condition increased to 0.58±0.29 kPa, for MPP-89 and 1.48±1.1 kPa, for REN cell line. For benign cells, the average stiffness grew to a value of 2.16±1.0

kPa. The enhanced cell stiffness, in the case of cell monolayer, was probably due to cell-cell contacts that strengthen cell cytoskeleton structure (Fig. 11b). Cell mechanical properties were also evaluated on PAAm substrates with different stiffness. Our results showed that MeT-5A sensed variations in substrate stiffness changing (Fig. 12). We measured an average stiffness of 0.36±0.1 kPa and 1.4±0.5 kPa on soft substrates (0.3 kPa and 4 kPa, respectively), that increased to 2.7±1.4 kPa on the stiffer substrate (30 kPa). Contrary to benign cells, MPP-89 and REN cell lines did not feel difference in substrate stiffness up to 0.3 kPa (Fig. 12). In fact, tumour cell elasticity measured on 0.3 kPa were 0.27±0.06 kPa (MPP-89) and 0.75±0.2 (REN) kPa, while the average stiffness estimated on 4 and 30 kPa were 0.45±0.1 kPa and 1.4±0.5, for MPP-89 and REN cells, respectively.

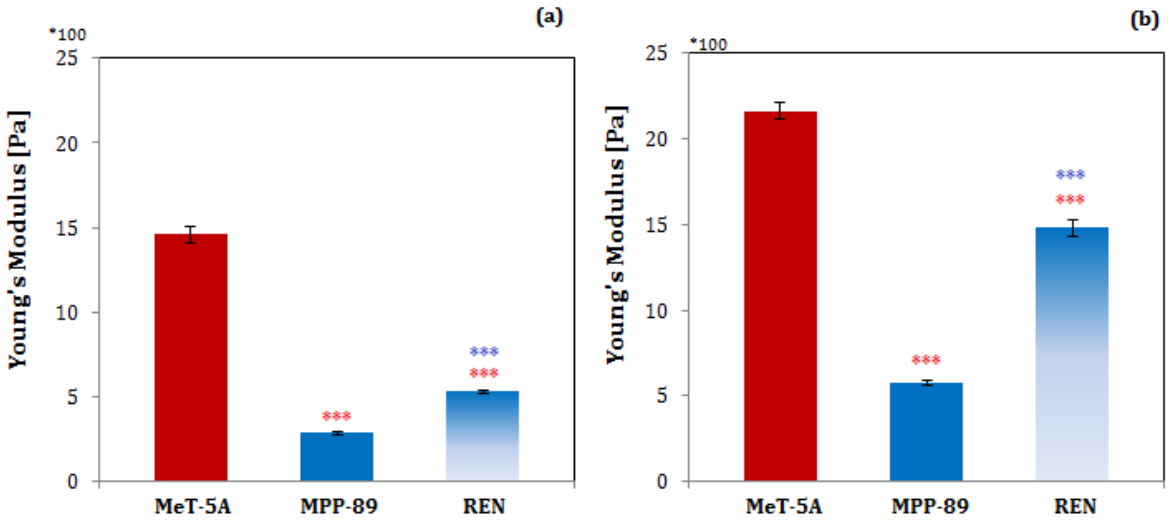

Figure 11 Apparent Young's modulus for benign MeT-5A and malignant REN and MPP-89, on glass, in two culture conditions: (a) single cells and (b) cell monolayer. In both cases, cancer cells showed reduction in stiffness with increasing metastatic potential Results were presented as mean ±S.E.M. Student's t test was applied to measure statistical differences. ***/***P<0.001 as compared to normal cells or MPP-89, respectively.

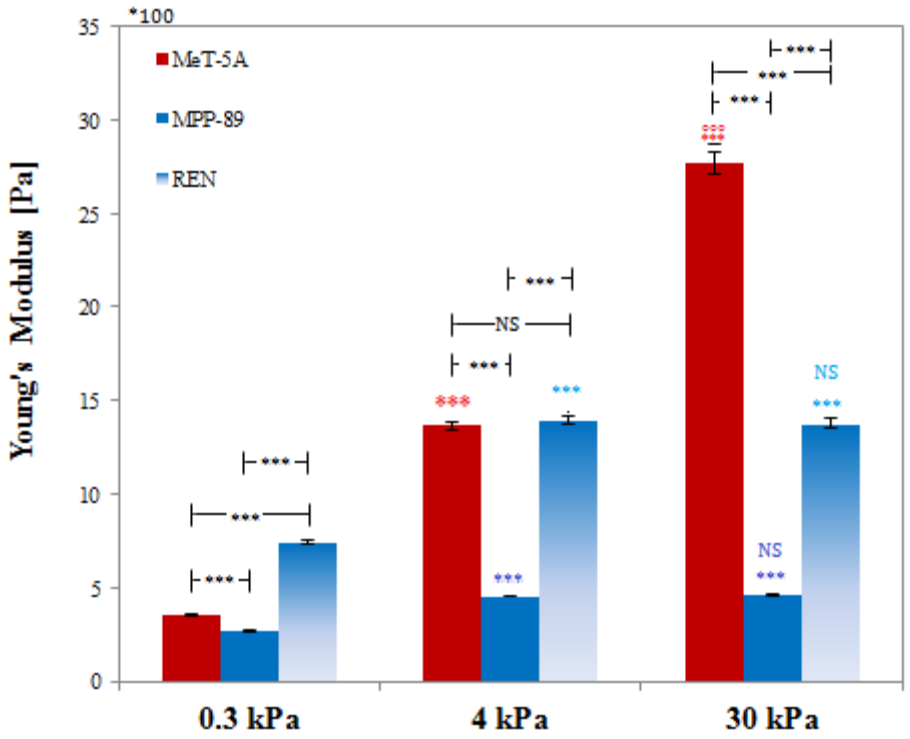

Figure 12 Apparent Young's modulus for benign MeT-5A and malignant REN and MPP-89 on PAAm. MeT-5A sensed variations in substrate stiffness changing, while MPP-89 and REN cell lines did not feel difference in substrate stiffness up to 0.3 kPa Results were presented as mean ±S.E.M and the number of cells analysed was indicated in the bars. Statistical comparisons were performed with a Student's unpaired test. ***/°°°P<0.001, NS P>0.05.

4.4 Discussion

MPM is a lethal cancer with increasing worldwide incidence. Unfortunately, MPM has a long latency period and then it is diagnosed in a late stage, when its resistance to conventional chemo- and radio-therapy is very strong. For these reasons, the identification of new and specific biomarkers is of relevant importance to guarantee an early diagnosis of MPM, but also to define more efficient treatments. To this purpose, a very promising contribute could come from the study of cell mechanical properties that can be considered as a label free marker of cancer progression (24–26). In fact, during cancer progression, cell undergoes from a fully mature, post mitotic state to a proliferating motile cancerous state, that involves a dramatic reorganization of the actin cytoskeleton and, consequently, a deviation from their mechanical properties (27–29).

In this work, we studied the mechanical properties (Young's modulus) of human lung mesothelial cells, by using AFM. Biophysical characterization supports the analysis of biological behaviour of cells, not only to discriminate malignant cells from benign ones, but also to identify the aggressiveness of tumour cells. In fact, it is well known that cancer cells are softer than their normal counterpart (30,31), but studying the correlation between cell mechanical properties and metastatic potential is an opening question. At this aim, in this study, we proposed the physiological behaviour and the mechanical characterization of a mesothelial cell line (MeT-5A) and two MPM cell lines (REN and MPP-89) of different aggressiveness, to better understand the consequence of malignant transformation.

Tumorigenesis is accompanied by alterations in cell cytoskeletal structure that plays a critical role in cellular processes, including cell proliferation and migration activities, and influences cell shape, adhesiveness and, consequently, mechanical properties (10,32). *In vitro* experiments on glass substrates revealed enhanced proliferative and migratory capacity of MPM cells (see Section 4.3.1). The increase in cell proliferative and migratory abilities is considered an hallmark of tumour transformation. The invasiveness of MPM cells was also investigated using wound healing scratch assay. During wound repair, we observed healthy cells moving together in sheet-like structures, maintaining cell-cell adhesions, due to the presence of cell-cell junctions. This collective migration was also a quick of REN cells. Unlike MeT-5A, REN cells had so high migration rate to be able to close the wound in the time of observation. Otherwise, MPP-89 showed an individual cell migration, because the function of cadherin, a cell-cell junction protein, was suppressed and cells moved as single cells. This feature suggested that a dedifferentiation of MPP-89 cells was proceeding. The distinct modes of cancer cell migration accorded to aggressiveness and differentiation state of cancer cells (33).

We analysed morphological and mechanical features of the proposed cell lines and we discovered that the morphology alone is not sufficient to discriminate malignant from benign cell. Previous experiments performed on cells from the pleural effusion samples, demonstrated that no correlation exists between *ex vivo* cultured cell morphology and expected measured stiffness. This lack of correlation suggest that it

is unlikely that *ex vivo* cultured morphological differences influence measured elasticity (16). We found that REN cells appeared morphologically similar to their heathy counterpart and they exhibited a great spreading area, about twice than that of MeT-5A cells. Nevertheless REN cells were more spread compared to MeT-5A, they appeared highly motile and able to repopulate the scratched area within 12 hours. Similarly to MeT-5A, REN cells migrated in the direction of wound closure, but, unlike healthy cells, they were able to close the wound in the time of observation. Furthermore, their mechanical properties resulted to be lower than those of healthy mesothelial cells, explaining their increased motility. The enhanced migration activities, the significantly reduction of cell mechanical properties confirmed the malignant behaviour of this cancer cell line. Moreover, the combination of biological and mechanical parameters could help to judge the aggressiveness of MPM. In fact, we noted that MPP-89 cells presented a very small spreading area, the ability to migrate rapidly and lower values of Young's modulus, compared to REN cells. The most important difference between REN and MPP-89 cells was in the way they closed scratched area in wound assay. As already said, REN cells preserved their ability to heal wounds, while wound healing process resulted to be seriously affected in the case of MPP-89 cells. In fact, MPP-89 cells lost their epithelial organization and gained the ability to detach from epithelial cell clusters in order to move as single cells in a mesenchymal fashion. All these features, recapitulated in Tab.1, underlined the differences between healthy and cancer cells and let us conclude that MPP-89 have a more aggressive potential than REN cells.

Plastic and glass cell culture systems lack the properties required to mimic *in vivo* environments. Consequently, *in vitro* cultured cells generally have an altered behaviour in terms of growth rate, morphology and intracellular metabolic activities. In this context, it is of paramount importance to design biomaterials with micro-structural and mechanical properties able to organize cells and support a more *in vivo* like behaviour and cellular phenotype. In particular, it has been widely demonstrated that the stiffness of extracellular environment has a large impact, similar to chemical stimuli, on the regulation of cell behaviours, in particular cell survival, proliferation, differentiation and migration (34). For example, changes in stiffness of glioma cells

due to the rigidity of the substrate (35,36) and the mechanical properties of cancer cells plated on soft collagen matrices have been reported (37). The importance to study the role of ECM mechanics is due to the changes of ECM composition and architecture in cancer. In fact, disease states are often accompanied by a local increase in ECM rigidity (38,39) due to local accumulation of a dense, crosslinked collagen matrix favouring detection of the tumour by physical palpation (40,41). Cells, that normally resides in soft environment, manifest enhanced proliferation and migration, a loss of cell polarity, when cultured on stiffer matrices (42). These aspects can be considered hallmarks of cancer cells, accompanying the transition from a relatively quiescent to a malignant phenotype, driven by local ECM remodelling and stiffening.

For these reasons, we also investigated how cellular functions and characteristics, such as cell migration, cell spreading area and mechanics were influenced by changes in substrate stiffness. To reproduce the environment that could better mimic the *in vivo* ECM, we had to consider that, in the body, tissues stiffness is not static, but changes during physiological processes and in pathological responses like tumorigenesis. In particular, the elastic modulus of a normal human lung has been measured at 0.44-7.5 kPa and this inhomogeneity depends in part on the region measured (alveolar wall or. airway wall or. airway epithelium, for example) (43). However, in case of lung cancer, the elastic modulus grows above 15 kPa (44). The increase in the stiffness of the ECM may lead to phenotypic cellular changes such as increased proliferation and migration (45,46). The stiffness interval we investigated in this study encompassed lung physiological range in healthy and disease conditions. Previous studies agreed that healthy cells have the ability, known as *mechano-sensing*, to detect and respond to the mechanical stiffness of the extracellular environment (34,47–51). Cancer cells do not show a clear behaviour. *In vitro* experiments on substrates of different stiffness demonstrated that only certain cancer cell lines exhibited a dependence on matrix rigidity for growth rate, spreading and migration (52). In particular, rigidity-dependent cancer cells grew better on stiff/rigid matrices and their lower growth rates, when plated on soft matrices, were caused at least in part by a selective alteration in cell cycle progression and by the induction of

apoptosis. On rigid substrates, cell lines which demonstrated rigidity-dependent growth also spread extensively, formed prominent stress fibres, mature focal adhesions and migrated rapidly, while they appeared rounded and failed to productively migrate on less rigid gels (45,52). The regulation of growth in response to rigidity was controlled by FAK, ERK, and the small GTPase Rho expression (42), or by an increase in cyclin D levels downstream of Rac activation (53). Rho GTPases and their downstream targets, which are critical mediators of cell spreading, migration, and contractility (54) may act as mechanosensory machinery that respond to the rigidity of the microenvironment.

In the present study, we found that matrix stiffness altered cytoskeletal structure and mechanical properties of normal and MPM cells. The less structured cytoskeleton, the decreased migration rate and the reduced Young's modulus on soft substrates was recently demonstrated for different lung cancer cell lines (55). Indeed, our results support these findings and bring more knowledge on the effects of substrate stiffness on lung cancer cells. Both normal mesothelial and MPM cells reacted to substrate stiffening by increasing spreading area and mechanical properties and by showing biphasic migration-velocity dependence on substrate stiffness, with a peak value reached on 13 kPa substrates in the case of normal cells and on 4 kPa substrates in the case of MPM cells. Importantly, on the softest substrate, cancer cells show a significantly reduction of migration rate, spreading area and Young's moduli, until reaching values similar to normal cells. Recent works study how the normal stroma exerts tumour-suppressive signals to control tissue homeostasis (56,57). It is demonstrated how the soft normal ECM can triggers the downregulation of cancer cells proliferation (56). Thus, our findings were oriented towards this new mechanism of ECM-mediated control of cancer cells behaviour.

	Cell Proliferation (Fold Increase)	**Single-cell Migration**	**Wound Closure Velocity**	**Cell Spreading Area**	**Single-Cell Mechanical Properties**
	%	μm/min	μm/min	μm^2	kPa
MeT-5A	3	0.28±0.15	0.23±0.1	1528±679	1.46±1.1
MPP-89	4.4	**0.5±0.26**	**0.14±0.05**	**688±270**	**0.29±0.16**
REN	4	**0.42±0.32**	**0.52±0.16**	**2422±761**	**0.53±0.23**

Table 1 Results of phenotypical and mechanical characterization of mesothelial and MPM cells. Data were presented as mean ± SEM. Statistical difference was shown as: **Mean ±SEM P<0.05**, **Mean ±SEM P<0.01**, **Mean ±SEM P<0.001** as compared to healthy cells.

4.5 Conclusions

In this work, we investigated the mechanical properties of MPM cells and their normal counterpart, using AFM. The AFM measurements helped to understand the correlation between cell structure, mechanics and functioning. The mechanical properties of MPM cells resulted to be lower than those of healthy mesothelial cells. The decrease of Young's moduli, due to malignancy, was consistent with morphological changes and cytoskeleton rearrangement observed by fluorescent microscopy. Our results showed that the malignant transformation altered cytoskeletal structure and, consequently, changed cellular functions, such as cell proliferation, migration and adhesion. Furthermore, cell mechanical properties were correlated to tumour cells aggressiveness. We noticed that cell stiffness declined with increase of the level of cancer transformation that could give benefits for tumour invasion. Moreover, we have taken a first step in characterizing the response of MPM cell lines to changes in the rigidity of surrounding microenvironment. We observed that both healthy and tumour cells reacted to substrate stiffening by increasing spreading area, cell migration and mechanical properties. Thus, extracellular environment has a large impact on the regulation of cell functions, in particular cell survival, proliferation and migration. In particular, ECM stiffness had a key role in the control and in the downregulation of cancer cell behaviour. In conclusion, our findings showed that cell mechanical properties could be considered a valid label free marker for cancer progression and the biophysical characterization of MPM cells may result an efficient support to the diagnosis of pleural effusions.

4.6 References of Chapter 4

1. Baas P, Schouwink H, Zoetmulder FAN. Malignant pleural mesothelioma. Ann Oncol. 1998;9(2):139–150.

2. Mossman BT, Shukla A, Heintz NH, Verschraegen CF, Thomas A, Hassan R. New Insights into Understanding the Mechanisms, Pathogenesis, and Management of Malignant Mesotheliomas. Am J Pathol. 2013 Apr;182(4):1065–77.

3. Sekido Y. Molecular pathogenesis of malignant mesothelioma. Carcinogenesis. 2013 Jul 1;34(7):1413–9.

4. Jean D, Daubriac J, Le Pimpec-Barthes F, Galateau-Salle F, Jaurand M-C. Molecular Changes in Mesothelioma With an Impact on Prognosis and Treatment. Arch Pathol Lab Med. 2012 Mar;136(3):277–93.

5. Han H-S, Yun J, Lim S, Han J-H, Lee KH, Kim ST, et al. Downregulation of cell-free miR-198 as a diagnostic biomarker for lung adenocarcinoma-associated malignant pleural effusion: miR-198 in malignant pleural effusion. Int J Cancer. 2013 Aug 1;133(3):645–52.

6. Hein S. The role of the cytoskeleton in heart failure. Cardiovasc Res. 2000 Jan 14;45(2):273–8.

7. Goldman JE, Yen S-H. Cytoskeletal protein abnormalities in neurodegenerative diseases. Ann Neurol. 1986 Mar;19(3):209–23.

8. Hall A. The cytoskeleton and cancer. Cancer Metastasis Rev. 2009 Jun;28(1–2):5–14.

9. Fife CM, McCarroll JA, Kavallaris M. Movers and shakers: cell cytoskeleton in cancer metastasis: Cytoskeleton and cancer metastasis. Br J Pharmacol. 2014 Dec;171(24):5507–23.

10. Alberts B, Johnson A, Lewis J. The Cytoskeleton and Cell Behavior. Vol. 4th edition. Molecular Biology of the Cell; 2002.

11. Ingber DE, Dike L, Hansen L, Karp S, Liley H, Maniotis A, et al. Cellular Tensegrity: Exploring How Mechanical Changes in the Cytoskeleton Regulate Cell Growth, Migration, and Tissue Pattern during Morphogenesis. In: International Review of Cytology [Internet]. Elsevier; 1994 [cited 2017 Jan 19]. p. 173–224. Available from: http://linkinghub.elsevier.com/retrieve/pii/S0074769608615429

12. Lin H-H, Lin H-K, Lin I-H, Chiou Y-W, Chen H-W, Liu C-Y, et al. Mechanical phenotype of cancer cells: cell softening and loss of stiffness sensing. Oncotarget. 2015 Aug 28;6(25):20946–58.

13. Lekka M, Pogoda K, Gostek J, Klymenko O, Prauzner-Bechcicki S, Wiltowska-Zuber J, et al. Cancer cell recognition – Mechanical phenotype. Micron. 2012 Dec;43(12):1259–66.

14. Guck J, Schinkinger S, Lincoln B, Wottawah F, Ebert S, Romeyke M, et al. Optical Deformability as an Inherent Cell Marker for Testing Malignant Transformation and Metastatic Competence. Biophys J. 2005 May;88(5):3689–98.

15. Cross SE, Jin Y-S, Tondre J, Wong R, Rao J, Gimzewski JK. AFM-based analysis of human metastatic cancer cells. Nanotechnology. 2008 Sep 24;19(38):384003.

16. Cross SE, Jin Y-S, Rao J, Gimzewski JK. Nanomechanical analysis of cells from cancer patients. Nat Nanotechnol. 2007 Dec;2(12):780–3.

17. Xu W, Mezencev R, Kim B, Wang L, McDonald J, Sulchek T. Cell Stiffness Is a Biomarker of the Metastatic Potential of Ovarian Cancer Cells. Batra SK, editor. PLoS ONE. 2012 Oct 4;7(10):e46609.

18. Zhou EH, Quek ST, Lim CT. Power-law rheology analysis of cells undergoing micropipette aspiration. Biomech Model Mechanobiol. 2010 Oct;9(5):563–72.

19. Fodil R, Laurent V, Planus E, Isabey D. Characterization of cytoskeleton mechanical properties and 3D-actin structure in twisted adherent epithelial cells. Biorheology. 2003;40(1–3):241–5.

20. Li Y, Wen C, Xie H, Ye A, Yin Y. Mechanical property analysis of stored red blood cell using optical tweezers. Colloids Surf B Biointerfaces. 2009 May;70(2):169–73.

21. Kirmizis D, Logothetidis S. Atomic force microscopy probing in the measurement of cell mechanics. Int J Nanomedicine. 2010;5(137):e45.

22. Park S, Lee YJ. AFM-based dual nano-mechanical phenotypes for cancer metastasis. J Biol Phys. 2014 Sep;40(4):413–9.

23. Faria EC, Ma N, Gazi E, Gardner P, Brown M, Clarke NW, et al. Measurement of elastic properties of prostate cancer cells using AFM. The Analyst. 2008;133(11):1498.

24. Brunner C, Niendorf A, Käs JA. Passive and active single-cell biomechanics: a new perspective in cancer diagnosis. Soft Matter. 2009;5(11):2171.

25. Suresh S. Biomechanics and biophysics of cancer cells☆. Acta Mater. 2007 Jul;55(12):3989–4014.

26. Lee GYH, Lim CT. Biomechanics approaches to studying human diseases. Trends Biotechnol. 2007 Mar;25(3):111–8.

27. Ketene AN, Schmelz EM, Roberts PC, Agah M. The effects of cancer progression on the viscoelasticity of ovarian cell cytoskeleton structures. Nanomedicine Nanotechnol Biol Med. 2012 Jan;8(1):93–102.

28. Lindberg U, Karlsson R, Lassing I, Schutt CE, Höglund A-S. The microfilament system and malignancy. Semin Cancer Biol. 2008 Feb;18(1):2–11.

29. Buda A, Pignatelli M. Cytoskeletal network in colon cancer: from genes to clinical application. Int J Biochem Cell Biol. 2004 May;36(5):759–65.

30. Lekka M, Laidler P, Gil D, Lekki J, Stachura Z, Hrynkiewicz AZ. Elasticity of normal and cancerous human bladder cells studied by scanning force microscopy. Eur Biophys J. 1999 May 25;28(4):312–6.

31. Prabhune M, Belge G, Dotzauer A, Bullerdiek J, Radmacher M. Comparison of mechanical properties of normal and malignant thyroid cells. Micron. 2012 Dec;43(12):1267–72.

32. Pawlak G, Helfman DM. Cytoskeletal changes in cell transformation and tumorigenesis. Curr Opin Genet Dev. 2001 Feb;11(1):41–7.

33. Yamazaki D, Kurisu S, Takenawa T. Regulation of cancer cell motility through actin reorganization. Cancer Sci. 2005 Jul;96(7):379–86.

34. Mason BN, Califano JP, Reinhart-King CA. Matrix Stiffness: A Regulator of Cellular Behavior and Tissue Formation. In: Bhatia SK, editor. Engineering Biomaterials for Regenerative Medicine [Internet]. New York, NY: Springer New York; 2012 [cited 2017 Jan 20]. p. 19–37. Available from: http://link.springer.com/10.1007/978-1-4614-1080-5_2

35. Sen S, Dong M, Kumar S. Isoform-Specific Contributions of α-Actinin to Glioma Cell Mechanobiology. Kreplak L, editor. PLoS ONE. 2009 Dec 23;4(12):e8427.

36. Sen S, Ng WP, Kumar S. Contributions of talin-1 to glioma cell-matrix tensional homeostasis. J R Soc Interface. 2012 Jun 7;9(71):1311–7.

37. Staunton JR, Doss BL, Lindsay S, Ros R. Correlating confocal microscopy and atomic force indentation reveals metastatic cancer cells stiffen during invasion into collagen I matrices. Sci Rep. 2016 Jan 27;6:19686.

38. Berry MF. Mesenchymal stem cell injection after myocardial infarction improves myocardial compliance. AJP Heart Circ Physiol. 2006 Jun 1;290(6):H2196–203.

39. Dean RG, Balding LC, Candido R, Burns WC, Cao Z, Twigg SM, et al. Connective Tissue Growth Factor and Cardiac Fibrosis after Myocardial Infarction. J Histochem Cytochem. 2005 Oct;53(10):1245–56.

40. Huang S, Ingber DE. Cell tension, matrix mechanics, and cancer development. Cancer Cell. 2005 Sep;8(3):175–6.

41. Levental KR, Yu H, Kass L, Lakins JN, Egeblad M, Erler JT, et al. Matrix Crosslinking Forces Tumor Progression by Enhancing Integrin Signaling. Cell. 2009 Nov;139(5):891–906.

42. Paszek MJ, Zahir N, Johnson KR, Lakins JN, Rozenberg GI, Gefen A, et al. Tensional homeostasis and the malignant phenotype. Cancer Cell. 2005 Sep;8(3):241–54.

43. White ES. Lung Extracellular Matrix and Fibroblast Function. Ann Am Thorac Soc. 2015 Mar;12(Supplement 1):S30–3.

44. Suki B. Assessing the Functional Mechanical Properties of Bioengineered Organs With Emphasis on the Lung: MECHANICAL PROPERTIES OF BIOENGINEERED ORGANS. J Cell Physiol. 2014 Sep;229(9):1134–40.

45. Ulrich TA, de Juan Pardo EM, Kumar S. The mechanical rigidity of the extracellular matrix regulates the structure, motility, and proliferation of glioma cells. Cancer Res. 2009 May 15;69(10):4167–74.

46. Wang Y, Wang G, Luo X, Qiu J, Tang C. Substrate stiffness regulates the proliferation, migration, and differentiation of epidermal cells. Burns. 2012 May;38(3):414–20.

47. Califano JP, Reinhart-King CA. Substrate Stiffness and Cell Area Predict Cellular Traction Stresses in Single Cells and Cells in Contact. Cell Mol Bioeng. 2010 Mar;3(1):68–75.

48. Deroanne C. In vitro tubulogenesis of endothelial cells by relaxation of the coupling extracellular matrix-cytoskeleton. Cardiovasc Res. 2001 Feb 16;49(3):647–58.

49. Reinhart-King CA, Dembo M, Hammer DA. Endothelial Cell Traction Forces on RGD-Derivatized Polyacrylamide Substrata †. Langmuir. 2003 Mar;19(5):1573–9.

50. Reinhart-King CA, Dembo M, Hammer DA. The Dynamics and Mechanics of Endothelial Cell Spreading. Biophys J. 2005 Jul;89(1):676–89.

51. Reinhart-King CA, Dembo M, Hammer DA. Cell-cell mechanical communication through compliant substrates. Biophys J. 2008 Dec 15;95(12):6044–51.

52. Tilghman RW, Cowan CR, Mih JD, Koryakina Y, Gioeli D, Slack-Davis JK, et al. Matrix Rigidity Regulates Cancer Cell Growth and Cellular Phenotype. Hotchin NA, editor. PLoS ONE. 2010 Sep 23;5(9):e12905.

53. Klein EA, Yin L, Kothapalli D, Castagnino P, Byfield FJ, Xu T, et al. Cell-Cycle Control by Physiological Matrix Elasticity and In Vivo Tissue Stiffening. Curr Biol. 2009 Sep;19(18):1511–8.

54. Jaffe AB, Hall A. RHO GTPASES: Biochemistry and Biology. Annu Rev Cell Dev Biol. 2005 Nov;21(1):247–69.

55. Shukla VC, Higuita-Castro N, Nana-Sinkam P, Ghadiali SN. Substrate stiffness modulates lung cancer cell migration but not epithelial to mesenchymal transition: SUBSTRATE STIFFNESS MODULATES LUNG CANCER CELL MIGRATION. J Biomed Mater Res A. 2016 May;104(5):1182–93.

56. Kaukonen R, Mai A, Georgiadou M, Saari M, De Franceschi N, Betz T, et al. Normal stroma suppresses cancer cell proliferation via mechanosensitive regulation of JMJD1a-mediated transcription. Nat Commun. 2016 Aug 4;7:12237.

57. Weaver VM, Petersen OW, Wang F, Larabell CA, Briand P, Damsky C, et al. Reversion of the Malignant Phenotype of Human Breast Cells in Three-Dimensional Culture and In Vivo by Integrin Blocking Antibodies. J Cell Biol. 1997 Apr 7;137(1):231–45.

5

MECHANICAL PHENOTYPING OF CELLS AND EXTRACELLULAR MATRIX AS GRADE AND STAGE MARKERS OF LUNG TUMOUR TISSUES

5.1 Introduction

The study of biomechanics and biophysics of cancer cells underline the role of the components of the cellular CSK in influencing some key functions such as cell mechanics, migration, differentiation, and neoplastic transformations (1–3). In fact modifications to the CSK induced by external stimuli, such as chemical, topographic and mechanical gradients embedded in the ECM, act in concert with the tumorigenic molecular signalling to affect malignant transformations (4–6).

In comparison with healthy cells, biomechanical investigations reported some common features of many types of tumour cell lines, such as a less structured CSK (7–9) with lower cell mechanical (10,11) and cytoadhesive (8,12,13) properties. All factors which, from a biophysical point of view, augment the metastatic potential of the cancer cells (7,8,10,13,14). The classical *in vitro* investigations focuses on the mechanical state of the cell and neglects the ancillary role of the tumour microenvironment in tumorigenesis and cancer progression. Indeed, the cancerous ECM foster some of the inherent malignant properties of transformed cells, and thus facilitated neoplastic progression, due to its ability to act as a storage compartment for growth-regulatory and antiapoptotic molecules, as well as a mechanical platform for cell attachment and movement (4,15,16). Going beyond the idea that tumorigenesis is mainly cell-autonomous process, in which progressive genetic derangement renders cells independent of the external context, following studies investigate how the transformation from health to malignancy alters the mechanical properties of cells within the tumour microenvironment (17).

Biophysical techniques reveal that cancer cells are more compliant than their healthy equivalents. This increase in cell deformability is accompanied by alterations in cytoarchitecture, associated with malignant transformation (18). Otherwise, the tissues affected by malignant tumours generally appear stiffer than healthy ones (19,20).

Part of this chapter is included in the paper *"Mechanical Phenotyping of Cells and Extracellular Matrix as Grade and Stage Markers of Lung Tumor Tissues"* , V. Panzetta, I. Musella; I. Rapa, M. Volante, P. A Netti, S. Fusco, submitted on Acta Biomaterialia (2017).

Therefore, for a very detailed mechanical phenotyping of tumours, it is necessary to consider the cross-talk between cells and their surrounding ECM. Indeed, a complex loop of interactions exists between cells and ECM: i) cells may modify the environment chemically by metalloproteinase secretion (21,22), or mechanically and topographically by generation and transmission of forces (23,24); ii) the ECM adapts and, thanks to its mechanical and topographic features, is able to induce structural modifications in the CSK and to trigger different cell functions and behaviours. To investigate the mechanical phenotyping of cells and tissues, have been used many techniques, like rheology or tissue elastography, suffering from poor spatial resolution and low force sensitivity. For this reason, it is supposed that the different mechanical characteristics of cancer cells could arise either from an imprecise mimicking of their *in vitro* micro-environment, or from an insufficient resolution of the mechanical characterization at a sub-cellular and sub-matricial level when tested *in vivo* or *ex vivo*.

In this work, human surgical tissue samples, removed from 10 patients affected by lung adenocarcinoma, were analysed using the multiple particles tracking (MPT) technique with the aim of mechanically phenotyping the tissues at cellular and ECM levels. A mechanical classification of the cells and the ECM of each sample was performed and compared with their healthy equivalents for all patients. Results and mechanical phenotypes were correlated to the stage and the grade of the tumour, previously assessed as part of the routine diagnostic procedure. In conclusion, we investigated and compared the ECM structure and morphology of both the tumour and the healthy tissues. This double-check mechanical characterization of *ex-vivo* biopsy tissues offers new diagnostic markers of the biophysical properties of the cells and the ECM (resolved at different spatial resolutions) and also gives new interpretative analytical points relating to cancer mechanobiology.

5.2 Materials and Methods

5.2.1 Samples

All experiments were performed in accordance with guidelines and regulations approved by the Research Ethics Committees of University of Naples and Turin. Experiments were performed on bioptic tissues from 10 patients with adenocarcinoma of the lung. One millimetre-thick tumour tissue fragments (approximately 1 cm^2) were isolated from fresh surgical specimens by means of a sterile scalpel. Corresponding healthy tissue samples were collected from lung parenchyma at least 3 cm away from the tumour nodule. After retrieval, tissue fragments were immediately prepared for cryopreservation as follows: samples were washed three times in a PBS buffer and transferred in 1.8 ml cryovials containing 1.5 ml of cryopreservation solution (RPMI 1640 medium supplemented with 10% fetal bovine serum and 10% DMSO). The cryovials were maintained at -20°C for 1h and then stored at -80°C. Tissues viability after cryopreservation was evaluated both with a Trypan blue assay and comparing the results of particle tracking experiments performed on a cryopreserved and 4% paraformaldehyde-fixed tissues.

Tissues were rapidly thawed in a 37°C water bath and maintained in complete medium during particle tracking experiments.

5.2.2 Cell culture

To study the effects of substrate stiffness on cell morphology and cytoskeletal structure, we used H522, an human lung cancer cell line. Cells were cultured at 37°C in 5% CO_2 in RPMI 1640 medium (GIBCO) supplemented with 10% Fetal Bovine Serum (FBS, GIBCO), 2mM L-glutamine (GIBCO), 5000 U/L penicillin (GIBCO), and 5000 μg/L streptomycin (GIBCO). Cells were plated at a concentration of 2000 cells/cm^2 on polyacrylamide gels of different stiffness.

5.2.3 Polyacrylamide substrata preparation and mechanical characterization

PAAm substrates were prepared by mixing acrylamide, methylene-bis-acrylamide to obtain from 0.3 kPa to 30 kPa hydrogels. The mechanical properties of PAAm

substrates were evaluated using a commercial AFM. The detailed preparation, functionalization and mechanical characterization of polyacrylamide substrates are described in Section 2.1.

5.2.4 Immunofluorescence labelling

Cells were plated at a density of 2000/cm^2 on 23 mm glass dishes (Fluorodish, World Precision Instrument). To evaluate the spreading area at 24h and 48h from seeding, cells were fixed and immunostained, as described in section 2.2.3.

5.2.5 Cell spreading area

Specimens were imaged using a Olympus IX81 inverted microscope and a 10× objective to quantify cell spreading. Fluorescent images were imported into ImageJ software (NIH, Bethesda, MD, USA) for postprocessing, analysis and quantification of the ventral cell area (cellular footprint). Individual cells were outlined and their areas were determined. More than 300 cells were analyzed for each substrate stiffness and for both time.

5.2.6 Ballistic injection and particle tracking intracellular and extracellular mechanics

Carboxyl-modified fluorescent polystyrene particles (0.50 μm diameter, Polyscience, Inc.) were introduced into the bioptic tissues using a ballistic gun (Bio-Rad, Hercules, CA). Helium gas at 2000 psi was used to force a macro-carrier disk coated with particles to crash into a stopping screen. The force of collision was transferred to the particles, causing their dissociation from the macro-carrier and the bombardment of tissues. Once bombarded, tissues were washed extensively with PBS and stained with vital DNA-specific dye, Hoechst 33342 (Life Technologies), at a 1:1000 dilution. Cell nuclei were stained in order to discriminate between cells and ECM during optical microscopy analyses. After incubation, tissues were washed with PBS and the motion of intra-cellular and extra-cellular fluorescent beads was recorded for a total of 5 s at 100 fps, as described in Section 2.3.1. The total number of analysed particles was at least 200 from more than 20 cells and regions for each sample.

PTM (see 2.3.1) allows the monitoring of local viscoelastic properties of living cells and the extra-cellular micro-environment with a high spatio-temporal resolution, collecting and analysing the Brownian motions of particles embedded in cytoplasm and ECM, respectively. The particle displacements were tracked from the very beginning of the videos taken of beads embedded into the cells and ECM. To generate the point tracking trajectories, an ad hoc Matlab (Matlab 7) code firstly detected the beads in each frame, and then it linked the points into trajectories. Each position was determined by intensity measurements through its centroid, and it was compared frame by frame to identify the trajectory for each particle, based on the principle that the closest positions in successive frames belong to the same particle (proximity principle). Once the nanoparticle trajectories had been obtained, MSDs were calculated (see 2.3.1). The particles embedded in regions with a thickness similar to or smaller than the particle diameter were excluded from the analysis (cell lamellar regions).

5.2.7 Tissue morphology

To prepare tissues for observation under microscope, they were embedded in OCT and then sliced (see 2.2.5). A Confocal Leica TCS SP5 II combined with a multi-photon laser source was used to investigate tissue morphology. The sectioned samples were stained for actin microfilaments and nucleus detections (see 2.2.5).

5.2.8 Immunohistochemical analysis

Basal membrane material was highlighted by immunohistochemical detection of laminin (Novocastra; clone 4C7, diluted 1:50). A standard automated (Dako Autostainer, Glostrup, Denmark) immunoperoxidase procedure was employed, and immunoreactions were shown by a biotin-free dextran-chain detection system (Envision, Dako), and developed using diaminobenzidine as the chromogen.

5.2.9 Statistical Analysis

Data are reported as mean ± standard error (SE), unless otherwise indicated. Statistical comparisons were performed with a Student's unpaired test. P values < 0.05 denote statistical significance.

5.3 Results

5.3.1 Tissue viability assay

Before performing particle tracking analyses of *ex vivo* lung tissues, a Trypan Blue assay was used in order to evaluate the viability of tissues after cryopreservation. The tissue samples were rapidly thawed in a 37°C water bath, maintained in complete medium and stained with Trypan Blue. The results (not shown) suggest that post-thaw tissue viability was maintained when cryopreserved by using DMSO. We also compared MSDs of cryopreserved and 4% paraformaldehyde-fixed tissues. MSDs of fixed tissues were close to the noise floor and appeared to flatten out, as consequence of cell death. On the contrary, MSDs of cryopreserved tissues indicated a sub-diffusive behaviour, which originated from actin network confinement and cytoskeletal hindrance (Fig.1).

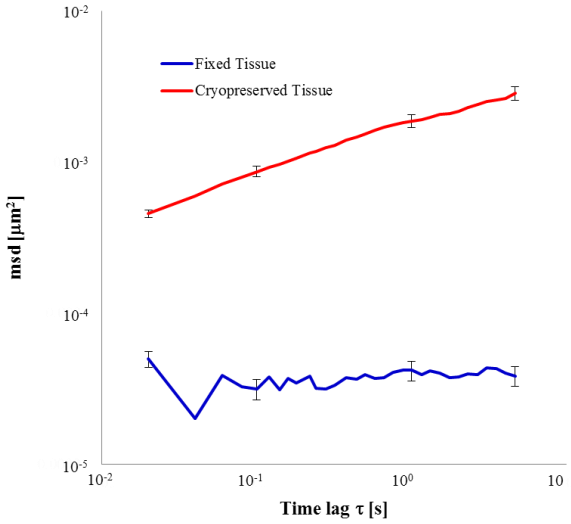

Figure 1 Ensemble-averaged MSDs of 500 nm fluorescent particles in cryopreserved and 4% paraformaldehyde-fixed tissues (both in cells and ECM). MSDs of fixed tissues were close to the noise floor and appeared to flatten out, as consequence of cell death. On the contrary, MSDs of cryopreserved tissues indicated a sub-diffusive behaviour, which originated from actin network confinement and cytoskeletal hindrance.

5.3.2 Particle tracking microrheology

Particle tracking microrheology allowed to analyse *ex vivo* lung tissues, distinguishing between cells and ECM contributions. Polystyrene beads (500 nm) were introduced through ballistic injection into the biopsy tissues. The spontaneous motion of the

probing beads across cell cytoskeleton and ECM structures was tracked to calculate the MSD. The amplitude and the slope of MSDs can be correlate to the mechanical properties of the intracellular and extracellular microenvironment. Tissue were stained with a fluorescent dye to label nuclei and thus, to distinguish cells from their surrounding ECM. In this way, we could compare the MSDs of particles exploring the cytoplasm and the ECM of healthy and tumour tissues. Fig. 2 shows that particles introduced in cells of adenocarcinoma tissues exhibited greater MSDs at all explored lag times as compared to cells of normal tissues.

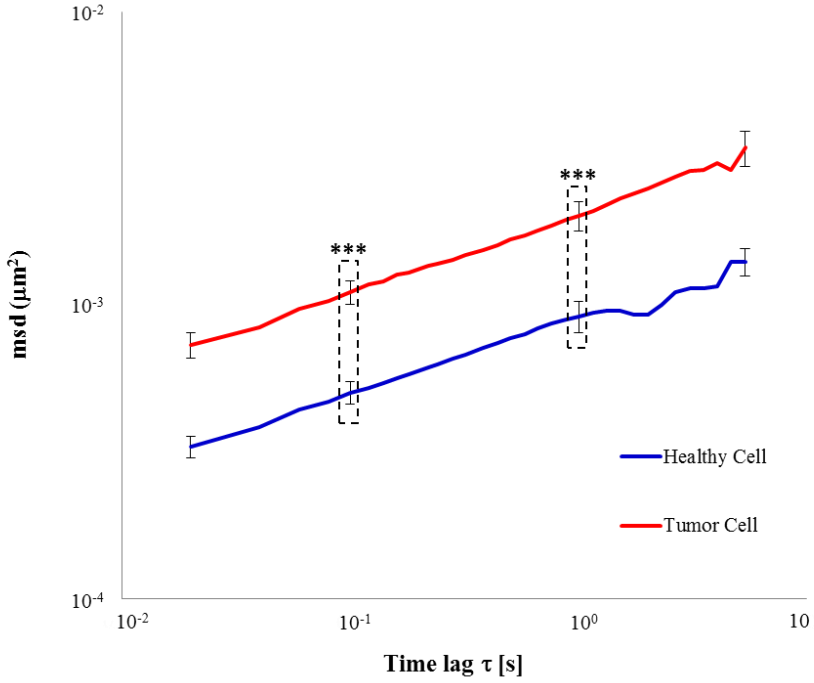

Figure 2 Ensemble-averaged MSDs of 500 nm fluorescent particles in cells of healthy (blue line) and adenocarcinoma (red line) tissues. ***, $p<0.001$; $n>700$ for all studied cases.

On the other side, particle tracking analyses revealed also that MSDs in tumour ECM are smaller in comparison to healthy tissues at all time lags (Fig.3).

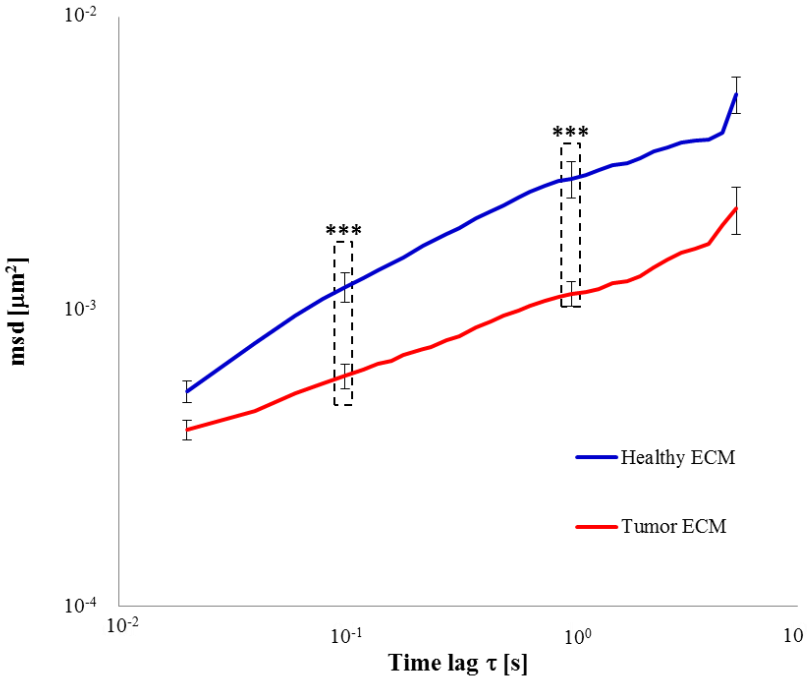

Figure 3 Ensemble-averaged MSDs of 500 nm fluorescent particles in ECM of healthy (blue line) and adenocarcinoma (red line) tissues. ***, p<0.001; n>700 for all studied cases.

We selected the averaged measured MSD at τ=1s (Fig.4). We observed that, from healthy to tumour tissues, MSDs amplitude of the probes embedded in the cells increased significantly of 2.5 times, while MSDs of ECM decreased of the same value (Fig. 4 a, b).

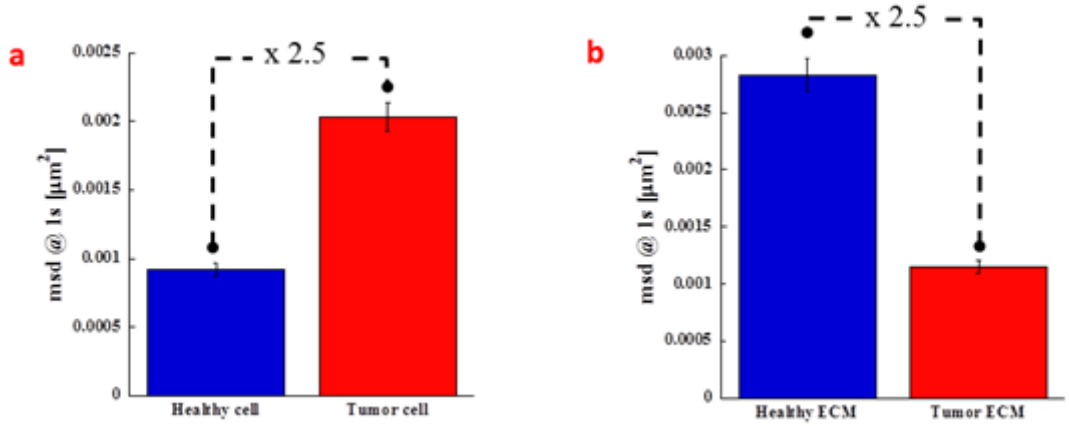

Figure 4 The average measured MSD at 1 s turned out to be 2.5 times higher in tumour cells than in healthy ones (a), indicating a cell softening during cancerous transformation. Contrarily, the decrease of MSD in tumour ECM indicated a matrix stiffening that promotes in several ways tumour progression.

These results highlighted that, in tumour tissues, cells resulted more compliant although they were located in a stiffer matrix. This aspect could be the consequence of a damaged mechanosensing due to pathological state. In order to investigate more thoroughly this aspect we cultured H522 cells from lung adenocarcinoma on polyacrylamide substrates which had different stiffness (see Fig.5). The polymeric substrates were fabricated mimicking an ECM stiffening from 4 to 30 kPa and evaluating the cell spreading area at 24 and 48 h. Cell spreading, in fact, represents a very good indicator of the mechanosensing process of cells (25). As shown in Fig.5, H522 cells presented a different morphology on the substrates, with a higher spreading area on the stiffer substrate (30 kPa). H522 sense the stiffness of the polyacrylamide substrates which increases the cell area and reorganizes their cytoskeleton when moving from 4 to 30 kPa. Nevertheless, from previous works it has been shown that the ability of mechanosensing may be different depending on the tumour cell line (26) and all the experimental evidence came from in vitro characterizations. During in vitro experiments we were able to recreate some physiological conditions, but it is impossible to control and replicate them all. As shown, in the comparison between the mechanical behaviour of cells in biopsy tissue and 2D culture, tumour cells could display different behaviours and characteristics, depending on the nature of the surrounding environment.

5.3.3 Dependence of Nanomechanical Properties on Tumour Grade and Stage

The analysed samples were classified according to the grade and the stage (Table 1), as they were defined by the most recent classification of lung tumours (27). Through particle tracking experiments, we also searched for a correlation between the nanomechanical properties of bioptic tissues and their grade and stage. Unfortunately, samples of grade 1 were missing in the sample patients (10) we investigated, but, as shown in Fig. 6a, we found a clear correlation between MSDs of cells and tumour grade. MSDs and cell deformability increase in a significant way when tumour grade passes from 2 to 3, resulting about 2 and 5 times higher than normal tissues in the case of grade 2 and 3, respectively.

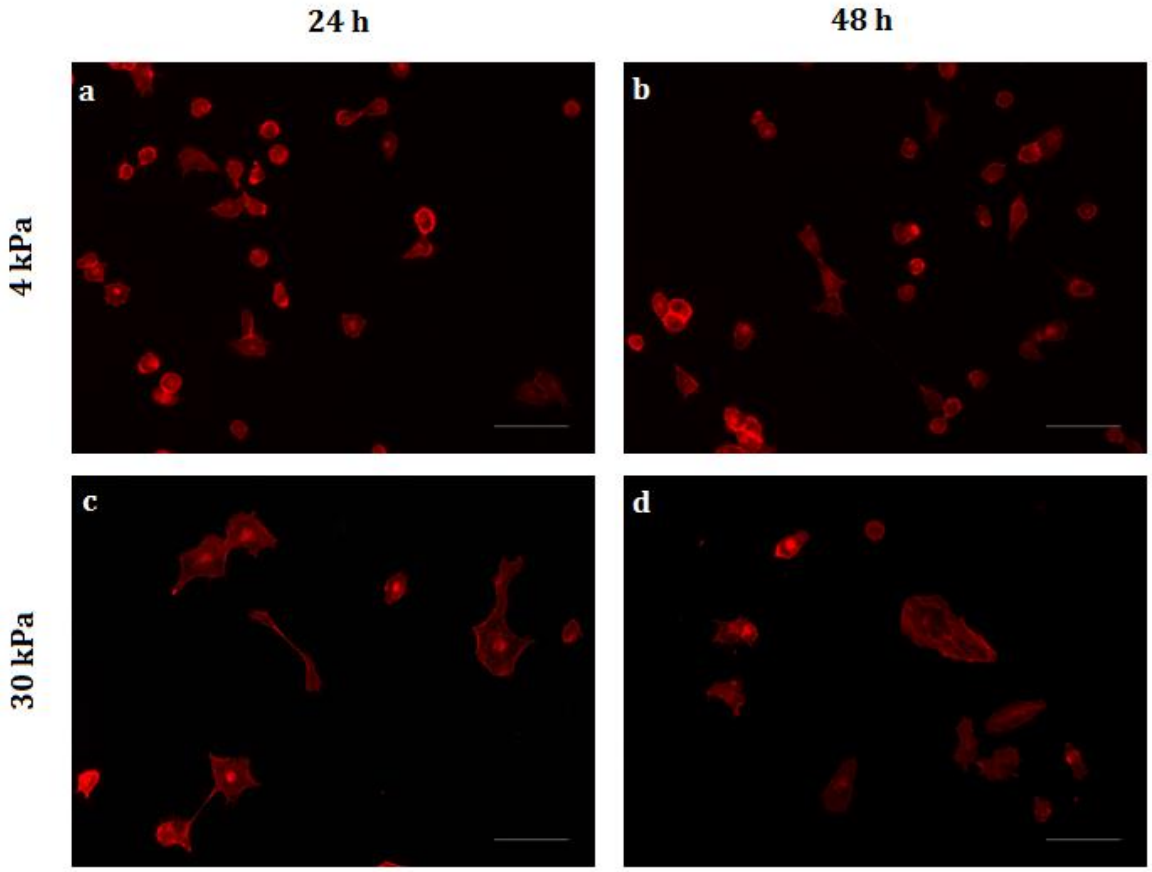

Figure 5 Analysis of H522 cells on polyacrylamide gels. Phalloidin staining of cells plated on substrates of different stiffness: 4 kPa (a), 30 kPa (b). Scale bars are 100 μm.

Conversely, Fig. 6b reports that the ECM stiffening process -we registered the passage from a normal to a tumour tissue- is not directly dependent on the tumour grade. In Fig. 7 is shown that the ensemble averaged MSDs of probes in cells of grade 3 samples resulted higher than those of particles in cells of grade 2 tissues and, consequently, healthy tissues. On the other hand, Fig. 8 shows that, MSDs of nanoparticles in ECM of adenocarcinoma tissues did not change with tumour grade and they resulted lower than MSDs of probes in ECM of normal tissues, for all time lag. Such findings are in agreement with tumour grading assessed by conventional morphological procedure for lung tumour (Fig. 6c-f). In fact, it is based on how much tumour cells differ morphologically and grow faster than normal cells and not on ECM structural changes during tumour progression.

Sample	Grade	Stage	Diameter (cm)	pT	pN	pL
1	2	1	2	pT1a	pN0	pL0
2	2	1	2.6	pT2b	pN0	pL0
3	2	1	2.7	pT1b	pN0	pL0
4	2	1	2.8	pT1b	pN0	pL0
5	2	1	3.2	pT2a	pN0	pL1
6	2	3	2.5	pT1b	pN2	pL0
7	2	3	2	pT1b	pN2	pL0
8	3	1	3.2	pT2a	pN0	pL0
9	3	3	2.8	pT1b	pN2	pL0
10	3	3	2.5	pT1b	pN2	pL0

Table 1 Parameters of classification of analyzed adenocarcinoma samples: grade, stage, size, pathological assessment of the primary tumor (pT), pathological assessment of the regional lymph nodes (pN), visceral pleural invasion (pL).

Notwithstanding the grade, the stage of the tumour resulted correlated strictly with the mechanical properties of both cells and ECM. In this case, it is very important for the classification also the tumour architecture, which is defined by evaluating the presence of sheets or solid nests with incorporating fibrotic tissue. In particular, MSDs of NPs in cells significantly increased when the tumour advances from stage 1 to 3 (Fig. 6g). Inversely, MSDs decreased sensitively in ECM from normal tissue to cancer at stage 1 and 3 (Fig. 6h). As in the case of the grade, the sample population lacked stage 2. By comparing the MSDs of tumour tissues at stage 1 and 3 we found an increase of 2.3- and 3.5-fold times for tumour cells compared to their healthy counterparts and a decrease of 2- and 4-fold times for ECM. In Fig. 9-10, we report the averaged MSDs of particles, respectively, in cells and ECM and we noticed a decreasing in cell mechanical properties and an increasing in ECM mechanics, with tumour stage growing.

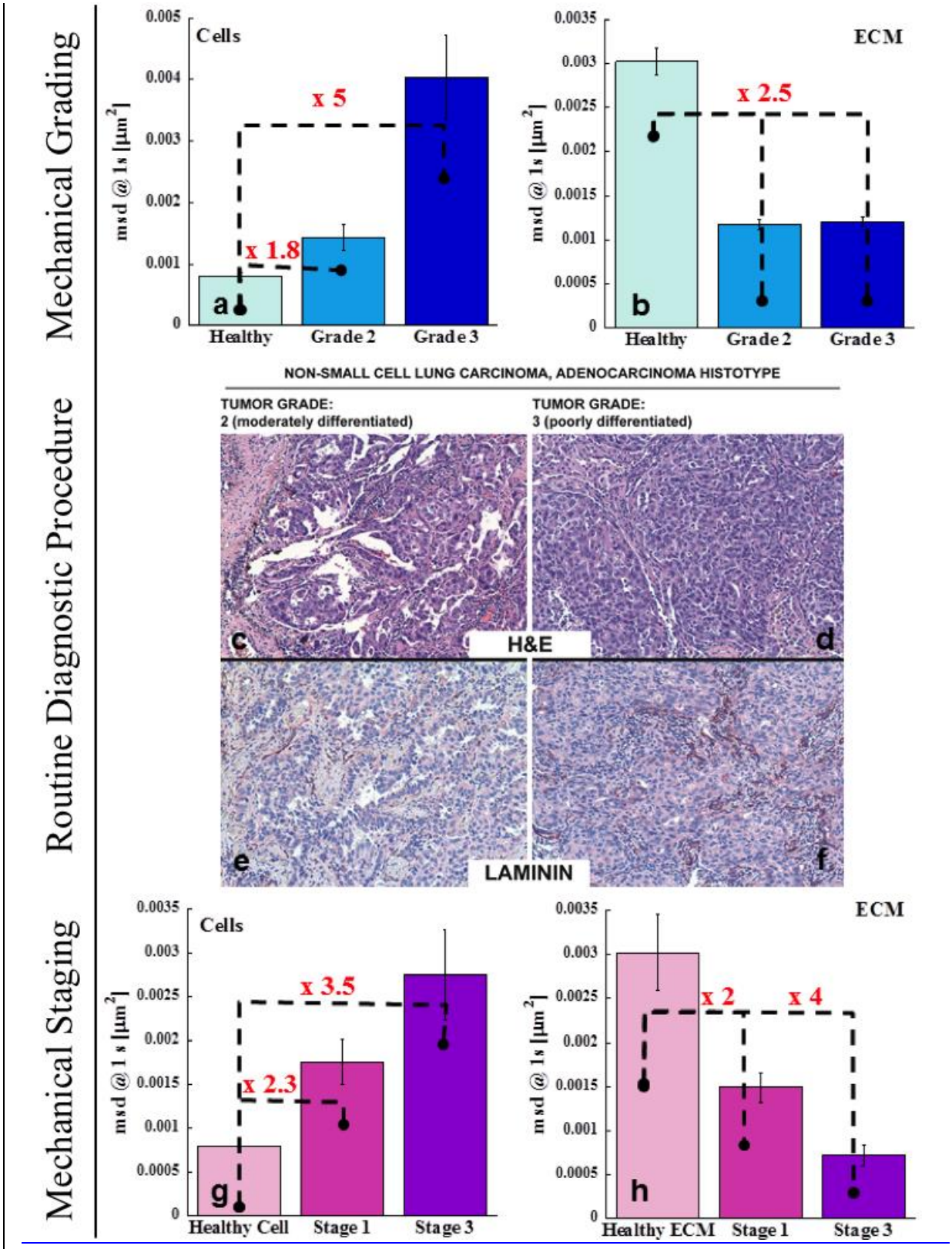

Figure 6 (a, b) MSDs of nanoparticles (NPs) inside the cells correlated directly with tumour grade, increasing 2- and 5-fold for tumour grade 2 and 3, respectively (a). Contrarily, it seems that there is not a strict correlation between cancer grade (2 and 3) and matrix stiffening (b). (c-f) Adenocarcinoma tumours were stained with hematoxylin and eosin (H&E) (top) and laminin (bottom). Original magnification, 200× for all images. (g, h)Both MSDs of NPs inside the cells and in the ECM correlated directly with the tumour stage.

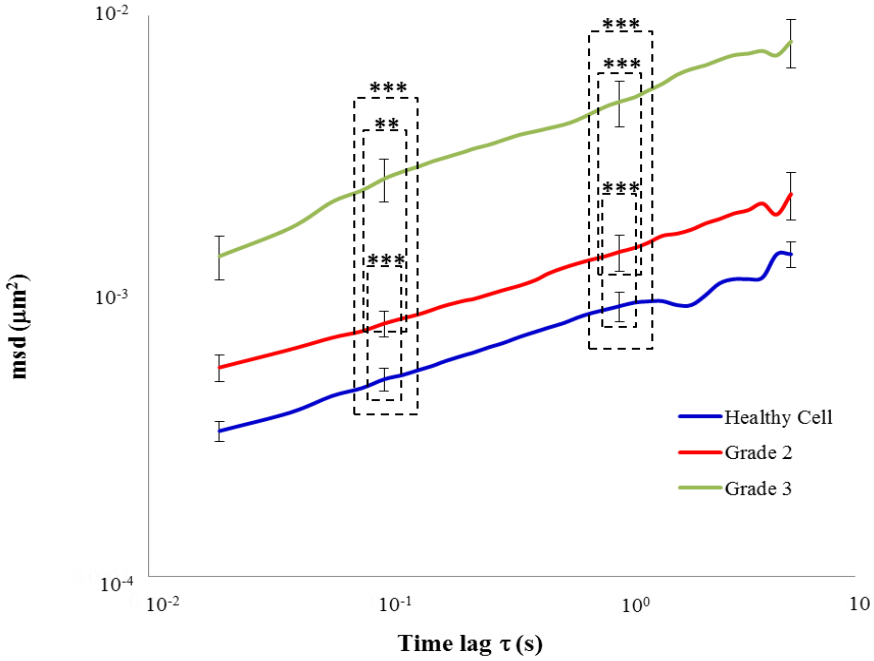

Figure 7 Ensemble-averaged MSDs of 500 nm fluorescent particles in cells of healthy (blue line) and adenocarcinoma grade 2 (red line) and grade 3 (green line) tissues. **, p<0.01, ***, p<0.001; n between 200 and 600 for all studied cases.

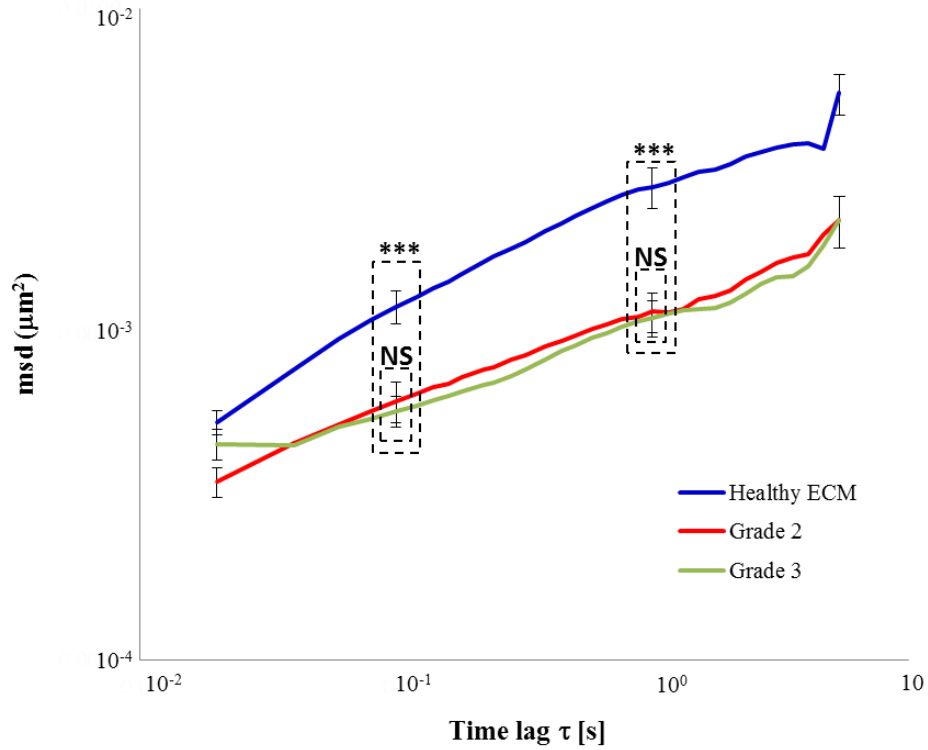

Figure 8 Ensemble-averaged MSDs of 500 nm fluorescent particles in ECM of healthy (blue line) and adenocarcinoma grade 2 (red line) and grade 3 (green line) tissues. **, p<0.01, ***, p<0.001; n between 200 and 600 for all studied cases.

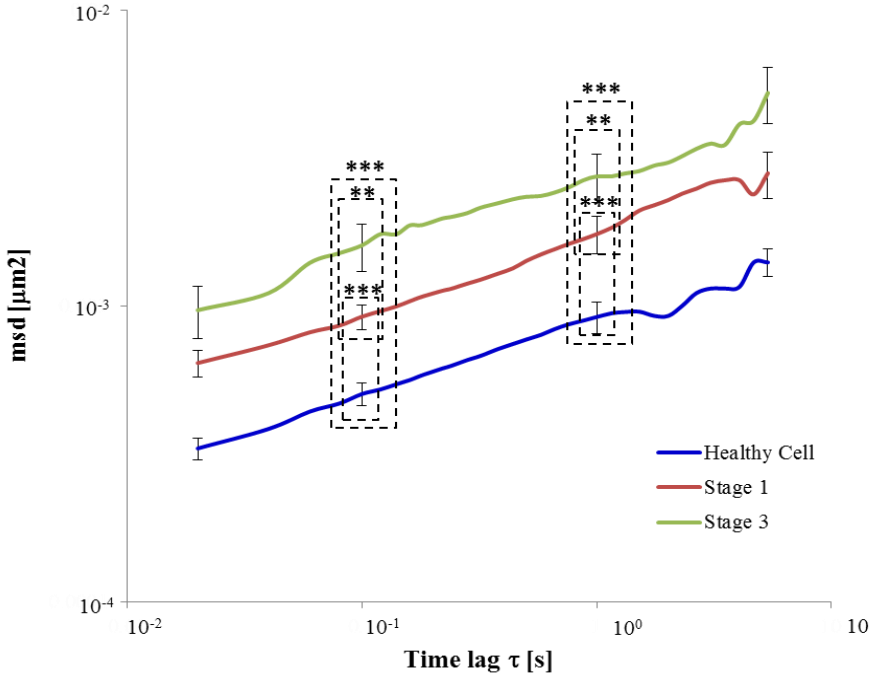

Figure 9 Ensemble-averaged MSDs of 500 nm fluorescent particles in cells of healthy (blue line) and adenocarcinoma stage 1 (red line) and stage 3 (green line) tissues. **, p<0.01, ***, p<0.001; n between 200 and 700 for all studied cases.

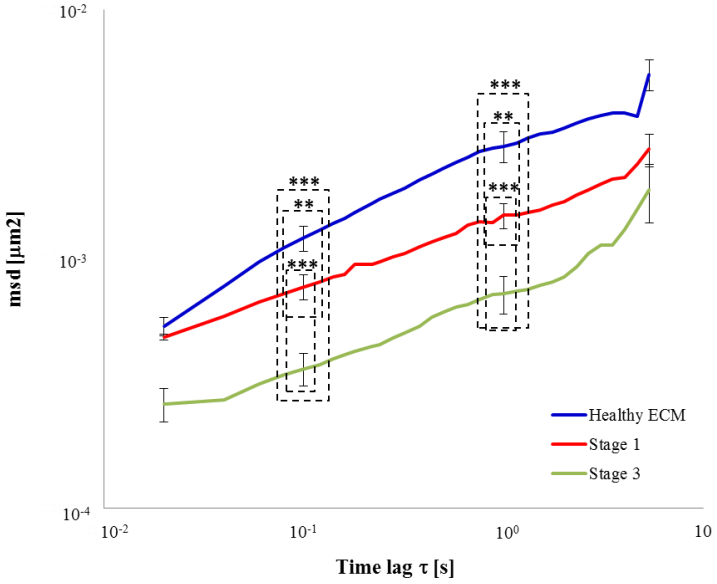

Figure 10 Ensemble-averaged MSDs of 500 nm fluorescent particles in ECM of healthy (blue line) and adenocarcinoma stage 1 (red line) and stage 3 (green line) tissues. **, p<0.01, ***, p<0.001; n between 200 and 700 for all studied cases.

5.3.4 Tissue morphology

By combining confocal fluorescence and second harmonic generation (SHG), we investigated the spatial distribution of cells and collagen in normal and tumour samples (Fig.11). The structural changes in tumour ECM architecture, which occur with transformation from healthy tissues to adenocarcinomas are clear. In normal lung tissues collagen fibres were curly, isotropically and uniformly distributed (Fig. 11b). In tumour tissues the bundles were thicker, linearized and presented a higher density, as the SHG reconstruction has higher average intensity (Fig. 11f). Moreover, cells were different in number and organization. Tumour slices presented a higher amount of cells which clumped in reservoirs between the collagen bundles.

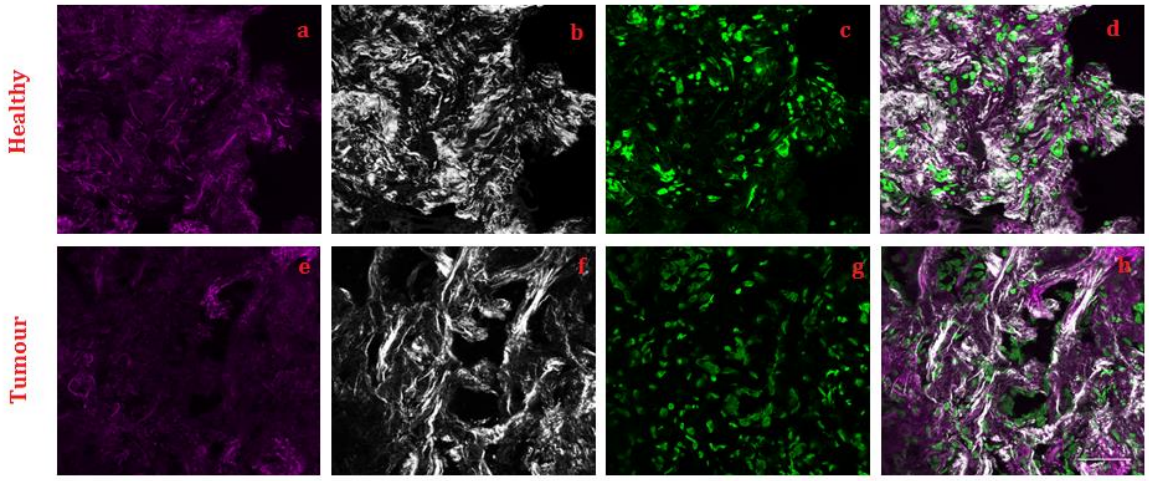

Figure 11 (a-h) Phalloidin staining of actin (magenta, a-e), collagen by second harmonic generation (SHG-white, b-f) and Hoechst staining of nuclei (green, c-g) of healthy (top) and tumor (bottom) lung biopsies. Scale bar, 50 μm.

5.4 Discussion and conclusions

Particle tracking microrheology was performed to correlate the nanomechanical properties of *ex vivo* lung tissue to its pathophysiological state. Biopsy tissues were stored cryopreserved (see 5.2.1), so the viability of sample was tested before particle tracking analyses. Fluorescent particles (500 nm) were introduced through a ballistic bombardment into the samples and tracked to obtain their motion across cell cytoskeleton and ECM structures. Tissue samples were stained with a fluorescent dye to label nuclei. In this way, we could distinguish cells from their surrounding ECM and

calculate the MSD of probes exploring both intra-cellular and extra-cellular environment. In this analysis, healthy/tumour cells and stromal cells were not distinguished basing on their morphological characteristics and specific functions. In fact, the purpose of this work was to evaluate the mechanical properties of the intra-cellular micro-environment by considering the collaborative and synergetic interactions between tumour and stromal cells in the emergence of the hallmarks of the cancer. As has already been demonstrated (28), the amplitude and the slope of MSD is inversely related to the mechanical properties of the environment probed by particles. Thus, we compared the MSDs of particles introduced in cytoplasm and in ECM of healthy and tumour lung removed from each patient. MPT analyses showed that the cancerous transformation of tissues had a remarkable effect on the dynamics of the tracer beads in tumour cells and their associated ECM. This evidence, obtained from averaging all the *ex vivo* samples investigated with no distinction between grade and stage of tumour, was in line with well-established results *in vitro* and with more recent *ex vivo* comparisons (17,29). The observed increased motion of particles in cells of adenocarcinoma tissue (Fig. 2) could be associated to a less structured cytoskeleton and then to an increase in the compliance or deformability of cells, as already observed in 2D (10,11) and 3D (30) *in vitro* systems. In fact, it was demonstrated that cell softening is strictly correlated with cancerous transformation, characterized by resistance to anoikis, cell anchorage-independent growth, capability to migrate and invade distant tissues (31). Furthermore, the onset of cancer is also characterized by a change in the mechanical properties of the extracellular-microenvironment, which becomes stiffer within malignant tissues. Indeed, MPT analyses revealed that MSDs in tumour ECM are smaller in comparison to normal tissue at all time lags (Fig. 3). During the last years there has been a gradual accumulation of evidence suggesting that a stiffening of the ECM promotes cancer progression and cell transformation from normal to malignant to metastatic (24,32,33). In particular, the enhancement of collagen cross-linking and consequently the ECM stiffness, results in increased integrin activity and focal adhesion signalling that promote tumour proliferation, survival and invasiveness (24).The alteration of integrin adhesions in malignancy are associated to the miR-18a circuit that is activated by tensile forces generated by stiffened ECM (34). In fact, increased EMC

stiffness influences miR-18a expression, leading to PI3K-dependent malignant progression (34). The increase of the mean square displacement when nanobeads were embedded in the cells and the decrease in the ECM (Fig. 4) suggest a sort of symmetric modification of the mechanical properties of the cells and the extra-cellular matrix caused by the onset of a tumour. Most unexpectedly, it was noted that cells in tumour tissues resulted as being more compliant although residing in a stiffer matrix. This suggests that damaged/compromised mechanosensing machinery may be present in cancer cells. This situation was accurately investigated culturing H522 cells from lung adenocarcinoma on polyacrylamide substrates of different stiffness (form 4 to 30 kPa) to mime an ECM stiffening. We evaluated the cell spreading area at 24 and 48h because this parameter represents a very good indicator of the mechanosensing process of cells (25). Our results show that H522 could sense the difference of substrate stiffness and exhibited a different morphology on them(Fig.5). Previously works demonstrated that the ability of mechanosensing may be different depending on the tumour cell line (26) and all the experimental evidence came from in vitro characterizations. During in vitro experiments was impossible to control and replicate all physiological conditions. Thus, not necessarily cells in adenocarcinoma biopsy tissues lost their mechanosensing capability, but surely, as shown, in the comparison between the mechanical behaviour of cells in biopsy tissue and 2D culture, tumour cells could display different behaviours and characteristics, depending on the nature of the surrounding environment.

Different ECM organizations in tumour biopsies are also revealed in the actin, nuclei and collagen stained sections (Fig. 11). The structural changes in tumour ECM architecture, which occur with transformation from healthy tissues to adenocarcinomas are clear. We observed curly, isotropically and uniformly distributed collagen fibres in normal lung tissues (Fig. 11b) while in tumour tissues the bundles were thicker, linearized and presented a higher density, as the SHG reconstruction has higher average intensity (Fig. 11f). Such linear collagen bundles were the fibrous substrate on which cells could migrate at high velocity and with high persistence (35). Moreover, cells were different in number and organization. Tumour slices presented a higher amount of cells which clumped in reservoirs between the

collagen bundles. This was indicative of a different production and remodelling of ECM from normal and tumour cells and, consequently, as already confirmed from MPT analysis, different mechanical properties.

We also investigated the existence of a correlation between the nanomechanical properties of biopsy tissues and their grade and stage as they were defined by the most recent classification of lung tumours (27). The sample population lacked the grade 1, but we found a clear correlation between MSDs of cells and tumour grade anyway. In particular, MSDs and cell deformability increase in a significant way when tumour grade passes from 2 to 3, resulting about 2 and 5 times higher than normal tissues in the case of grade 2 and 3, respectively (Fig. 6a). This observation supports the idea that cells undergo a trans-differentiation process during tumour progression (36). Conversely, Fig. 6b reports that the ECM stiffening process -we registered the passage from a normal to a tumour tissue- is not directly dependent on the tumour grade. Such findings are in agreement with tumour grading assessed by conventional morphological procedure for lung tumour (Fig. 6c-f). In fact, it is based on how much tumour cells differ morphologically and grow faster than normal cells and not on ECM structural changes during tumour progression. In particular, the most important factor in grading analysis of lung adenocarcinoma is the degree of cytologic atypia, defined by nuclear pleomorphism and presence of distinct nucleoli. Fig. 6 shows representative H&E stained-sections of tumour of grade 2 and grade 3. In the case of grade 2 (Fig. 6c), tumour shows a solid and glandular growth and cells with moderately pleomorphic nuclei and greater nucleus/cytoplasm ratio. The grade 3 tumour presented almost entirely solid nests or cords of cells with very poorly pleomorphic nuclei and a variable quantity of cytoplasm. In addition, in the case of the grade 3 tumour, it is possible to observe a more abundant deposition of laminin around the tumour cell nests, confirming the observation of more bountiful ECM components that contribute to increase ECM stiffness.

Notwithstanding the grade, the stage of the tumour resulted correlated strictly with the mechanical properties of both cells and ECM. In this case, it is very important for the classification also the tumour architecture, which is defined by evaluating the presence of sheets or solid nests with incorporating fibrotic tissue. In particular,

MSDs of NPs in cells significantly increased when the tumour advances from stage 1 to 3 (Fig. 6g). Inversely, MSDs decreased sensitively in ECM from normal tissue to cancer at stage 1 and 3 (Fig. 6h). As in the case of the grade, the sample population lacked stage 2. A linear progression of the softening process occurring during the trans-differentiation pathway of the tumour was observed by analysing the mechanical properties of the cells. In fact, by comparing the MSDs of tumour tissues at stage 1 and 3 we found an increase of 2.3- and 3.5-fold times for tumour cells compared to their healthy counterparts and a decrease of 2- and 4-fold times for ECM. As reported in the Table. 1, at stage 1 tumour cells were not found in regional lymph nodes in any of the tissues (tumours were classified as N0), while in tumours at stage 3, N was assigned a value of 2, indicating that the tumour had spread to regional lymph nodes. Lymph node invasion may mean that the cancer is growing fast and represents one of the first steps in the pathogenesis of metastasis, increasing the probability of developing a secondary tumour (37,38). A recent study demonstrated that cancer cells which metastasized to the lymph nodes up-regulate most important ECM proteins, in particular collagen I fibres, forming a “freeway” for metastasis (39). In particular, in the case of lung cancer, it was observed that an altered ECM cross-linking is found within lung cancer: high laminin-5 expression and Lysyl oxidase-mediated collagen cross-linking correlated with lung cancer invasiveness (40). This result is consistent with our findings that tumour stage and cancer stiffening are closely associated.

5.5 References of Chapter 5

1. Fletcher DA, Mullins RD. Cell mechanics and the cytoskeleton. Nature. 2010 Jan 28;463(7280):485–92.

2. Connelly JT, Gautrot JE, Trappmann B, Tan DW-M, Donati G, Huck WTS, et al. Actin and serum response factor transduce physical cues from the microenvironment to regulate epidermal stem cell fate decisions. Nat Cell Biol. 2010 Jul;12(7):711–8.

3. Yamaguchi H, Condeelis J. Regulation of the actin cytoskeleton in cancer cell migration and invasion. Biochim Biophys Acta BBA - Mol Cell Res. 2007 May;1773(5):642–52.

4. Comoglio, P. M.; Trusolino, L. Cancer:the matrix is now in control.pdf. Nature medicine; 2005.

5. Yilmaz M, Christofori G. EMT, the cytoskeleton, and cancer cell invasion. Cancer Metastasis Rev. 2009 Jun;28(1–2):15–33.

6. Pathak A, Kumar S. Biophysical regulation of tumor cell invasion: moving beyond matrix stiffness. Integr Biol. 2011;3(4):267.

7. Lin Z, Han Y, Wu B, Fang W. Altered cytoskeletal structures in transformed cells exhibiting obviously metastatic capabilities. Cell Res. 1990 Dec;1(2):141–51.

8. Raz A, Geiger B. Altered organization of cell-substrate contacts and membrane-associated cytoskeleton in tumor cell variants exhibiting different metastatic capabilities. Cancer Res. 1982 Dec;42(12):5183–90.

9. Panzetta V, De Menna M, Bucci D, Giovannini V, Pugliese M, Quarto M, et al. X-RAY IRRADIATION AFFECTS MORPHOLOGY, PROLIFERATION AND MIGRATION RATE OF HEALTHY AND CANCER CELLS. J Mech Med Biol. 2015 Apr;15(2):1540022.

10. Cross SE, Jin Y-S, Rao J, Gimzewski JK. Nanomechanical analysis of cells from cancer patients. Nat Nanotechnol. 2007 Dec;2(12):780–3.

11. Lekka M, Laidler P, Gil D, Lekki J, Stachura Z, Hrynkiewicz AZ. Elasticity of normal and cancerous human bladder cells studied by scanning force microscopy. Eur Biophys J. 1999 May 25;28(4):312–6.

12. Cavallaro U, Christofori G. Cell adhesion and signalling by cadherins and Ig-CAMs in cancer. Nat Rev Cancer. 2004 Feb;4(2):118–32.

13. Oka H, Shiozaki H, Kobayashi K, Inoue M, Tahara H, Kobayashi T, et al. Expression of E-cadherin cell adhesion molecules in human breast cancer tissues and its relationship to metastasis. Cancer Res. 1993 Apr 1;53(7):1696–701.

14. Volk T, Geiger B, Raz A. Motility and adhesive properties of high- and low-metastatic murine neoplastic cells. Cancer Res. 1984 Feb;44(2):811–24.

15. Lu P, Weaver VM, Werb Z. The extracellular matrix: A dynamic niche in cancer progression. J Cell Biol. 2012 Feb 20;196(4):395–406.

16. Bissell MJ, Radisky D. Putting tumours in context. Nat Rev Cancer. 2001 Oct;1(1):46–54.

17. Plodinec M, Loparic M, Monnier CA, Obermann EC, Zanetti-Dallenbach R, Oertle P, et al. The nanomechanical signature of breast cancer. Nat Nanotechnol. 2012 Oct 21;7(11):757–65.

18. Suresh S. Biomechanics and biophysics of cancer cells☆. Acta Mater. 2007 Jul;55(12):3989–4014.

19. Butcher DT, Alliston T, Weaver VM. A tense situation: forcing tumour progression. Nat Rev Cancer. 2009 Feb;9(2):108–22.

20. Sinkus R, Lorenzen J, Schrader D, Lorenzen M, Dargatz M, Holz D. High-resolution tensor MR elastography for breast tumour detection. Phys Med Biol. 2000 Jun;45(6):1649–64.

21. Egeblad M, Werb Z. New functions for the matrix metalloproteinases in cancer progression. Nat Rev Cancer. 2002 Mar;2(3):161–74.

22. Deryugina EI, Quigley JP. Matrix metalloproteinases and tumor metastasis. Cancer Metastasis Rev. 2006 Mar;25(1):9–34.

23. Malik R, Lelkes PI, Cukierman E. Biomechanical and biochemical remodeling of stromal extracellular matrix in cancer. Trends Biotechnol. 2015 Apr;33(4):230–6.

24. Levental KR, Yu H, Kass L, Lakins JN, Egeblad M, Erler JT, et al. Matrix Crosslinking Forces Tumor Progression by Enhancing Integrin Signaling. Cell. 2009 Nov;139(5):891–906.

25. Guarnieri D, Muscetti O, Falanga A, Fusco S, Belli V, Perillo E, et al. Surface decoration with gH625-membranotropic peptides as a method to escape the endo-lysosomal compartment and reduce nanoparticle toxicity. Nanotechnology. 2015 Oct 16;26(41):415101.

26. Li J, Wu Y, Schimmel N, Al-Ameen MA, Ghosh G. Breast cancer cells mechanosensing in engineered matrices: Correlation with aggressive phenotype. J Mech Behav Biomed Mater. 2016 Aug;61:208–20.

27. Travis WD, Brambilla E, Burke AP, Marx A, Nicholson AG. Introduction to The 2015 World Health Organization Classification of Tumors of the Lung, Pleura, Thymus, and Heart. J Thorac Oncol. 2015 Sep;10(9):1240–2.

28. Hoffman BD, Massiera G, Van Citters KM, Crocker JC. The consensus mechanics of cultured mammalian cells. Proc Natl Acad Sci. 2006 Jul 5;103(27):10259–64.

29. Tian M, Li Y, Liu W, Jin L, Jiang X, Wang X, et al. The nanomechanical signature of liver cancer tissues and its molecular origin. Nanoscale. 2015;7(30):12998–3010.

30. Baker EL, Lu J, Yu D, Bonnecaze RT, Zaman MH. Cancer Cell Stiffness: Integrated Roles of Three-Dimensional Matrix Stiffness and Transforming Potential. Biophys J. 2010 Oct;99(7):2048–57.

31. Liotta LA, Kohn E. Anoikis: Cancer and the homeless cell. Nature. 2004 Aug 26;430(7003):973–4.

32. Paszek MJ, Zahir N, Johnson KR, Lakins JN, Rozenberg GI, Gefen A, et al. Tensional homeostasis and the malignant phenotype. Cancer Cell. 2005 Sep;8(3):241–54.

33. Provenzano PP, Inman DR, Eliceiri KW, Knittel JG, Yan L, Rueden CT, et al. Collagen density promotes mammary tumor initiation and progression. BMC Med [Internet]. 2008 Dec [cited 2017 Jan 18];6(1). Available from: http://bmcmedicine.biomedcentral.com/articles/10.1186/1741-7015-6-11

34. Mouw JK, Yui Y, Damiano L, Bainer RO, Lakins JN, Acerbi I, et al. Tissue mechanics modulate microRNA-dependent PTEN expression to regulate malignant progression. Nat Med. 2014 Mar 16;20(4):360–7.

35. Condeelis J, Segall JE. Intravital imaging of cell movement in tumours. Nat Rev Cancer. 2003 Dec;3(12):921–30.

36. Thiery JP. Epithelial–mesenchymal transitions in tumour progression. Nat Rev Cancer. 2002 Jun;2(6):442–54.

37. Alitalo K, Tammela T, Petrova TV. Lymphangiogenesis in development and human disease. Nature. 2005 Dec 15;438(7070):946–53.

38. Gupta GP, Massagué J. Cancer Metastasis: Building a Framework. Cell. 2006 Nov;127(4):679–95.

39. Rizwan A, Bulte C, Kalaichelvan A, Cheng M, Krishnamachary B, Bhujwalla ZM, et al. Metastatic breast cancer cells in lymph nodes increase nodal collagen density. Sci Rep. 2015 May 7;5:10002.

40. Wood SL, Pernemalm M, Crosbie PA, Whetton AD. The role of the tumor-microenvironment in lung cancer-metastasis and its relationship to potential therapeutic targets. Cancer Treat Rev. 2014 May;40(4):558–66.

6

Conclusions

6.1 Conclusions

Tumour tissues exhibit specific biological and biophysical characteristics that distinguish them from healthy tissues. The features accompanying tumour progression have been grouped in nine hallmarks of cancer (see 1.2) and they take into account both changes in cells and ECM properties, variations in cell-cell adhesions and in cell-ECM interactions. Among these hallmarks, the mechanical properties of cells and their surrounding ECM have a fundamental role to define the malignant transformation. Cancer cells show an altered behaviour compared to normal cells, due to genetic defects and functional capabilities that allow them to survive, proliferate and disseminate towards distant tissues. Biological and functional alterations are combined with abnormalities in the physical and structural characteristics of the cells. The studies of the biomechanical properties of tumour cells show that, for most of the cancer types, the cancer cells are more compliant than their healthy counterparts (1–4). Furthermore, cell stiffness decreases with increasing cancer invasiveness and metastatic potential (5,6). A key role, during tumour progression, is attributed to the tumour microenvironment, which greatly contributes to the response of tumour cells. Research findings show that tumours display unique mechanical properties: they are stiffer than normal tissues (7,8). The clear difference existing between normal and tumour tissue mechanics has been employed to cancer detection. In fact, oncologists often diagnose cancer based on a change of tissue stiffness sensed by palpation. Nevertheless, this difference can be exploit also in cancer treatment. The mechanical microenvironment may cause malignant transformation, possibly through activation of oncogenic pathways and inhibition of tumour suppressor genes. In addition, the mechanical microenvironment may promote tumour progression by influencing cellular processes, enhancing cell survival through autophagy, but also by affecting sensitivity of tumour cells to therapeutics. Furthermore, multiple intracellular signalling pathways results to be sensitive to the mechanical properties of the microenvironment. Among these processes, the epithelial to mesenchymal transition (EMT) is recently proposed as an indicator of cancer progression and metastasis.

In the first part of this study, we have analysed murine fibroblast cells to identify several biophysical parameters for the screening of the cancer. We have performed the research examining, in parallel, the alterations, caused by cell virus transformation, of normal cell functions and cell mechanical properties . We have found that cellular structure, functions and mechanics are strictly correlated. In particular, we have found that the malignant phenotype was marked by an increased proliferation, reduced adhesion to substrate, altered cellular morphology, enhanced migration capacity and lower cell mechanical properties. All the altered cellular activities and functions seem to be directly dependent on the changes which occur at level of cytoskeleton architecture. Considering these experimental observations, we have concluded that the evaluation of cytoskeleton mechanical properties could be a useful diagnostic indicator of cell malignant transformation. In the second part of our project, we have tried to take advantage of the key biophysical parameters, previously identified, to support the hard diagnosis of malignant human pleural effusions. We have examined human lung cells, discriminated healthy from cancer cells and distinguished cancer cells with different aggressiveness. In fact, we have found that cell mechanical properties were correlated to tumour cell aggressiveness: the reduction of cell stiffness, with the level of cancer transformation, seems to promote tumour invasion. Nevertheless, the investigation of the mechanical phenotyping of tumours cannot be limited to the mechanical state of the cell. Cells are not isolated system, but a complex loop of interactions exists between cells and their surroundings. Preliminary experiments using hydrogels of different stiffness for cell culture have demonstrated that the stiffness of the substrate has a large impact on cellular functions. Thus, in order to reach a more profound understanding of the role of extracellular mechanics in tumour progression, we have characterized the mechanics of *ex vivo* human biopsy tissues. For the first time, we have used the particle tracking microrheology to study the mechanics of *ex vivo* human biopsy tissues. This technique offers the opportunity to probe the sample in 3D, and, thus, to examine how malignant transformation influences the mechanical properties of cells within the tumour microenvironment. The application of the microrheology technique allowed the simultaneous characterization of the mechanics of cells and extracellular environment. We have observed that the malignant transformation

causes a reduction in cell mechanical properties, as already observed *in vitro* conditions, combined to a stiffening of their surroundings. What is more important and interesting, particle tracking results permitted to establish a correlation between the nanomechanical properties of biopsy tissues and the grade and stage of lung tumours. Our results underscore the importance of the mechanical properties of ECM in tumour progression. It is important to underline that by using the particle tracking technique we cannot derive quantitative indications of biopsies stiffness, but a comparison between the mechanical properties of healthy and tumour tissues can be performed. The simultaneous mechanical phenotyping of cells and ECM appear an efficient additional support in the diagnosis of cancer, even if the technique requires the surgical intervention, because it cannot be applied *in vivo*. However, this technique appears highly advantageous to a deeper understanding of cancer mechanobiology and in the definition of new therapeutic tools for lung cancer.

6.2 Future perspectives

Understanding the changes associated with the ECM surrounding cells would be critical in the cancer treatment. In fact, according to the results achieved in the latter part of PhD, we have hypothesized that by orchestrating, reengineering or normalizing the microenvironment from a mechanical point of view it could be possible to reverse typical EMT process of cancer cells and turn the microenvironment from a tumour supportive to a non-supportive one. In order to determine how changes in matrix rigidity influence cell properties, we have performed preliminary *in vitro* experiments to find out if tumour cells behaviour respond to dynamic changes in substrate stiffness, on which they are seeded. In particular, gelatine substrates, whose elasticity is comparable to that of cancer lung tissue, are used for cell culture. A specific enzyme (collagenase) is used to, partially and in a controlled way, degrade the substrate, decreasing its mechanical properties in order to obtain gelatine substrates with an elasticity comparable to that of healthy lung tissue. Several of the biophysical parameters selected in the first part of this work, such as cell migration and cell spreading, can be measured before and after enzyme treatment to verify if normal cell behaviour can be restored by softening the

microenvironment. Moreover, E-cadherin and N-cadherin are used as epithelial and mesenchymal markers, respectively, to test the reversion of the EMT process. In theory, the restoring up-regulation of E-cadherin and down-regulation of N-cadherin into invasive epithelial cell lines, would abrogate their invasive potential. If these results will be confirmed, a list of therapeutic agents could be tested to verify their ability to reengineering the cancer microenvironment to a state of normalcy. The study of the mechanics of cell and extracellular environment could provide information about the state of tissue and, thus, support the diagnosis of tumour. Moreover, tissues mechanical properties could also be involved in cancer treatment. In particular, the ECM can be considered a powerful target to normalize the aggressive and invasive behaviour of cancer cells.

6.3 References of Chapter 6

1. Li QS, Lee GYH, Ong CN, Lim CT. AFM indentation study of breast cancer cells. Biochem Biophys Res Commun. 2008 Oct;374(4):609–13.

2. Kirmizis D. Atomic force microscopy probing in the measurement of cell mechanics. Int J Nanomedicine. 2010 Mar;137.

3. Guck J, Schinkinger S, Lincoln B, Wottawah F, Ebert S, Romeyke M, et al. Optical Deformability as an Inherent Cell Marker for Testing Malignant Transformation and Metastatic Competence. Biophys J. 2005 May;88(5):3689–98.

4. Remmerbach TW, Wottawah F, Dietrich J, Lincoln B, Wittekind C, Guck J. Oral Cancer Diagnosis by Mechanical Phenotyping. Cancer Res. 2009 Feb 10;69(5):1728–32.

5. Cross SE, Jin Y-S, Rao J, Gimzewski JK. Nanomechanical analysis of cells from cancer patients. Nat Nanotechnol. 2007 Dec;2(12):780–3.

6. Swanton C, Burrell RA, Futreal PA. Breast cancer genome heterogeneity: a challenge to personalised medicine? Breast Cancer Res [Internet]. 2011 Feb [cited 2017 Feb 7];13(1). Available from: http://breast-cancer-research.biomedcentral.com/articles/10.1186/bcr2807

7. Plodinec M, Loparic M, Monnier CA, Obermann EC, Zanetti-Dallenbach R, Oertle P, et al. The nanomechanical signature of breast cancer. Nat Nanotechnol. 2012 Oct 21;7(11):757–65.

8. Yu H, Mouw JK, Weaver VM. Forcing form and function: biomechanical regulation of tumor evolution. Trends Cell Biol. 2011 Jan;21(1):47–56.